AD/A-003 751

GEOMAGNETICALLY TRAPPED RADIATION

Michael Schulz

Aerospace Corporation

Prepared for:

Space and Missile Systems Organization

17 December 1974

UNCLASSIFIED

SECURITY CLASSIFICATION OF THIS PAGE (When Data Entered)

AD/A003 757

REPORT DOCUMENTATION PAGE

READ INSTRUCTIONS BEFORE COMPLETING FORM

1. REPORT NUMBER: SAMSO-TR-74-264	2. GOVT ACCESSION NO.
3. RECIPIENT'S CATALOG NUMBER	
4. TITLE (and Subtitle): GEOMAGNETICALLY TRAPPED RADIATION	5. TYPE OF REPORT & PERIOD COVERED: Interim
6. PERFORMING ORG. REPORT NUMBER: TR-0075(5260-20)-2	
7. AUTHOR(s): Michael Schulz	8. CONTRACT OR GRANT NUMBER(s): F04701-74-C-0075
9. PERFORMING ORGANIZATION NAME AND ADDRESS: The Aerospace Corporation, El Segundo, Calif. 90245	10. PROGRAM ELEMENT, PROJECT, TASK AREA & WORK UNIT NUMBERS
11. CONTROLLING OFFICE NAME AND ADDRESS: Space and Missile Systems Organization, Air Force Systems Command, Los Angeles, Calif. 90045	12. REPORT DATE: 17 December 1974
	13. NUMBER OF PAGES: ~~112~~ 116
14. MONITORING AGENCY NAME & ADDRESS (if different from Controlling Office)	15. SECURITY CLASS. (of this report): Unclassified
	15a. DECLASSIFICATION/DOWNGRADING SCHEDULE

16. DISTRIBUTION STATEMENT (of this Report)

Approved for public release; distribution unlimited

17. DISTRIBUTION STATEMENT (of the abstract entered in Block 20, if different from Report)

18. SUPPLEMENTARY NOTES

19. KEY WORDS (Continue on reverse side if necessary and identify by block number)

Radiation belts

Magnetospheric physics

20. ABSTRACT (Continue on reverse side if necessary and identify by block number)

This review covers the major developments in radiation-belt phenomenology of the past four years (1970-1973). This has been a period characterized by consolidation and refinement of ideas and measurements related to geomagnetically trapped particles. Significant progress has been made in understanding ion and electron pitch-angle distributions within the context of radial diffusion and pitch-angle diffusion, respectively. Comparison of alpha-particle and proton distributions has helped to clarify the relative strengths of known radial-diffusion mechanisms. Careful measurements

DD FORM 1473 (FACSIMILE)

19. KEY WORDS (Continued)

20. ABSTRACT (Continued)

have indicated the directional flux of cosmic-ray-albedo neutrons, which constitute (through beta decay) a major source of high-energy (≥20-MeV) inner-belt protons. Inclusion of radial-diffusion and geomagnetic-secular effects has brought the theory of the inner proton belt into reasonable agreement with observation. At very low L values ($L \lesssim 1.2$) atmospheric collisions have been found to facilitate the radial transport of 40-keV protons and 2-MeV electrons. The plasmapause has been identified as an important boundary for plasma instabilities (wave-particle interactions) that lead to particle precipitation and red-arc excitation. Suggestions have followed for artificially simulating such plasmaspheric effects by magnetospheric injection of cold barium or lithium plasma.

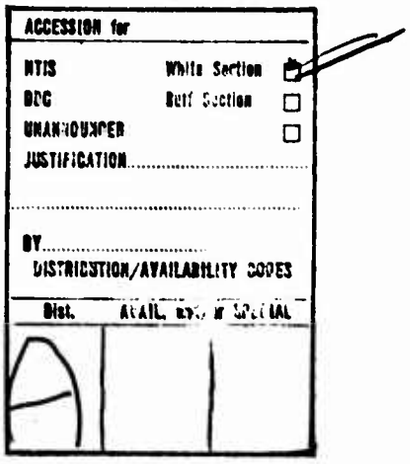

Approved

G. A. Paulikas, Director
Space Physics Laboratory

Publication of this report does not constitute Air Force approval of the report's findings or conclusions. It is published only for the exchange and stimulation of ideas.

Jean Bogert, 2nd Lt.
United States Air Force
Technology Development Division
Deputy for Technology

PREFACE

This article is based on an invited review that was presented 19 June 1974 at the International Symposium on Solar-Terrestrial Physics in São Paulo, Brazil. The author is pleased to thank Prof. S. A. Bowhill for issuing the original invitation, as well as for his patience in awaiting delivery of the manuscript. The author has profited from the helpful comment of Dr. R. W. Fredricks, Dr. Antonio Mogro-Campero, Dr. Lawrence R. Lyons, and Prof. Ruth Gall, and from encouraging remarks by Prof. Juan G. Roederer, Dr. J. B. Blake, and Dr. G. A. Paulikas. Finally, it is a pleasure to thank Mrs. Dorothy M. Monroe for typing the final manuscript with great skill in a short time.

CONTENTS

TABLE

FIGURES

1. INTRODUCTION

The earth's radiation belts consist of energetic electrons and ions (mainly protons) which execute quasi-periodic trajectories under the constraining influence of the geomagnetic field. The adiabatic theory of charged-particle motion (Northrop and Teller, 1960) provides the kinematical framework for characterizing radiation-belt particles. The kinematical state of a particle is defined by specifying the three invariant action integrals J_i and three conjugate phases φ_i associated with the particle's gyration about a guiding field line (i = 1), bounce motion between magnetic mirror points (i = 2), and azimuthal drift around the earth (i = 3). This hierarchy typically applies for particle momenta $p \ll 60(Z/L^2)$ GeV/c, where Z is the charge number (Z = 1 for protons and electrons, Z = 2 for alpha particles, etc.). Moreover, the bounce and drift integrals are well-defined only for values of the shell parameter $L \leq 10$, since the outer magnetosphere is too distorted to support adiabatic motion.

Dynamically interesting phenomena are those that violate the adiabatic invariants, which are respectively proportional to the action integrals J_i. The first invariant $M \equiv |q|(J_1/2\pi m_0 c) = p_\perp^2/2m_0 B$ is equal to m/m_0 times the particle's magnetic moment. The second invariant $J \equiv J_2 = \oint p_\parallel ds$ is evaluated along the particle's guiding field line, and the third invariant $\Phi \equiv (c/q)J_3$ is equal to the magnetic flux enclosed by the drift shell. In accordance with Hamilton-Jacobi theory, the characteristic frequency $\dot{\varphi}_i/2\pi$ associated with the action integral J_i is given

by $\dot{\varphi}_i/2\pi = \partial W/\partial J_i$, where W is the particle's energy (kinetic plus potential). Representative frequency contours are shown in Figure 1 for particles mirroring at the equator of an idealized geomagnetic dipole field, with no electrostatic fields superimposed (Schulz and Lanzerotti, 1974).

Processes that violate either or both of the first two invariants lead to particle diffusion in pitch angle and/or energy. Processes that violate the third invariant lead to radial diffusion. In particular, processes that conserve the first two invariants while violating the third produce a kind of radial diffusion that energizes particles as they diffuse into the magnetospheric interior from an external source, e.g., from the plasma sheet or the solar wind (see Figure 2).

The plasma sheet is an electrically resistive medium extending across the magnetospheric tail in a dawn-to-dusk electric field ~1 V/km. The resistivity is not collisional but anomalous (plasma-kinetic), and the plasma-sheet temperature amounts to several keV (with $T_p > T_e$). The main source of particles for the plasma sheet is most likely the shocked solar wind, but (according to Axford, 1970) plasma from the earth's polar ionosphere may also contribute via the "polar wind", which flows out along open field lines (see Figure 3).

Magnetospheric plasma tends to drift as illustrated in Figure 2 under the influence of electrostatic and magnetostatic fields. The earth's rotation leads to a quasi-stable capture of equatorial and mid-latitude ionospheric plasma within a sharply bounded region known as the plasmasphere. Here the plasma temperature is ~1 eV or less, but the equatorial

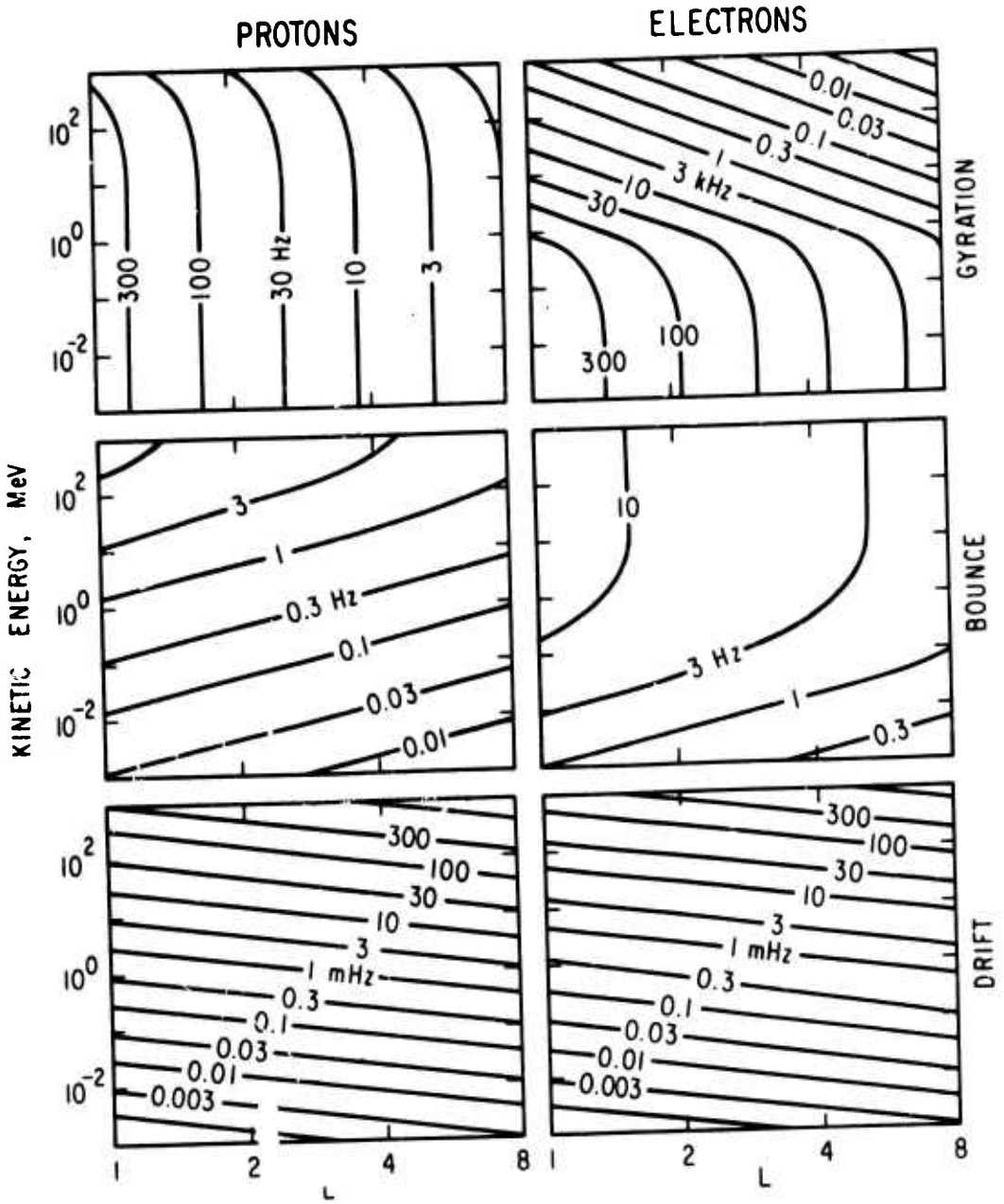

Fig. 1. Contours of constant adiabatic gyration, bounce, and drift frequency for equatorially mirroring particles in geomagnetic dipole field. The approximation of an adiabatic hierarchy of motions is seen to fail around the upper corners (E ~1 GeV, L ~ 8), where $\Omega_1 \sim \Omega_2 \sim \Omega_3$.

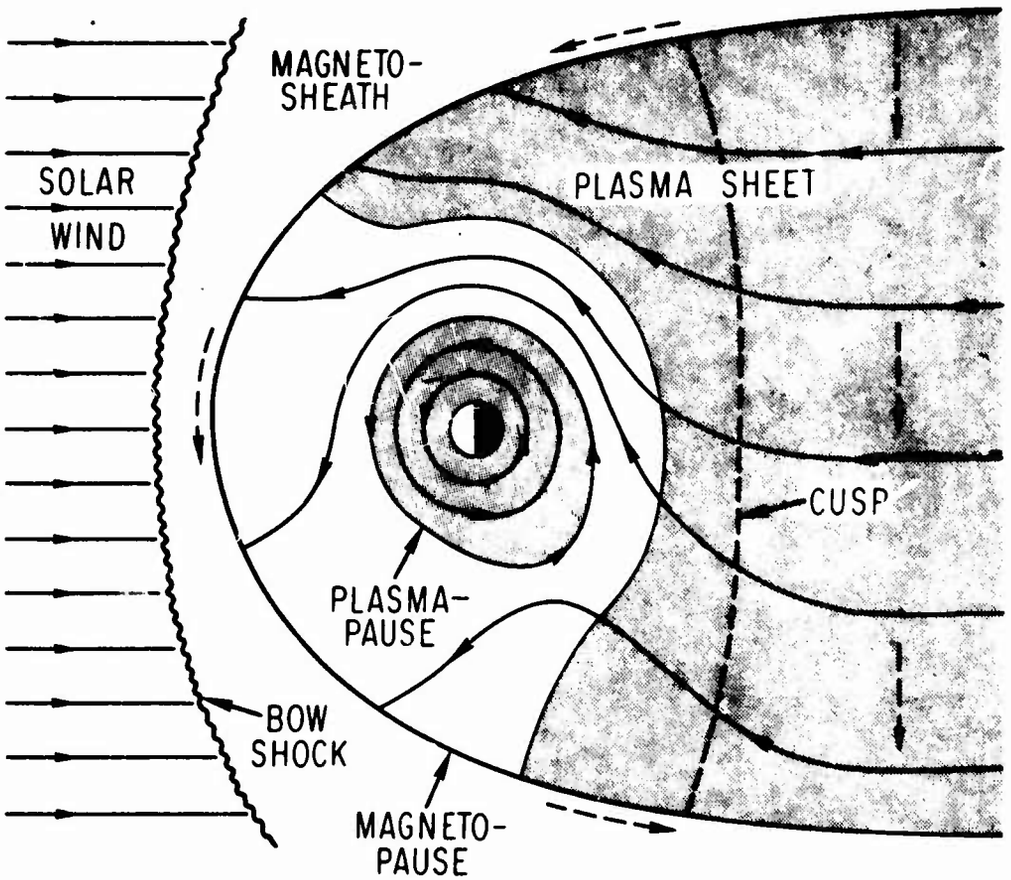

Fig. 2. Distribution (shaded areas) and flow pattern (solid arrows) of magnetospheric plasma in the equatorial plane. Dashed arrows indicate electric-current pattern. The plasmasphere is the shaded region inside the plasmapause. Field lines beyond the magnetic cusp are "open", forming a neutral-sheet configuration maintained by plasma-sheet currents. However, the plasma sheet also extends (presumably by diffusion) onto closed field lines sunward of the cusp.

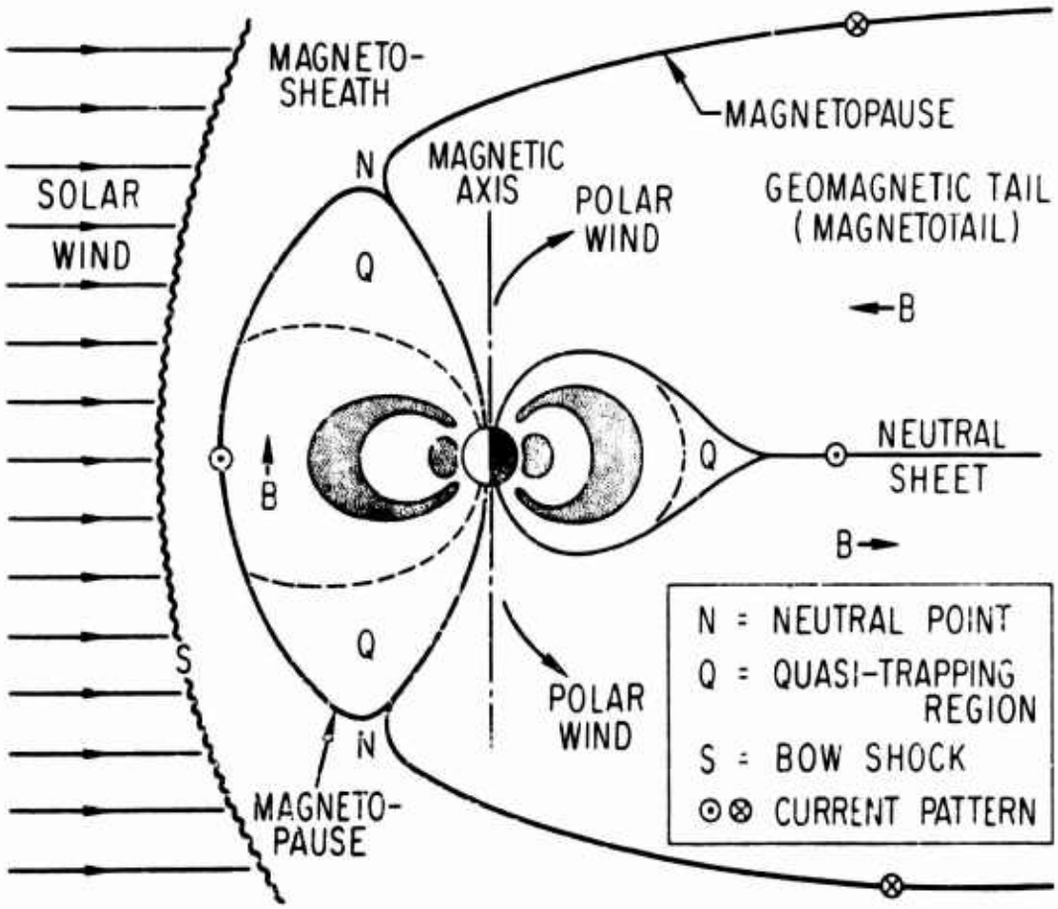

Fig. 3. Magnetospheric configuration in the noon-midnight meridional plane. Shaded regions correspond to electron radiation belts (omnidirectional flux $I_{4\pi} \geq 10^6$ $cm^{-2}sec^{-1}$ at kinetic energies $E \geq 0.5$ MeV). Quasi-trapping regions (bounded by dashed curves) contain the mirror points of particles which, because of the distorted magnetic-field configuration, cannot complete an adiabatic drift orbit around the earth.

density is high ($\sim 10^3 e^{4-L}$ cm^{-3}, according to Chappell et al., 1970) compared with that in regions beyond the plasmapause (≤ 1 cm^{-3}). Since the cold-plasma density strongly affects dispersion relations and resonance conditions, the plasmapause (see Figure 2) is also a boundary for phenomena dependent on magnetospheric wave-particle interactions.

In addition to the above-described plasma sheet, there are other important sources of geomagnetically trapped radiation. Energetic solar-flare protons ($E \sim 1 - 100$ MeV) can enter the magnetosphere more-or-less directly from interplanetary space. Such particles are not strongly affected by traversal of the magnetosheath, nor by large-scale electric fields in the magnetosphere. They can enter the magnetosphere through the tail (perhaps also at the dayside neutral points) and can gain access to closed drift shells through an intrinsic breakdown of the adiabatic hierarchy, a breakdown that is characteristic of high-rigidity particles in the outer magnetosphere.

Solar-flare protons striking the atmosphere can eject energetic neutrons by spallation of nitrogen and oxygen nuclei. The beta decay of such albedo neutrons within the magnetosphere (a process known as SPAND, for solar-proton-albedo-neutron decay) constitutes a minor source of radiation-belt protons. The analogous reaction, induced by more energetic cosmic-ray particles from the galaxy, is know as CRAND (for cosmic-ray-albedo-neutron decay) and accounts in a major way for the injection of energetic protons into the inner radiation zone ($L \leq 3$). A final source of geomagnetically trapped radiation, operative during the years 1958 – 62, consisted of the fission debris from high-altitude (≥ 200 km)

nuclear detonations (e.g., Walt, 1971). The beta decay of such fission fragments led to the formation of artificial radiation belts having various widths in L and various distributions in pitch angle, and the analysis of data on such artificial radiation belts has provided valuable diagnostic information about the magnetospheric environment.

The purpose of the present review is to cover the major developments in radiation-belt phenomenology of the past four years (1970-1973). The selection of topics is somewhat subjective, and the omission of some possibly important contributions (e.g., those not understood by the present reviewer) is unavoidable. The intent is to provide a coherent and somewhat critical review of recent progress in radiation-belt physics, and to suggest some promising ideas for further investigation.

2. ADIABATIC DRIFT SHELLS

Although the dynamically interesting phenomena of radiation-belt physics require (by the present definition) a violation of one or more adiabatic invariants, there exist two interesting kinematical phenomena (known as shell splitting and quasi-trapping) which arise from the magnetosphere's inherent azimuthal asymmetry. If the magnetosphere were azimuthally symmetric about the earth's dipole axis, the tracing of particle drift shells would consist simply of rotating each field line about the axis of symmetry. Two particles mirroring on the same field line,

regardless of their energies or equatorial pitch angles, would generate the same adiabatic drift shell.

However, the real magnetosphere is not azimuthally symmetric. There is a day-night asymmetry with respect to the magnetic field, and a dawn-dusk asymmetry with respect to the magnetospheric electric field. In consequence of these asymmetries, particle drift shells tend to intersect rather than coincide. Two particles, even if they have the same kinetic energy on a given field line, will (in general) execute different drift shells unless they also have the same equatorial pitch angle on the given field line. This effect is known as shell splitting.

Evidence for shell splitting in a given field model is obtained by considering the drift trajectory of a particle having a vanishing second invariant J. This trajectory must, of course, conserve the first invariant M and total (kinetic plus potential) energy W. It must also track a local minimum in the field magnitude B (with respect to arc length s) on each field line that it crosses. In analytical terms, the surface generated by the drift paths of particles having $J = 0$ is the surface on which $\partial B/\partial s = 0$ $\partial^2 B/\partial s^2 \geq 0$, where $\partial/\partial s \equiv \hat{\underset{\sim}{B}} \cdot \underset{\sim}{\nabla}$. It was noted by Mead (1964) that, in his field model, the $J = 0$ surface bifucates into two separate sheets on the day side of the magnetosphere. Shabansky and Antonova (1968) suggested that a particle having $J \approx 0$ will select either the northern or the southern sheet, according to the instantaneous value of its bounce phase φ_2 at the site of bifurcation.

The drift path of a particle having J = 0 is a contour conserving both M and W on the surface described above. (Neglecting electrostatic potentials, it is a path of constant B.) Shell splitting is indicated by an azimuthal variation of $\partial^2 B/\partial s^2$ along this path of constant M and W (Roederer and Schulz, 1969; 1971).

It may happen that a particle has well-defined M and J on a given field line, but cannot execute a complete adiabatic drift shell without encountering the magnetospheric surface (either at the magnetopause or at the neutral sheet, Figure 3). Such a particle is said to be quasi-trapped, and its mirror points are said to occupy a quasi-trapping region for the energy (W) in question. One example of quasi-trapping is the fate of particles having vanishing kinetic energy beyond the plasmapause (see Figure 2). Such particles encounter the magnetopause before completing a drift orbit of 2π radians. (Despite the azimuthal asymmetry, there is no shell splitting in the limit of vanishing M and J. Such particles follow electrostatic equipotentials, which coincide with magnetic field lines in most accepted models.)

The geometry of the magnetic field alone is relevant to the motion of those particles having sufficiently high energy to justify the neglect of electrostatic potentials, but having sufficiently low rigidity to move adiabatically. The criterion on rigidity (cf. Taylor and Hastie, 1971) can be made more precise by introducing the traceless tensor

$$\underset{\sim}{\epsilon} \equiv (pc/qB^2)\, \underset{\sim}{\nabla B} \qquad (1)$$

and requiring that each rectangular component of $\underset{\sim}{\epsilon}$ be much less than unity in absolute value. This criterion is fortunately satisfied by most of the particles one chooses to study in the context of radiation-belt physics. Special methods of numerical analysis, designed to trace the details of each particle trajectory, are obligatory in situations where the components of $\underset{\sim}{\epsilon}$ are not sufficiently small (e.g., Smart et al., 1969).

The tracing of charged-particle orbits, whether by numerical trajectory analysis or by the theory of adiabatic invariance, requires the specification of a field model. Recent developments in field modeling are reviewed elsewhere (e.g., Morfill, 1975). It will be sufficient here to recall three rather old models. The first, due to Mead (1964), is a 13-term expansion of the geomagnetic scalar potential V (such that $\underset{\sim}{B} = -\underset{\sim}{\nabla} V$) in spherical harmonics having the north-south and dawn-dusk symmetries appropriate to the case of a solar wind normally incident on a dipolar magnetic field. Mead required the solar-wind plasma to undergo specular reflection from the self-consistent magnetopause that forms thereby (Mead and Beard, 1964). The result is a field pattern illustrated in Figure 4a.

If one adopts a microscopic view and allows the solar-wind plasma to penetrate the magnetopause (e.g., Bird and Beard, 1972), the resulting gyration and drift currents are found to generate a self-consistent magnetotail (cf. Figure 3). Williams and Mead (1965) simulated this effect by adding to the 13-term model an equatorial current

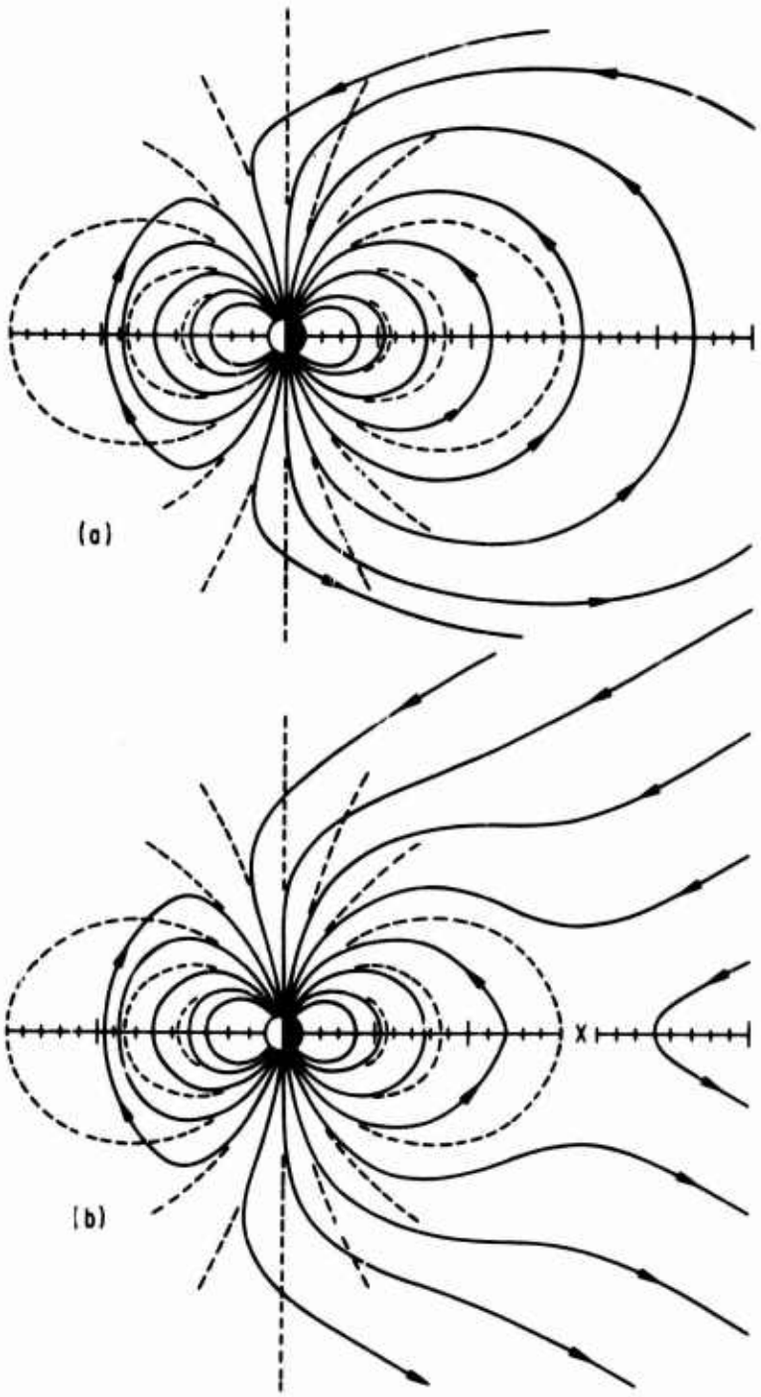

Fig. 4. Schematic representation of meridional field lines in (a) the 13-term and (b) the 3-term Mead magnetospheres (solid curves). Corresponding dipole field lines (dashed curves) are shown for invariant latitudes $\Lambda = 65^{\circ}$, 70°, 75°, 80°, 85° and 90°, but omitted for $\Lambda = 60^{\circ}$. The symbol X marks the location of the nightside neutral line that automatically appears in the 3-term model (Schulz and Lanzerotti, 1974).

strip across the nightside magnetosphere from dawn to dusk. However, one gets a similar effect without the current strip (see Figure 4b) by simply truncating the expansion of Mead (1964) after the third term. The resulting three-term model, actually suggested by Mead (1964), contains the salient features of the actual magnetospheric topology. It is derivable from the scalar potential

$$V = - g_1^0 (a/r)^2 z - \bar{g}_1^0 (a/b)^3 z - \sqrt{3}\, \bar{g}_2^1 (a/b)^3 (x/b)\, z , \qquad (2)$$

where r is the geocentric distance (radial coordinate), z is the distance north of the equator (along the dipole axis), and x is the projected distance from the dipole axis (measured along the earth-sun line, positive on the night side). The expansion coefficients g_n^m and $\bar{g}_n^m$ are Schmidt-normalized (Chapman and Bartels, 1940). The symbols $\underline{a}$ and $\underline{b}$ represent the radius of the earth and the geocentric "stand-off" distance to the subsolar point on the magnetopause, respectively.

Using the field model of Williams and Mead (1965), Roederer (1967) has studied the quasi-trapping phenomenon in situations for which electrostatic potentials can legitimately be neglected. He has found that a particle having one mirror point in each of the two quasi-trapping regions on the noon meridian (regions Q in Figure 3) will fail to complete a drift orbit of 2π radians, conserving M and J. Such a particle would have to preserve the magnitude of its mirror field B_m in the course of azimuthal

drift, while conserving also the quantity K^2 ($\equiv J^2/8m_0M$). This proves to be impossible, and the particle's drift shell instead crosses the nightside boundary between closed and open field lines.

The foregoing conclusion applies to bounce trajectories that cross the equatorial plane, i.e., to mirror-field intensities B_m that exceed the magnitude of B in the equatorial plane along a given field line, in the noon meridian. Roederer (1967) did not consider the motion of particles trapped in the higher-latitude field minima that exist near the magnetopause on the day side. Thus, his discovery of a nightside quasi-trapping region (marked Q in Figure 3), characteristic of particles mirroring too near the magnetic equator, must be received with caution (cf. Shabansky and Antonova, 1968).

Particles having K = 0 do, however, show evidence of quasi-trapping in the three-term field model of Mead (1964). It can be shown (cf. Roederer and Schulz, 1969) that the value of $\partial^2B/\partial s^2$ is correctly given, in the equatorial plane of this field model, by the expression

$$r^2B(\partial^2B/\partial s^2)_{eq} = 9B^2 + 9\bar{g}_1^0(a/b)^3[3B + 2\bar{g}_1^0(a/b)^3] + 6(\bar{g}_2^1)^2(a/b)^6(r/b)^2(1 + 15\cos^2\varphi) - \sqrt{3}\,\bar{g}_2^1(a/b)^3(r/b)[39B + 48\,\bar{g}_1^0(a/b)^3]\cos\varphi. \quad (3)$$

where φ is the longitude measured eastward from the midnight meridian. The azimuthal variation of a positive $(\partial^2B/\partial s^2)_{eq}$ demonstrates the existence of shell splitting in this model. Moreover, it follows from (3) that $\partial^2B/\partial s^2$ vanishes in the equatorial plane along the contour given by

$$\sqrt{3}\cos\varphi = (2\bar{g}_2^1/7g_1^0)(r/b)^4 + (3g_1^0/7\bar{g}_2^1)(b/r)^4 - (3\bar{g}_1^0/7\bar{g}_2^1)(b/r). \quad (4)$$

This contour marks the aforementioned bifurcation of the K = 0 surface. Moreover, the magnitude of B vanishes in the equatorial plane along the contour given by

$$\sqrt{3}\cos\varphi = -(g_1^0/\bar{g}_2^1)(b/r)^4 - (\bar{g}_1^0/\bar{g}_2^1)(b/r). \quad (5)$$

This contour marks the boundary between closed and open field lines (see Figure 4b). Both of these important contours are plotted in Figure 5, using

$$g_1^0 = 1.24\,\bar{g}_1^0 = -2.56\,\bar{g}_2^1 = -0.31 \text{ gauss}, \quad (6)$$

as recommended by Mead (1964). Both contours intersect the equatorial trace of the magnetopause calculated self-consistently (i.e., in the model containing many more than three spherical-harmonic coefficients) by Mead and Beard (1964). The analytical continuation of B = 0 and $(\partial^2 B/\partial s^2)_{eq} = 0$ beyond the Mead-Beard surface is indicated by dashed curves, but presumably has no physical meaning.

It is convenient, following Stone (1963), to label a field line with the parameter

$$L_0 \equiv |g_1^0/B_0|^{1/3}, \quad (7)$$

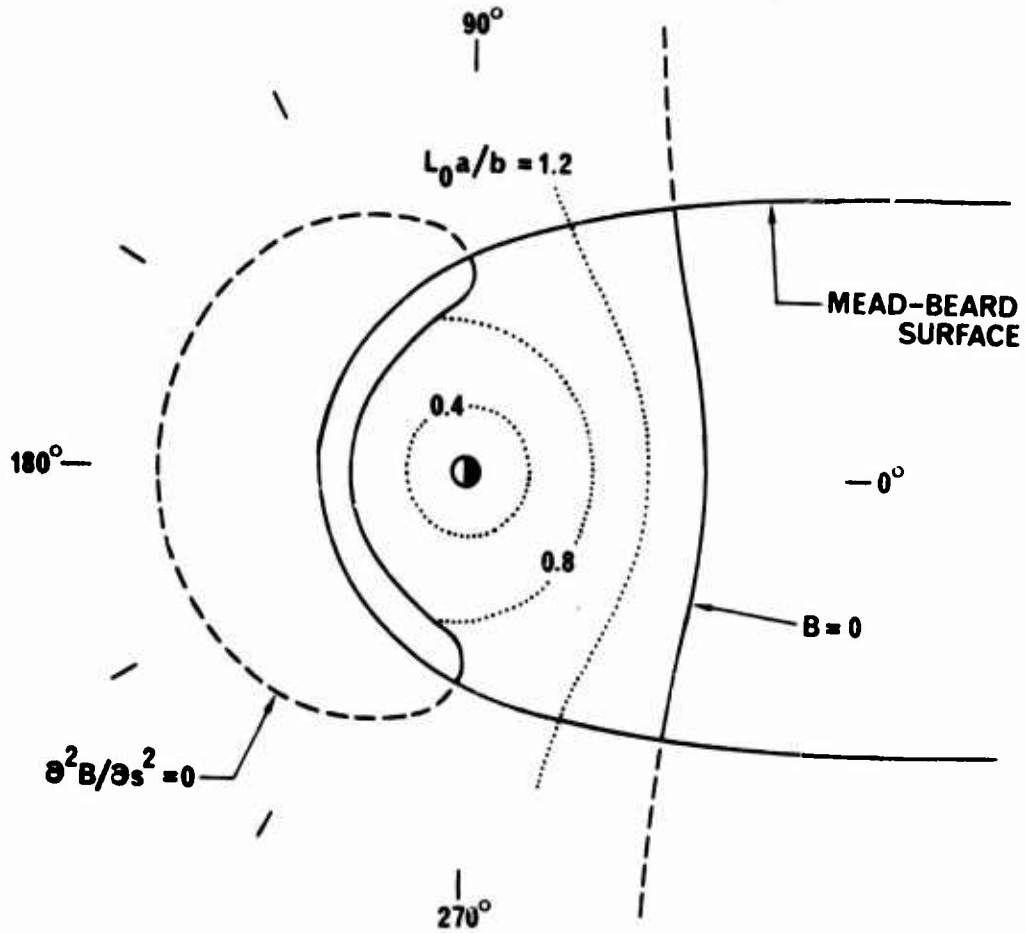

Fig. 5. Equatorial-plane contours of constant B and of $\partial^2 B/\partial s^2 = 0$ in the three-term Mead field. Dashed curves represent the analytical continuation of contours $B = 0$ and $\partial^2 B/\partial s^2 = 0$ beyond the magnetospheric surface calculated by Mead and Beard (1964). Dotted curves represent azimuthal-drift trajectories of particles having $J = 0$. The contour $L_0 = 1.2b/a$ illustrates quasi-trapping (cf. Figure 3), and the contour $L_0 = 0.8b/a$ illustrates dayside bifurcation of the azimuthal-drift trajectory.

where B_0 is the minimum value of B along the field line. The parameter L_0 thus serves also as a label for the drift path of a particle having K = 0. Figure 5 thus illustrates (by means of dotted curves) both stable trapping (L_0 = 0.4 b/a) and quasi-trapping (L_0 = 1.2 b/a) at K = 0, as well as an intermediate case (L_0 = 0.8 b/a) in which the drift path bifurcates at $\partial^2 B/\partial s^2 = 0$. Further analysis would be required to determine whether the drift path L_0 = 0.8 b/a closes within the magnetosphere in this model of the earth's field.

The above results tend to confirm the suggestion by Roederer (1967) that there is a nightside quasi-trapping region containing the mirror points of particles having small values of K. In both studies, however, the field models used contain elements of inconsistency. In the present study, the three-term representation of the field is manifestly inconsistent with the magnetopause determination of Mead and Beard (1964), which would require at least the 13-term field model for self-consistency. In the case of Roederer's study, the field model contained an infinitely wide current sheet (Williams and Mead, 1965) extending from the dawn horizon to the dusk horizon. The currents in that model thus did not properly close over the rounded surface of the magnetotail (cf. Figure 3). It remains an open question whether any particles having K = 0 can show quasi-trapping in a self-consistent model of the geomagnetic field and its boundary. A study based on the 13-term model of Mead (1964) would help to resolve this essentially topological question, although the inclusion of a self-consistently modeled neutral sheet would

be necessary in order to resolve the question of quasi-trapping in the real geomagnetic field.

Although presented above as a means of particle escape from the magnetosphere, quasi-trapping can equally well be viewed as a means of particle access. The equations of motion are quite reversible in space and time. However, such access from outside the magnetosphere would be only transient if unaccompanied by some means of radial diffusion from the partial (quasi-trapped) drift shell to a closed drift shell. One may consider in this context the access of solar-wind plasma to the earth's plasma sheet, by way of the dayside polar "cusp" (e.g., Frank, 1971), which extends roughly from either neutral point down to the earth's surface (see Figure 3).

It has been noted above, following equation (3), that shell splitting is present even under the simplest idealization of the day-night magnetospheric asymmetry. Shell splitting is, of course, present also in more nearly realistic field representations, such as the model of Williams and Mead (1965). Roederer (1967) traced the adiabatic drift shells of this field model and thereby estimated the amount by which drift shells are split apart. Pfitzer et al. (1969) carried the analysis a significant step further by using a shell-tracing program to map the distribution function of geomagnetically trapped particles from one longitude to another. They used data from an elliptically orbiting spacecraft (OGO-3) to determine the radial distribution of electron intensity at each equatorial pitch angle. Applying Liouville's theorem, they then used the shell-tracing program

to predict the diurnal variations of electron intensity at synchronous altitude (specifically at the site of ATS 1). The good agreement between prediction and reality is illustrated in Figure 6, where x denotes the cosine of the equatorial pitch angle, B_t is the tail-field intensity (an adjustable parameter of the Mead-Williams model), and $1\ \gamma \equiv 10^{-5}$ gauss.

It is interesting to notice that shell splitting thus leads to an anomalous pitch-angle distribution, i.e., a distribution having a relative minimum at $x = 0$, in the general vicinity of midnight. The pitch-angle distribution is normal (essentially compatible with the lowest eigenmode of pitch-angle diffusion) at the noon meridian (1200 LT). The explanation is not difficult. At $L \geq 5$, the distribution of electron intensity at fixed energy decreases with increasing drift-shell radius. In other words, the radiation resides in a belt. Particles having $x = 0$ travel a path of constant equatorial B, and must pass nearer the earth at midnight than at noon in order to do so. Particles having $x = 0.42$ (for example) mirror in the relatively less distorted inner magnetosphere, and so execute a more nearly symmetrical drift shell. Thus, the ATS-1 spacecraft at midnight samples electrons from a larger drift shell for $x = 0$ than for $x = 0.42$; the ordering of shell diameters is reversed when the spacecraft is at noon.

One immediately observes from Figure 6 that the midnight pitch-angle distribution is more strongly anomalous in the higher-energy channel. This empirical fact was scrutinized more thoroughly by Lucas and Brice (1973), using the electron data of West et al. (1973). Representative

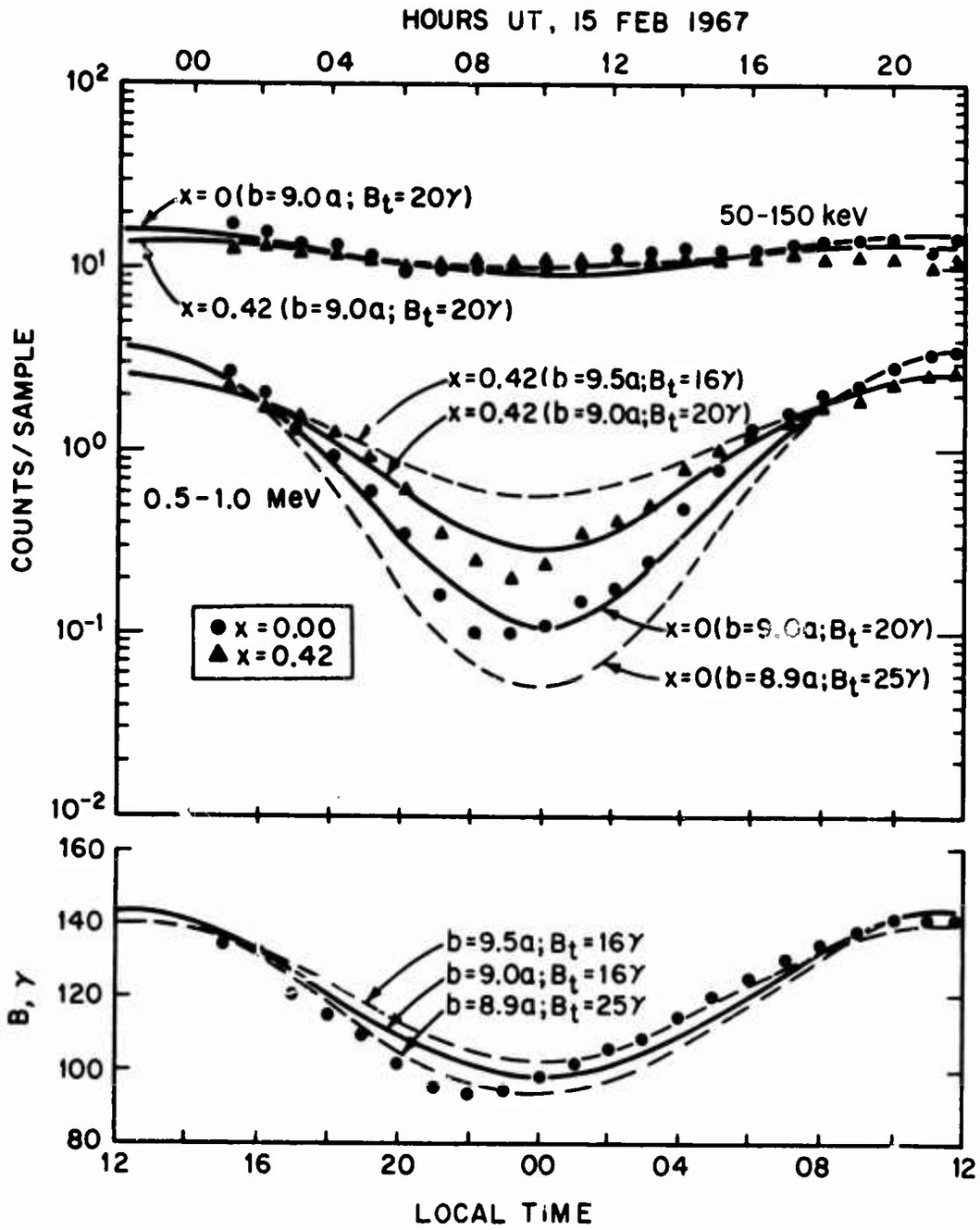

Fig. 6. Diurnal variation of electron fluxes and magnetic field (data points) observed at synchronous altitude (ATS 1), as compared with predictions (dashed and solid curves) based on Mead-Williams field models (b/a, B_t) and distribution function $\bar{f}(M, J, \Phi)$ deduced from OGO-3 electron data (Pfitzer et al., 1969).

nightside (left panel) and morningside (right panel) pitch-angle distributions are shown in Figure 7. Even at the lower energies, where the nightside distribution remains normal, one detects a relative flattening of the pitch-angle distribution on the night side. West et al. (1973) obtained pitch-angle distributions at a great variety of longitudes. On examining their characterizations (here called normal vs anomalous), one detects a gradual rotation of the predominant asymmetry from day-night toward dawn-dusk with decreasing electron energy. This rotation is qualitatively compatible with the incipient contribution of the magnetospheric electric field to drift-shell splitting (see Roederer and Schulz, 1971; Stern, 1971).

Although shell splitting itself is a purely adiabatic phenomenon (conserving all three invariants), it can lead, in the presence of particle collisions with the atmosphere, to an enhanced form of radial diffusion (called "neoclassical" diffusion in the language of laboratory plasma physics). This may be an important process for inner-zone electrons ($L \lesssim 1.2$), where other known radial-diffusion mechanisms are relatively ineffective. The shell splitting at such low L values arises not much from the gross magnetospheric asymmetries discussed above, but rather from higher-order internal multipoles (magnetic anomalies) of the earth's main field. The magnitude of this internal shell splitting is derivable from Figure 8 (Roederer et al., 1973), in which the subscript 0 is used to emphasize that $\partial^2 B/\partial s^2$ has been evaluated along a path of constant B ($= B_0$) on a warped surface defined by the condition $\partial B/\partial s = 0$ (see above). The

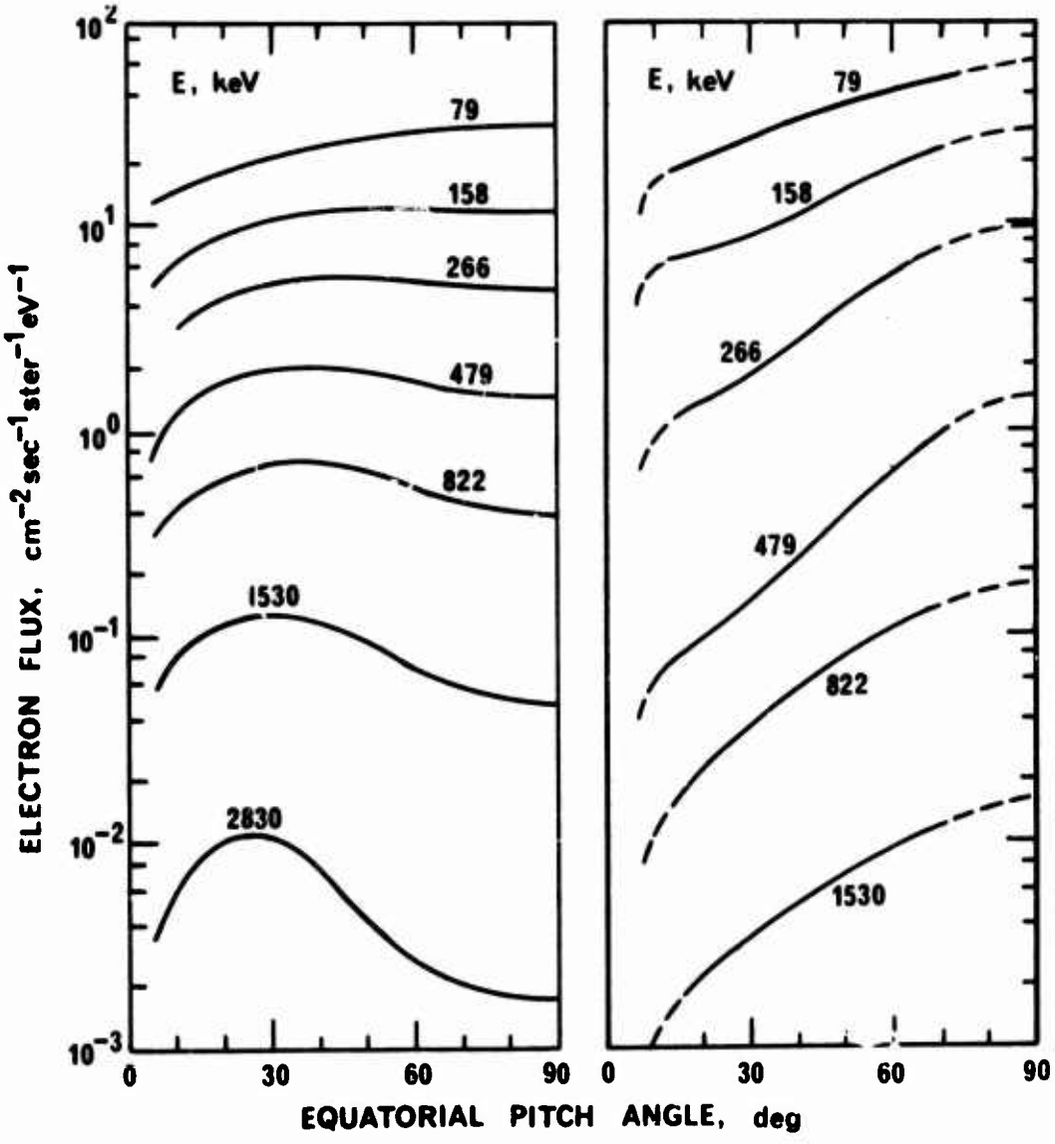

Fig. 7. Typical nighttime (18 September 1968) and morningside (30 March 1968) pitch-angle distributions of energetic electrons at L ~ 7 (from West et al., 1973). The data were transformed to equatorial latitude; the dashed portions of the curves are extrapolations (Lucas and Brice, 1973).

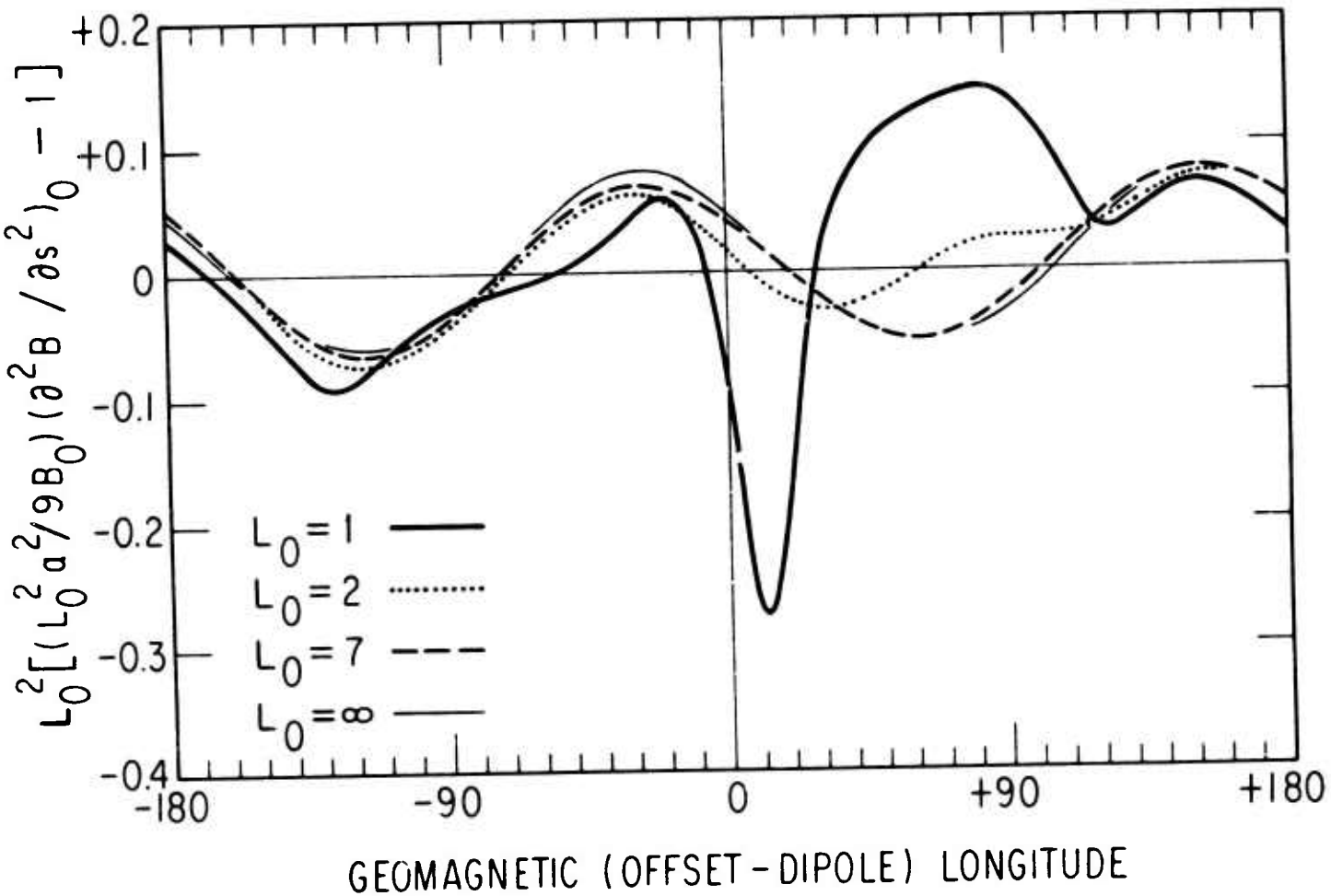

Fig. 8. Normalized shell-splitting function associated with internal geomagnetic multipoles, shown for selected contours of constant $B(= -g_1^0/L_0^3)$ on the equatorial ($\partial B/\partial s = 0$) surface (Roederer et al., 1973).

minimum-B surface is no longer planar, as it was in equations (2)-(5). The definition of L_0 is still given by (7) with the interpretation that g_1^0 is to be evaluated in offset-dipole coordinates (Chapman and Bartels, 1940). Shell splitting, here as elsewhere, is indicated by the azimuthal variation of $\partial^2 B/\partial s^2$ along a path of constant B ($= B_0$) on the surface K = 0. The main features discernible at $L_0 \sim 1$ are the South American ($\varphi \approx 0^\circ$-30°) and South African ($\varphi \approx 40^\circ$-110°) anomalies. The main asymptotic contribution to shell splitting (actually dwarfed by gross magnetospheric asymmetries at $L_0 \geq 2$) arises from the internal octupole (n = 3, m = 2).

3. PARASITIC PITCH-ANGLE DIFFUSION

Following a major disturbance (either natural or artificial) of the magnetospheric environment, one generally observes a temporal decay of enhanced electron intensities toward the levels characteristic of magnetically quiet periods. For kinetic energies $E \geq 100$ keV, the decay is typically exponential, yielding a lifetime τ that depends upon E and L. A compilation of such electron lifetimes, based on observations of the integral flux at $E > 0.5$ MeV, is illustrated in Figure 9. The lifetimes ~ 200 days (filled circles) at the two lowest L values are compatible with the theory of atmospheric scattering (Walt, 1966). However, the decay rates observed beyond $L \approx 1.5$ clearly demand

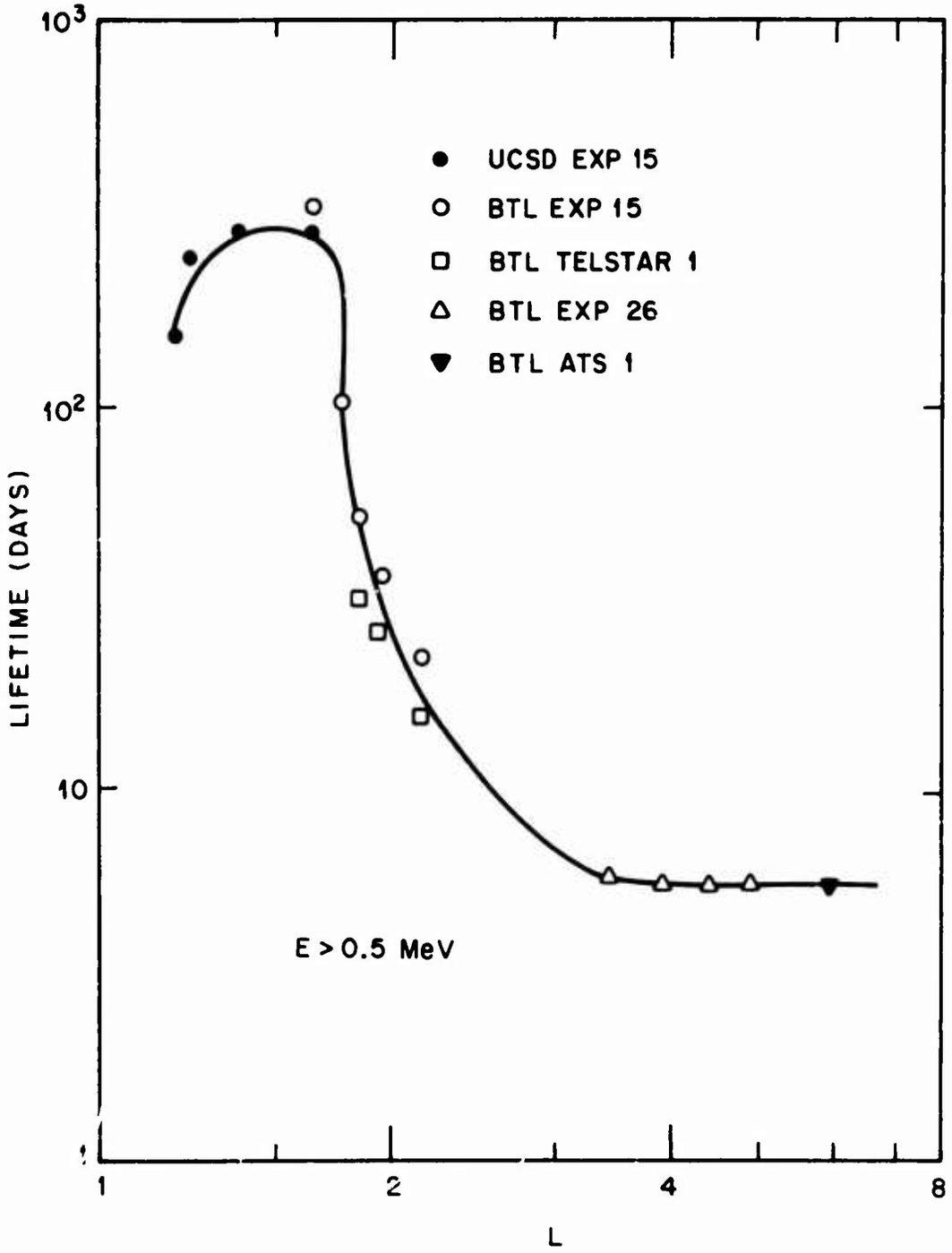

Fig. 9. Observed lifetimes of near-equatorial electron fluxes in the inner and outer zones, as compiled by Roberts (1969).

another explanation. It is by now generally accepted that wave-particle interactions are the responsible scattering agent, and that within the plasmasphere the relevant waves are electromagnetic.

Since the decay of electron intensities at $E \geq 100$ keV is typically exponential, it must be that the waves responsible for the particle scattering are not primarily generated by the particles being scattered. The waves may have arisen from some other source, e.g., a population of lower-energy particles residing elsewhere in the magnetosphere, or they may have arisen in part from earth-based radio sources. A minor fraction of the magnetospheric VLF wave energy can be attributed to "whistlers" created by lightning discharges. Since the particles of interest here thus "feed upon" wave energy not of their own creation, their pitch-angle diffusion is said to be parasitic. No evil connotation is intended.

The empirical consequence of magnetospheric wave-particle interactions is a particle decay rate that increases monotonically with L. This conclusion is reinforced by Figure 10, which is a compilation of post-storm electron lifetimes in three energy channels (Williams et al., 1968). Here the lifetime τ is seen to be a monotonically increasing function of particle energy and (as noted) a monotonically decreasing function of L.

Early efforts to model the interaction between geomagnetically trapped particles and electromagnetic waves generally focused on an

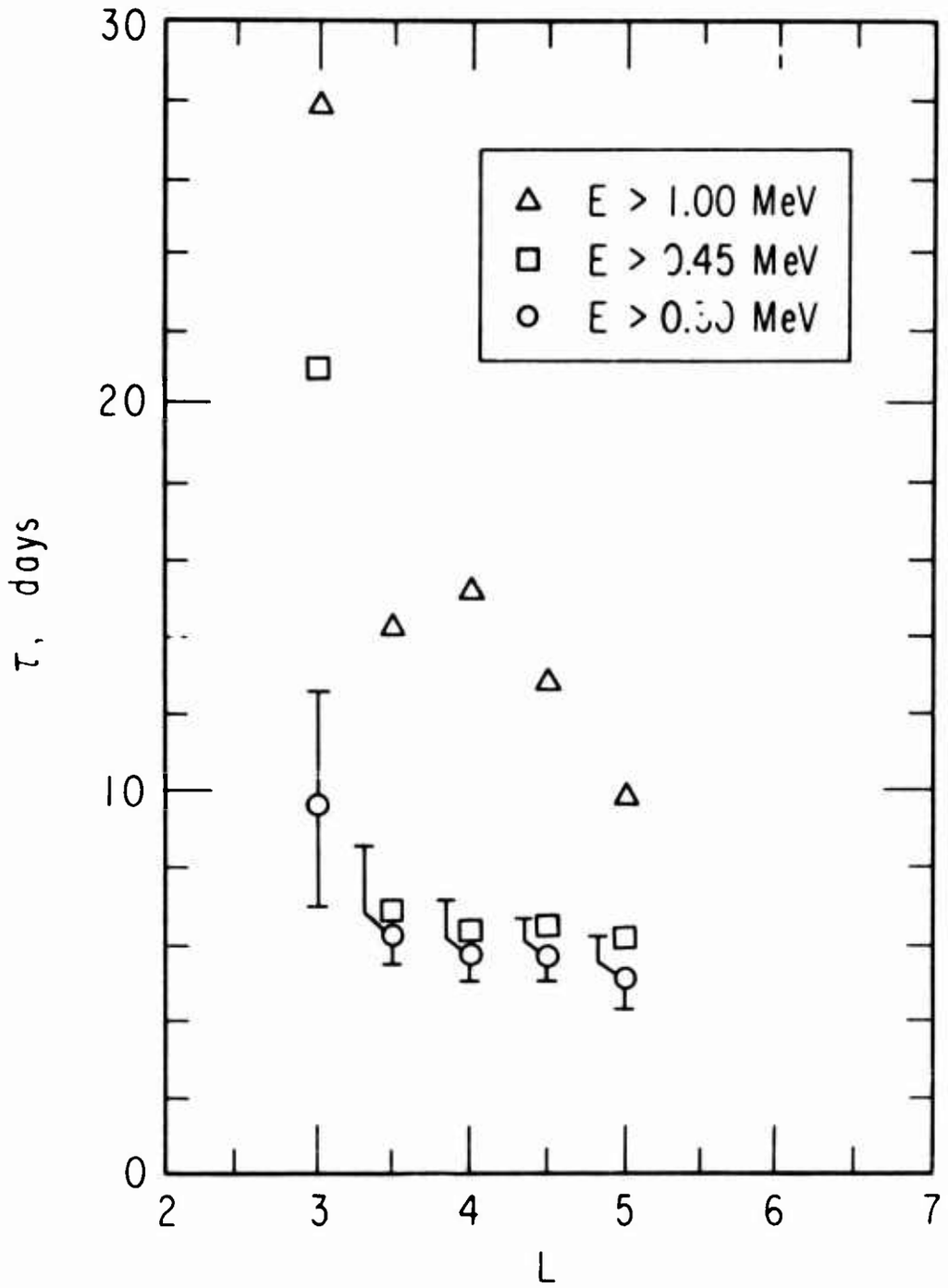

Fig. 10. Lifetimes of near-equatorial unidirectional electron fluxes, as determined from Explorer-26 data (Williams et al., 1968) for the period 22.5 April 1965 to 3.0 May 1965.

equatorial interaction via cyclotron resonance, as specified by the condition

$$\omega - k_{\parallel} v_{\parallel} = \Omega, \tag{8}$$

where $\omega/2\pi$ is the frequency of the wave, $\Omega/2\pi$ is the relativistic gyrofrequency of the particle, and $k_{\parallel} v_{\parallel}$ is the Doppler shift associated with the particle's component of motion along $\underset{\sim}{B}$. The main difficulty with (8) is that particles mirroring too near the equator fail to interact effectively with a reasonable wave spectrum.

The problem of parasitic pitch-angle diffusion has recently been examined in greater generality by Lyons et al. 71, 1972) and by Lyons and Thorne (1972). They considered not only the case of wave propagation ($\underset{\sim}{k}$) parallel to $\underset{\sim}{B}$, as covered by (8), but more generally the case of wave propagation oblique to $\underset{\sim}{B}$. This expanded outlook leads to resonance under conditions for which

$$\omega - k_{\parallel} v_{\parallel} = n\Omega, \tag{9}$$

where n is any integer. The case n = 1 recovers the primary cyclotron resonance in the form of (8), but additional cyclotron resonances (n = 2, 3, 4, . . .) facilitate the interaction of higher-energy electrons with the wave spectrum. Moreover, the Landau resonance (n = 0) enables particles mirroring very near the equator to interact effectively with a reasonable wave spectrum (see Figure 11).

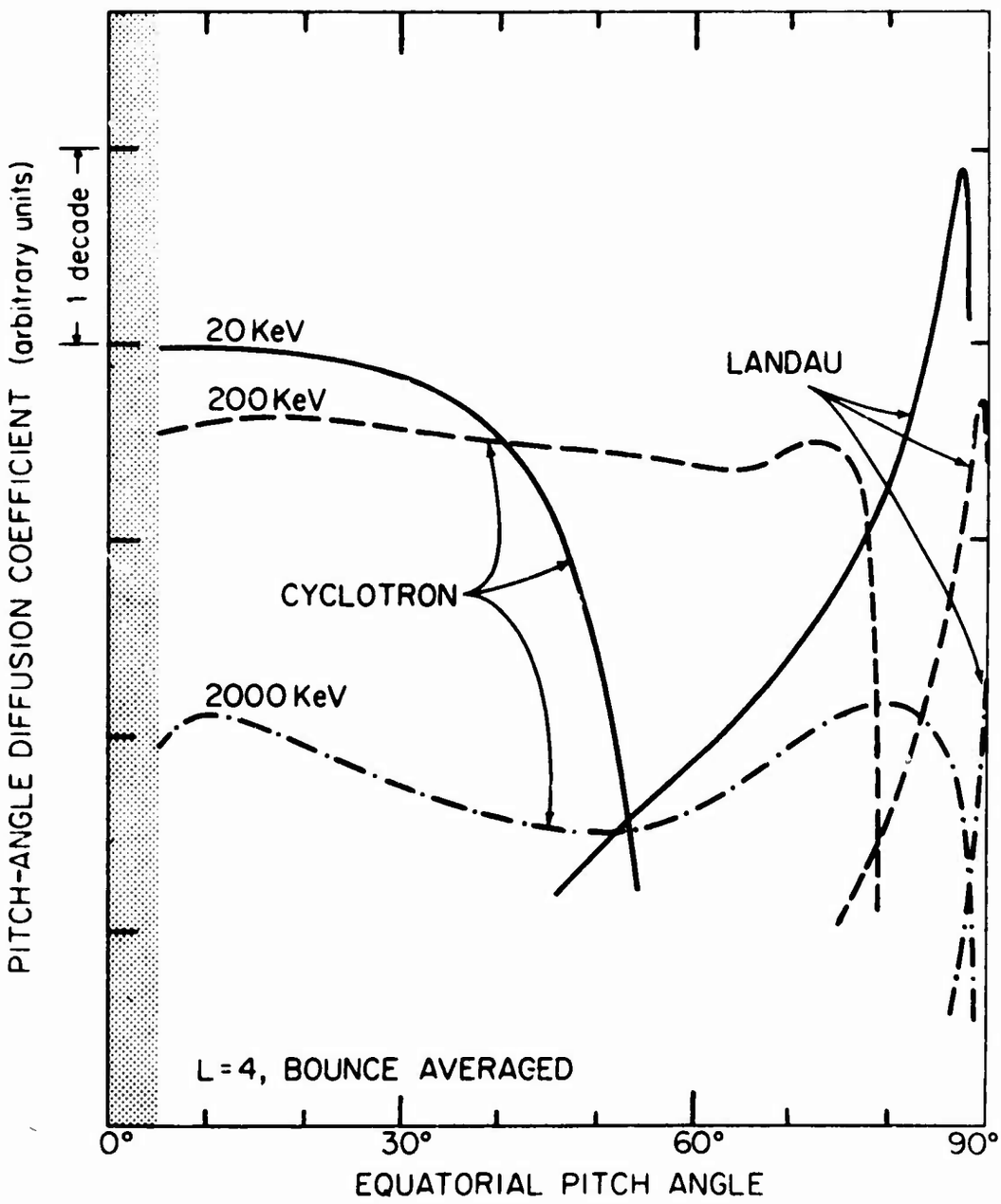

Fig. 11. Bounce-orbit averaged contributions from cyclotron resonance (including harmonics) and Landau resonance to the pitch-angle diffusion coefficient for various electron energies at L = 4, as determined by Lyons et al. (1972).

Recognizing that wave-particle interactions need not be confined to the equatorial plane, Lyons et al. (1972) assumed a uniform distribution of wave energy throughout the plasmasphere and performed a properly weighted bounce average to obtain D_{xx}, i.e., the diffusion coefficient for the cosine of the equatorial pitch angle. They considered a broad Gaussian wave spectrum (half-width = 300 Hz at 1/e) centered at 600 Hz, and imposed a lower cut-off at 300 Hz. The angular distribution of wave vectors was taken as proportional to the function

$$\Theta(\hat{\underset{\sim}{k}}) = \exp\left[0.04 - 0.04\,(\hat{\underset{\sim}{k}} \cdot \hat{\underset{\sim}{B}})^{-2}\right]. \tag{10}$$

Lyons et al. (1972) tentatively neglected the electric-field component of the waves, and so assured that the resulting pitch-angle diffusion would be perfectly elastic. This assumption justified a diffusion equation (for the phase-space distribution function f) of the form

$$\frac{\partial f}{\partial t} = \frac{1}{xT(y)} \frac{\partial}{\partial x} \left[xT(y)\, D_{xx} \frac{\partial f}{\partial x} \right]_{E,L} \tag{11}$$

which Lyons et al. (1972) solved for its longest-lived eigenfunction $g_0(x)$. The Jacobian $xT(y)$ is well approximated by use of the formula

$$T(y) = 1.3802 - 0.3198\,(y + y^{1/2}) \tag{12}$$

given by Lenchek et al. (1961), where $y \equiv (1 - x^2)^{1/2}$. The eigenfunctions $g_n(x)$ are required to be even functions of x and to vanish at the edge of the loss cone (shaded area in Figure 11).

Inserting a root-mean-square wave field of 35 mγ, Lyons et al. (1972) obtained the lifetimes shown in Figure 12. The corresponding eigenfunctions $g_0(x)$ are shown in Figure 13, superimposed with arbitrary normalization on a collection of data provided by H. I. West (personal communication). The "shoulders" of the predicted pitch-angle distribution in Figure 13 correspond to the "bottleneck" in the pitch-angle diffusion coefficient in Figure 11. It is a remarkable triumph of such a simply formulated theory to find that these "shoulders" in the predicted distribution function correspond so closely in pitch angle to similar features in the observational data. (R. W. Fredricks points out, in a personal communication, that the integration of Lyons' pitch-angle distribution over the angular aperture of West's instrument would further improve the quantitative agreement.)

Inclusion of the wavelike electric field in such an analysis is straightforward in principle. The wave-particle interaction in this case becomes slightly inelastic at high energies ($E \gtrsim 100$ keV), and rather strongly inelastic at low energies ($E \lesssim 50$ keV). Formally speaking, the diffusion coefficient becomes a second-rank tensor accommodating stochastic changes in E and x, as well as their correlation. The procedure for evaluating this diffusion tensor has been outlined by Lyons (1974).

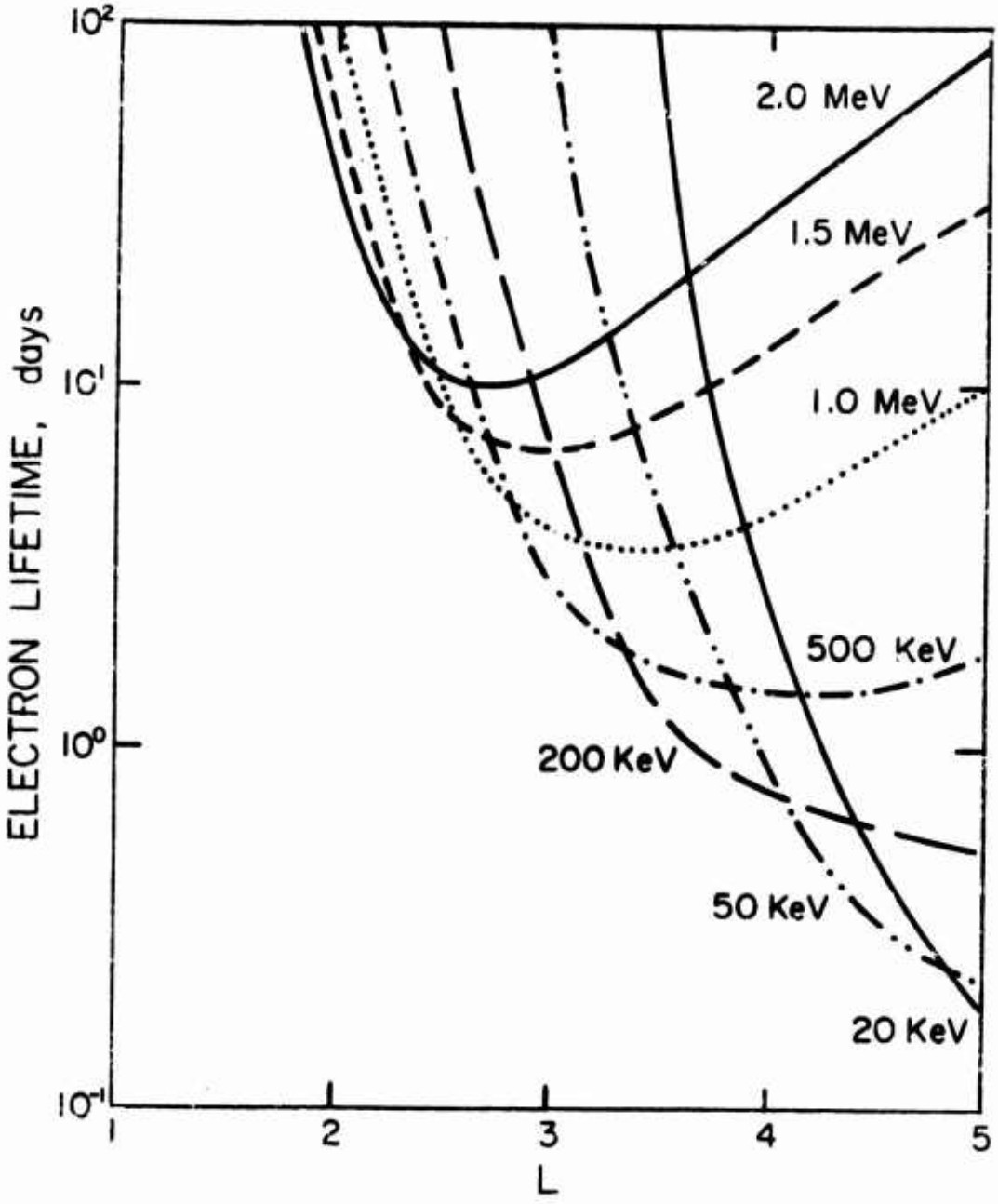

Fig. 12. Theoretical lifetimes of lowest pitch-angle eigenmode, within the plasmasphere, as determined by Lyons et al. (1972).

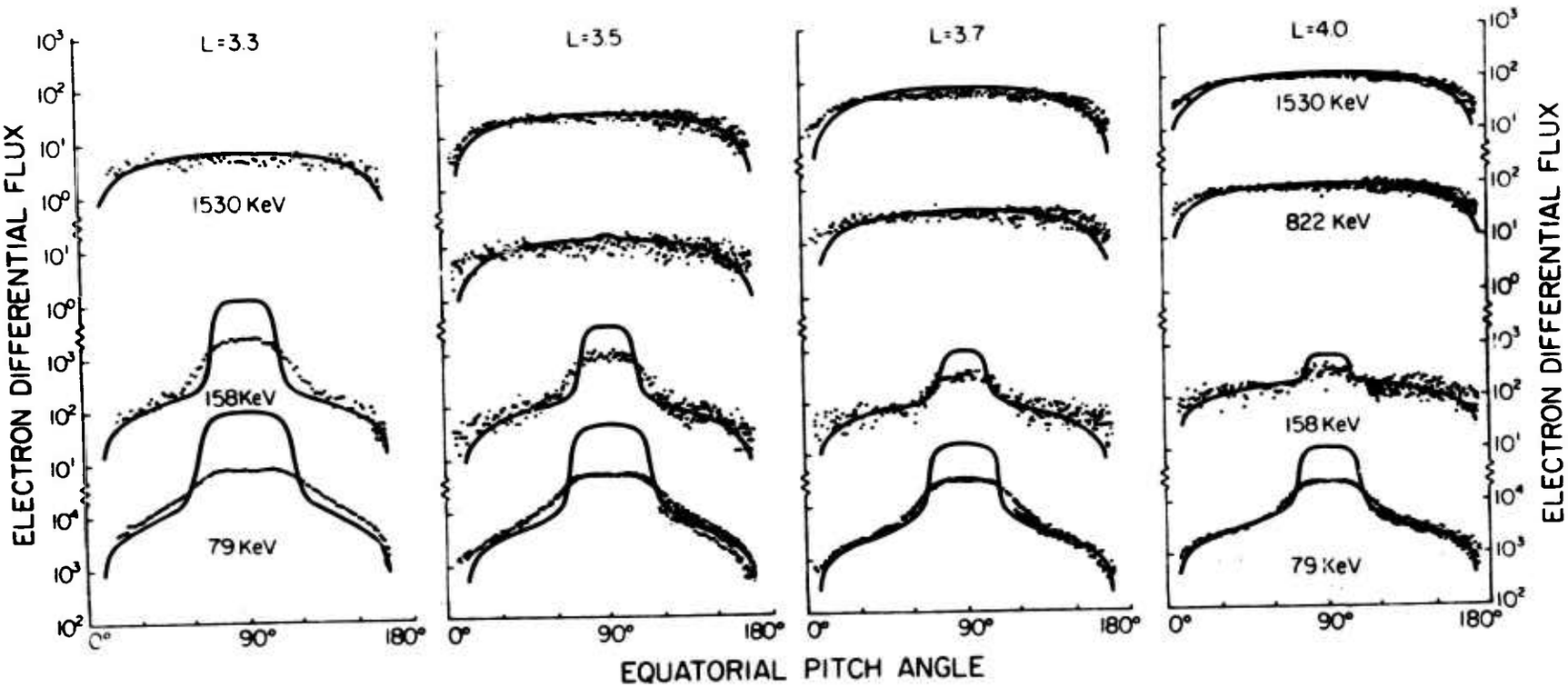

Fig. 13. Comparison of calculated equatorial pitch-angle distributions (lowest eigenmode, arbitrarily normalized) with equatorial electron distributions observed in the slot region during the decay phase following an injection event. Calculations were made by Lyons et al. (1972), observations by H. I. West (personal communication, 1971).

4. FORMATION OF INNER ELECTRON BELT

It is understandably customary to detect radiation-belt particles by means of instruments calibrated with respect to energy and angle of incidence, rather than with respect to the adiabatic invariants. Thus, although the adiabatic invariants would have been the more natural coordinates for describing the distribution of geomagnetically trapped radiation, most available maps of radiation intensity provide flux profiles plotted against L at fixed energy and equatorial pitch angle. Electron-flux profiles obtained in this format, especially during geomagnetically quiet periods, define two seemingly distinct radiation belts separated by a deep "slot". This pattern is illustrated in the left panel of Figure 14. The center of the "slot" is located typically between $L = 2.5$ and $L = 3.5$, depending on the particle energy considered.

The quiet-time "slot" region becomes filled in with particles during a magnetic storm, presumably because of enhanced radial diffusion. The result is illustrated in the right panel of Figure 14. At the lower energies ($E \sim 300$ keV in this example) the replenishment is so complete that the two-zone structure qualitatively disappears. At the higher energies the replenishment serves to shift the apparent "slot" position to L values less than $L = 2$.

During the period of decay following a storm, the electron-flux profiles return to their respective quiet-time configurations, as represented by the left panel of Figure 14, and this pattern remains essentially

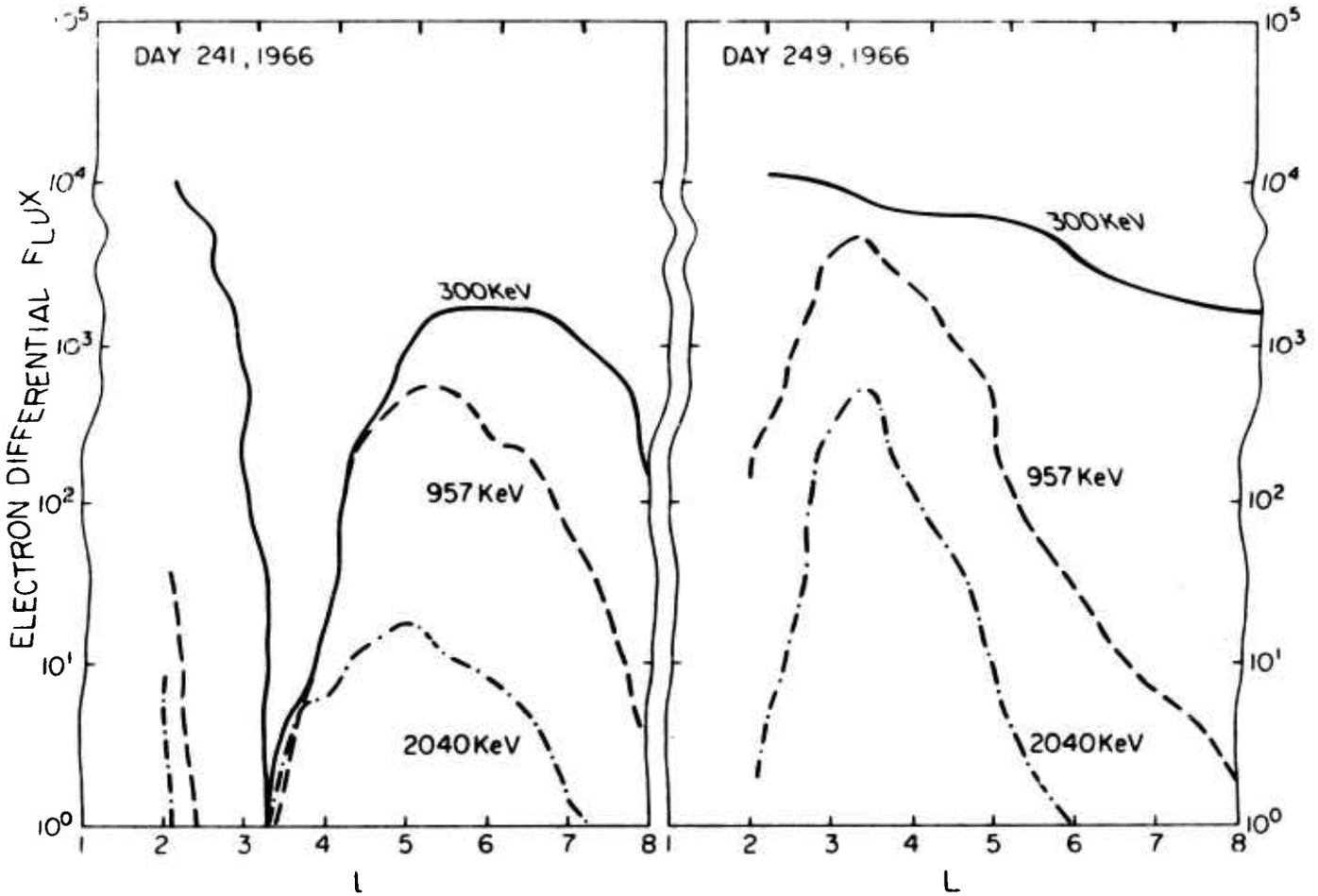

Fig. 14. Local $J_\perp$, $cm^{-2}sec^{-1}ster^{-1}keV^{-1}$, observed along the orbit of OV3-3 before and immediately after the magnetic storm of 4 September (Day 247) 1966. Following Day 249 the slot-region fluxes decayed away, and the two-zone structure (characteristic of quiet times) formed again (from Vampola, 1972; Lyons et al., 1972).

stationary until the next major geomagnetic disturbance. One could imagine that the process (presumably pitch-angle diffusion) responsible for the decay of radiation intensity is extinguished upon restoration of the quiet-time configuration, and that particle motion thereafter remains perfectly adiabatic. This would be wrong. A more reasonable interpretation of radiation-belt dynamics is that the processes responsible for radial diffusion and pitch-angle diffusion during disturbed periods persist (perhaps with modified intensity) during the intervening quiet periods, and that the static flux profiles observed during quiet periods represent a detailed balance between the effects of radial diffusion and pitch-angle diffusion.

Lyons and Thorne (1973) have explored this likely possibility by solving the radial-diffusion equation

$$\frac{\partial f}{\partial t} = L^2 \frac{\partial}{\partial L}\left[\frac{1}{L^2} D_{LL} \frac{\partial f}{\partial L}\right]_{M,K} - \frac{f}{\tau_w} - \frac{f}{\tau_c} = 0 \qquad (13)$$

for the quasi-static phase-space distribution function f, which is equal to $J_\perp/2m_0MB$, where $J_\perp$ denotes the differential electron flux per unit solid angle in a direction perpendicular to $\underset{\sim}{B}$. Lyons and Thorne (1973) included loss terms both for atmospheric Coulomb scattering (τ_c) and for wave-particle interactions (τ_w). They derived the former lifetimes from Walt (1966), and the latter from Figure 12. They considered the radial diffusion to be caused by electrostatic impulses (thereby defining

an M-dependent form for D_{LL}) and solved (13) for f at K = 0. The results, normalized to a common value at L = 5.5, are shown in the left panel of Figure 15. Since f must vanish at $L \approx 1$, it is inevitable in this formulation of the problem that f will emerge as a monotonic function of L at fixed M. Thus, the left panel of Figure 15 contains no hint of a two-zone structure.

Lyons and Thorne (1973) next applied these results for f at fixed M to obtain profiles of $J_\perp$ at fixed kinetic energy E, using an observed energy spectrum at L = 5.5 to normalize the distribution function. The outcome of this transformation is shown in the right panel of Figure 15. The two-zone structure thus arises quite naturally from a monotonic distribution in phase space, a distribution consistent with the radial diffusion of energetic electrons from an external source (beyond L = 5.5) to an atmospheric sink. Moreover, the "slot" between the radiation belts becomes increasingly pronounced with increasing energy, in agreement with the observational data.

The next reasonable step in this area of investigation would be to combine radial diffusion and pitch-angle diffusion explicitly in the same equation. The effective lifetimes τ_c and τ_w used in (13) correspond to a pitch-angle distribution in its lowest eigenmode. However, as Walt (1970) has pointed out, radial diffusion can have the effect of distorting the pitch-angle distribution. When both processes act simultaneously, the radial profile and pitch-angle distribution should

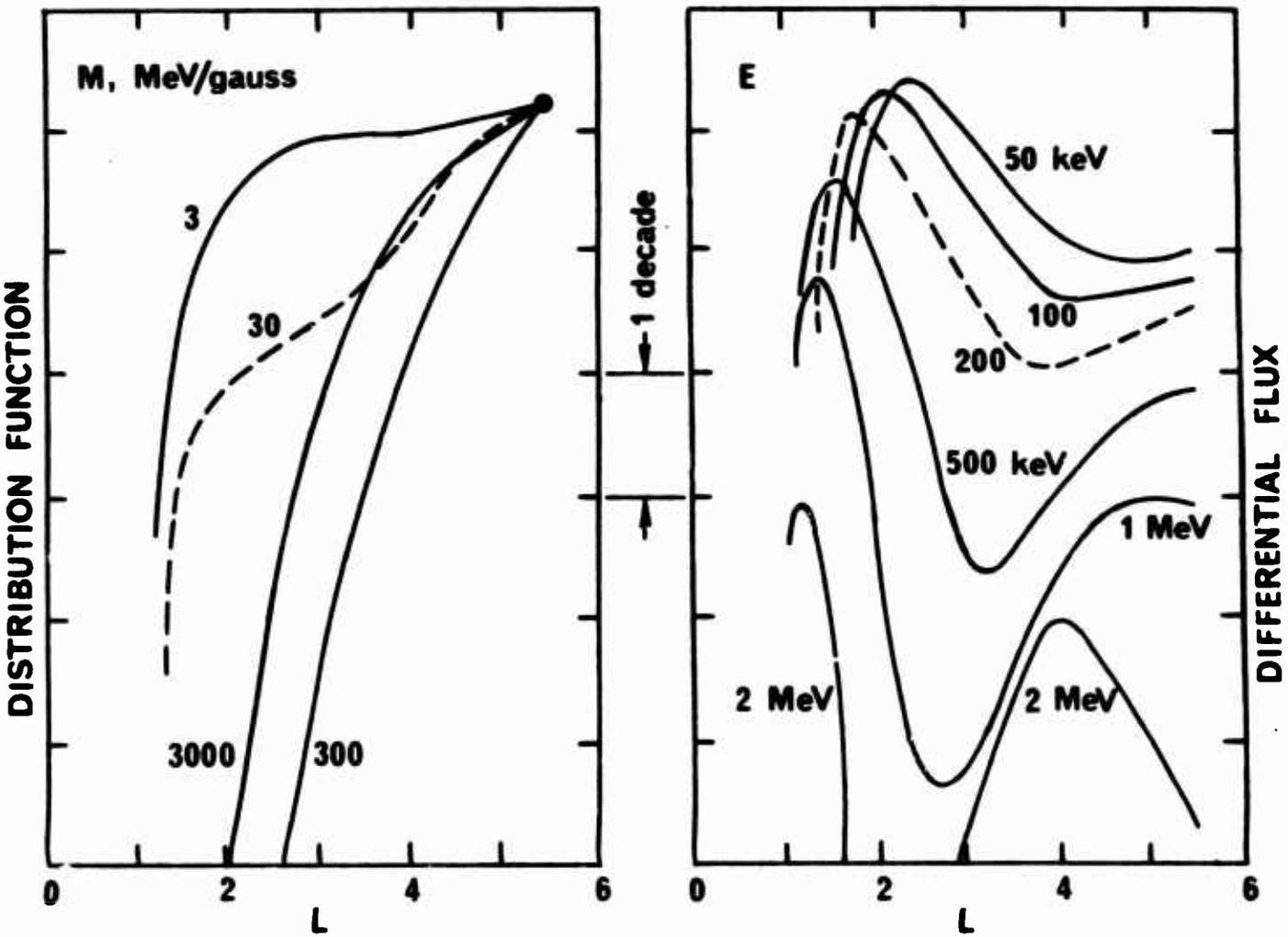

Fig. 15. Predicted steady-state profiles of $J_\perp/MB$ at constant M (left panel) normalized to a common value at $L = 5.5$, and of $J_\perp$ at constant E (right panel) normalized by prescribing the energy spectrum at $L = 5.5$ (from Lyons and Thorne, 1973).

really be determined in a self-consistent manner, by including both radial diffusion and pitch-angle diffusion on an equal footing in the basic equations.

5. ARTIFICIAL RADIATION BELTS

Prior to the international treaty of 1963, both the USA and the USSR had conducted nuclear tests in the atmosphere and in space. The high-altitude detonations (see Table 1) were the source of large numbers of energetic electrons that became trapped in the geomagnetic field, thus forming artificial radiation belts. Some of the spacecraft aloft at the time of the high-altitude detonations suffered severe radiation damage. Others launched immediately following several of the respective detonations, however, served to provide a wealth of data on the dynamics of artificial radiation belts. Moreover, since the dynamical processes affecting artificial radiation belts after their formation are essentially the same processes that affect natural radiation belts, one thus acquired large amounts of data concerning the behavior of radiation belts in general. Interpretation of these data continues, even at the present time.

Several of the artificial detonations provided the observer with particularly interesting distributions of geomagnetically trapped radiation. For example, the Soviet detonation of 28 October 1962 yielded an anomalous pitch-angle distribution, i.e., an off-equatorial maximum

Table 1. *Data on high-altitude nuclear detonations (as compiled by Van Allen, 1966; Hess, 1968; Walt, 1971)*

Name of Event	Date of Event	Universal Time	Total Yield	Latitude	Longitude	Altitude	Value of L^*	Lifetime τ, days
Teak	1 Aug 58	1050:05	~1 MT	17°N	169°W	77 km	1.12	"few"
Orange	12 Aug 58	1030:08	~1 MT	17°N	169°W	43 km	1.12	~1
Argus 1	27 Aug 58	0230:00	1-2 kT	38°S	12°W	~200	1.7	~20
Argus 2	30 Aug 58	0320:00	1-2 kT	50°S	8°W	~250	2.1	~20
Argus 3	6 Sept 58	2210:00	1-2 kT	50°S	10°W	~500	2.0	~30
Starfish	9 July 62	0900:	1.4 MT	17°N	170°W	~400	1.12	~600
USSR 1	22 Oct 62	0340:46	≪ 1 MT				1.8	~30
USSR 2	28 Oct 62	0441:18	< 1 MT				1.8	~30
USSR 3	1 Nov 62	0913:	~ 1 MT				1.75	~30

in the radiation intensity at $L \approx 1.9$ (Roberts, 1969). The detonation of 1 November 1962 yielded a radiation belt confined to an especially narrow interval in L (see Figure 16). These two space experiments thus led naturally to analytical studies of pitch-angle diffusion and radial diffusion, respectively.

Roberts (1969) fitted the anomalous pitch-angle distribution following the 28 October event to a superposition of the three lowest eigenfunctions of (11), making the convenient approximation that $T(y) \approx T(1)$ outside the loss cone. He thus accounted for the disappearance of the off-equatorial maximum in radiation intensity on a shorter time scale than the decay of this artificial belt as a whole.

Brown (1966) fitted the narrow radial profile following the 1 November event to a temporally expanding Gaussian. He found the squared full width at half maximum (FWHM) to increase by about 7×10^{-5} units of L^2 per day. Schulz and Lanzerotti (1974) translated this result into an equivalent radial-diffusion coefficient $D_{LL} \sim 6 \times 10^{-6}$ day^{-1} at fixed energy. Newkirk and Walt (1968a) had earlier performed a more sophisticated analysis, transforming the observed profile into an equivalent distribution function at fixed M and K (= 0) by assuming an equilibrium fission spectrum (see below) for the initial profile. They similarly obtained $D_{LL} \sim 6 \times 10^{-6}$ day^{-1}, but their method of analysis was superior since it properly conserved M and K under radial diffusion. In neither analysis could radial diffusion account for more than about one-third of

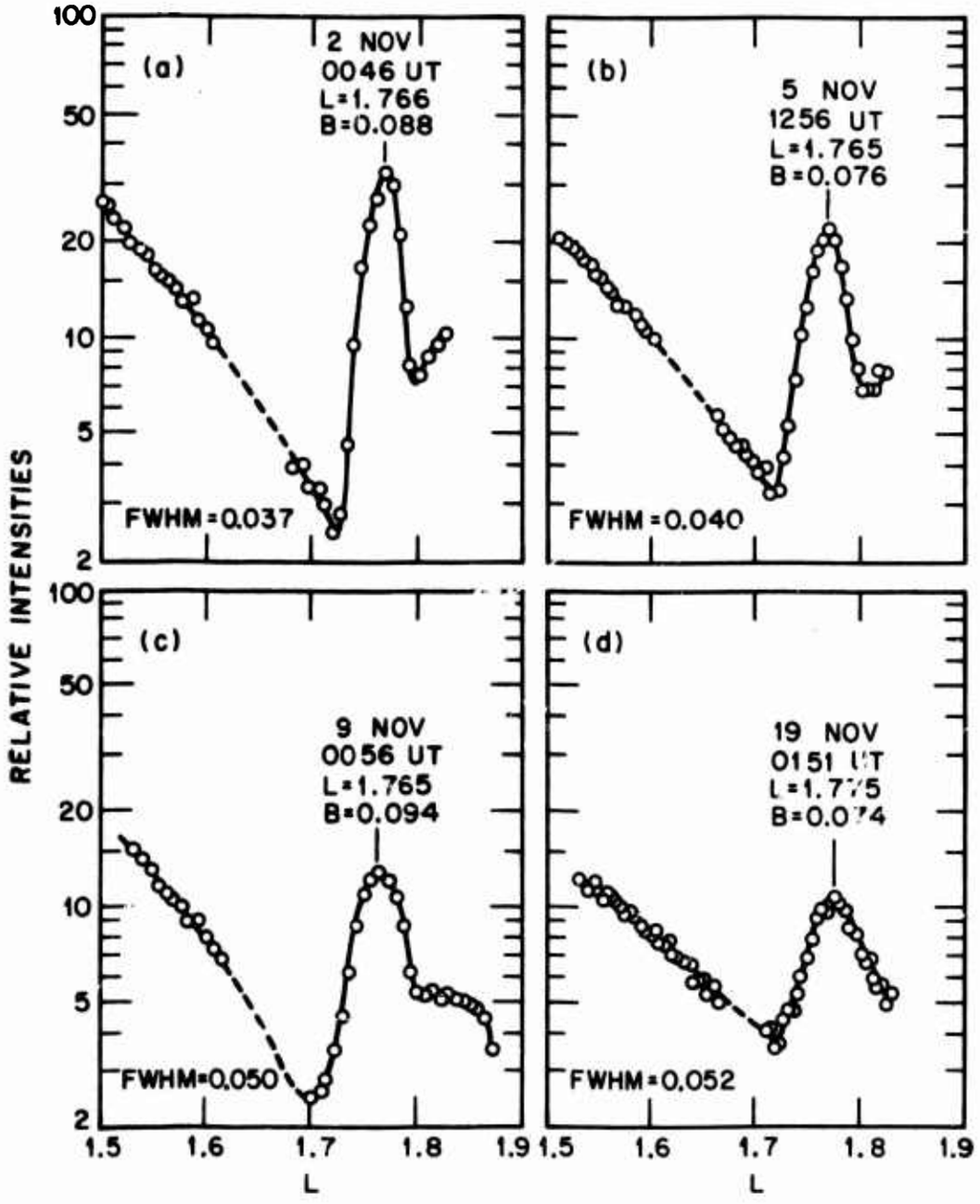

Fig. 16. Evolution of inner-zone electron-flux profile (E > 1.9 MeV, omnidirectional) observed on Explorer 15 following high-altitude nuclear explosion of 1 November 1962 (Brown, 1966).

the observed decline in maximum electron intensity (the peak at L = 1.765). For this, one must postulate pitch-angle diffusion with a characteristic lifetime of 15-20 days, as in (13).

The mechanism for creating an artificial radiation belt has been described by Davidson and Hendrick (1971). The high-altitude nuclear detonation first creates a partially ionized plasma that expands hydrodynamically until the plasma pressure (P) only balances the magnetic pressure ($B^2/8\pi$). Plasma expansion along $\underset{\sim}{B}$ is unimpeded, except perhaps by gravity (since the plasma ions are heavy, being fission products). Plasma expansion across $\underset{\sim}{B}$ is presumably mediated by turbulent diffusion until $\beta (\equiv 8\pi P/B^2)$ decreases to about unity. The plasma ions and electrons thereafter expand along $\underset{\sim}{B}$, and the neutral fission products expand irrespective of $\underset{\sim}{B}$. The fission-product nuclei are undergoing beta decay all the while, and some of the resulting (beta) electrons are emitted with velocity vectors compatible with trapping by the geomagnetic field. Although injected over a relatively narrow range of longitudes, these are the electrons that ultimately constitute the artificial radiation belt. The belt forms by drift-phase mixing (dispersion in φ_3), since the constituent electrons differ somewhat from each other in energy, equatorial pitch angle, and L value (and therefore in drift frequency $\Omega_3/2\pi$). The artificial radiation belt thereafter becomes subject to the natural processes leading to radial diffusion and pitch-angle diffusion, and so the deterministic history of each individual particle becomes obscured.

The solid curves in Figure 17 (based on Crowther and Harless, 1971) represent the prediction of such a model for a nuclear detonation, having a fission yield of one megaton ($= 4.186 \times 10^{22}$ erg), at altitude 200 km on the field line $L = L^*$. The ordinate here is a damage-equivalent flux of 1-MeV electrons, but can be considered for present purposes as an integral flux of the fission electrons. The form of the spectrum, following Carter et al. (1959), should be well approximated by the function

$$J_{4\pi}(E) \propto (v/c) \exp \left[- 0.2938 (\gamma - 1) - 0.0144 (\gamma - 1)^2 \right], \qquad (14)$$

where v is the particle speed, c is the speed of light, and γ is the ratio of relativistic mass (m) to rest mass (m_0). As a rough scaling law to fission yields Y other than one megaton, the belt width (in L) should be proportional to $Y^{1/3}$, and the peak radiation intensity should be proportional to $Y^{2/3}$.

The dashed line in Figure 17 represents a flux $I_{4\pi}^* \sim 7 \times 10^{10} L^{-4}$ $cm^{-2} sec^{-1}$. This is the maximum stable intensity obtained from the theory of Kennel and Petschek (1966) for a pitch-angle distribution having normal anisotropy. A larger flux of electrons ($I_{4\pi} > I_{4\pi}^*$) would lead to the spontaneous generation of electromagnetic noise in the whistler mode, and the resulting pitch-angle diffusion would quickly reduce the particle intensity to $I_{4\pi}^*$. The stable-trapping limit of Kennel and Petschek (1966) stands far below the condition $\beta = 1$ (solid line), under which the particle energy density equals $B^2/8\pi$. Thus, an artificial radiation belt cannot

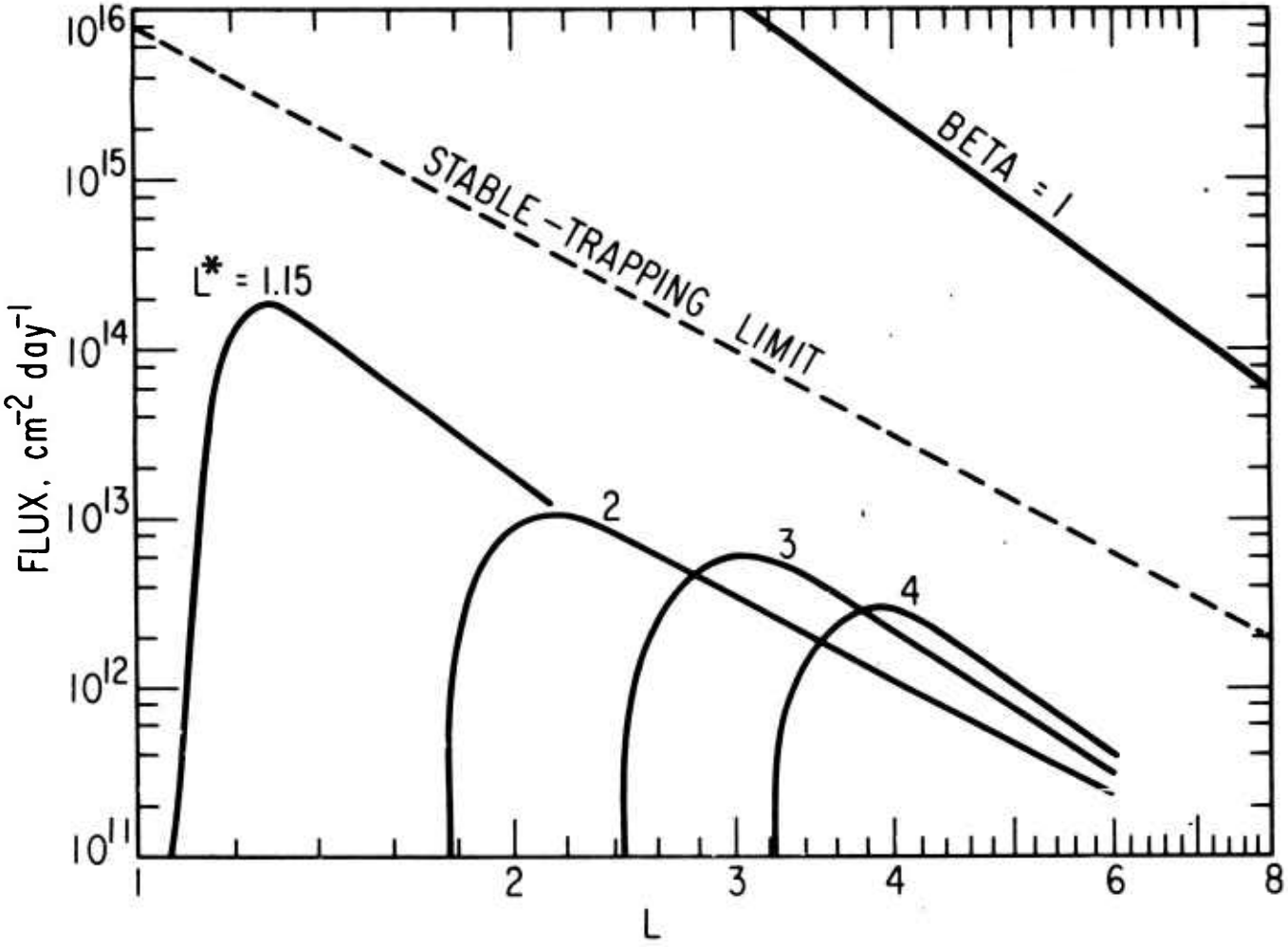

Fig. 17. Profiles of equatorial omnidirectional electron flux (solid curves) expected to result from nuclear detonation (one-megaton fission yield) at 200-km altitude on the field line L = L^* (from Crowther and Harless, 1971). Dashed line and solid line correspond to saturation levels characteristic of microscopic and macroscopic plasma instabilities, respectively.

significantly distort the geomagnetic field. Moreover, the stable-trapping limit exceeds the peak radiation intensity for a one-megaton belt by a factor ≤ 40 at all values of L^*. Thus, one would expect the Kennel-Petschek limit to operate initially in the case of a single one-megaton detonation if injection were confined to a longitude interval $\leq 10^{\circ}$ in width. The spectrum of fission electrons, however, differs considerably from the spectrum used by Kennel and Petschek (1966) in calculating the limiting value $\sim 7 \times 10^{10} L^{-4} cm^{-2} sec^{-1}$ on the integral omnidirectional flux $I_{4\pi}^*$. A calculation of $I_{4\pi}^*$ based on (14) would thus be very much in order, before firm conclusions can be drawn concerning the relevance of the Kennel-Petschek mechanism to artificial radiation belts.

The "Teak" and "Orange" events of August 1958 surprised many observers by injecting many energetic electrons onto quasi-adiabatic trajectories. The site conjugate to detonation lay deep in the dense atmosphere (in the South Pacific region), and one might thus have expected all but a few of the fission electrons to be in the loss cone. Davidson (1973) has recently proposed another interesting plasma instability to account for the discrepancy. He notes that the fission-beta electrons from the nuclear debris formed a particle beam (through the ambient plasma) directed toward the southern hemisphere. The beam-plasma interaction should have generated electromagnetic cyclotron waves, according to Davidson (1973), and the resulting pitch-angle diffusion should have enabled a large fraction of the fission-beta electrons to

escape from the loss cone (onto quasi-adiabatic trajectories) before reaching their southern mirror points. Productive research thus continues on the topic of artificial radiation belts, many years after the last such belt ceased to exist (circa 1966).

6. EMPIRICAL STUDIES OF PARTICLE DIFFUSION

The purpose of analyzing radiation-belt observations is to summarize the behavior of the particle distributions concisely within the framework of known physical laws. This normally means to specify the numerical values of the transport (Fokker-Planck) coefficients to which the particles have been subjected. One can, of course, adopt a "brute-force" approach and insert all conceivable combinations of D_{LL}, D_{xx}, etc., into a numerical program that theoretically predicts the evolution of the distribution function $f(M, J, \Phi; t)$. From the output one can select the prediction that best agrees with the data, and thereby identify the optimal set of transport coefficients, i.e., the set used in generating the best-fitting prediction.

Reviewed here are approaches that seem somewhat more imaginative, in that the optimum trial values for D_{LL} and/or D_{xx} are extracted from the observational data directly. One such approach, the variational method, entails a linear least-squares determination of that D_{LL} which makes D_{xx} (a function of L) deviate minimally from a

constant in time. Another, the spatial-quadrature method, treats (13) as a first-order differential equation for D_{LL}. In both methods, the spatial and temporal derivatives of f are treated as given by the observational data.

Having obtained trial values of D_{LL} and/or D_{xx} by such empirical methods, one would be prudent to test those values in the usual way, by inserting the trial transport coefficients into the diffusion equation and seeking to predict the observed temporal evolution or stationary form of f. However, the trial-and-error aspects of the more traditional approach are thus averted.

The data shown in Figure 18 were extracted from satellite observations of integral fluxes in two energy channels ($E > 0.5$ MeV and $E > 1.9$ MeV) by assuming a power-law energy spectrum (Lanzerotti et al., 1970). A major magnetic storm began on 17 December 1962. This led to a redistribution of J_1/MB which continued for about three weeks, until the quiet pre-storm configuration was approximately restored. The redistribution was presumably accomplished by a superposition of radial diffusion and pitch-angle diffusion, as described by the coefficients D_{LL} and D_{xx}, respectively. The magnitude of D_{LL} (and perhaps also of D_{xx}) was presumably enhanced during the disturbed period (e.g., 17-21 December).

Lanzerotti et al. (1970) employed a variational method to extract D_{LL} and D_{xx} from the full set of data described above. They assumed

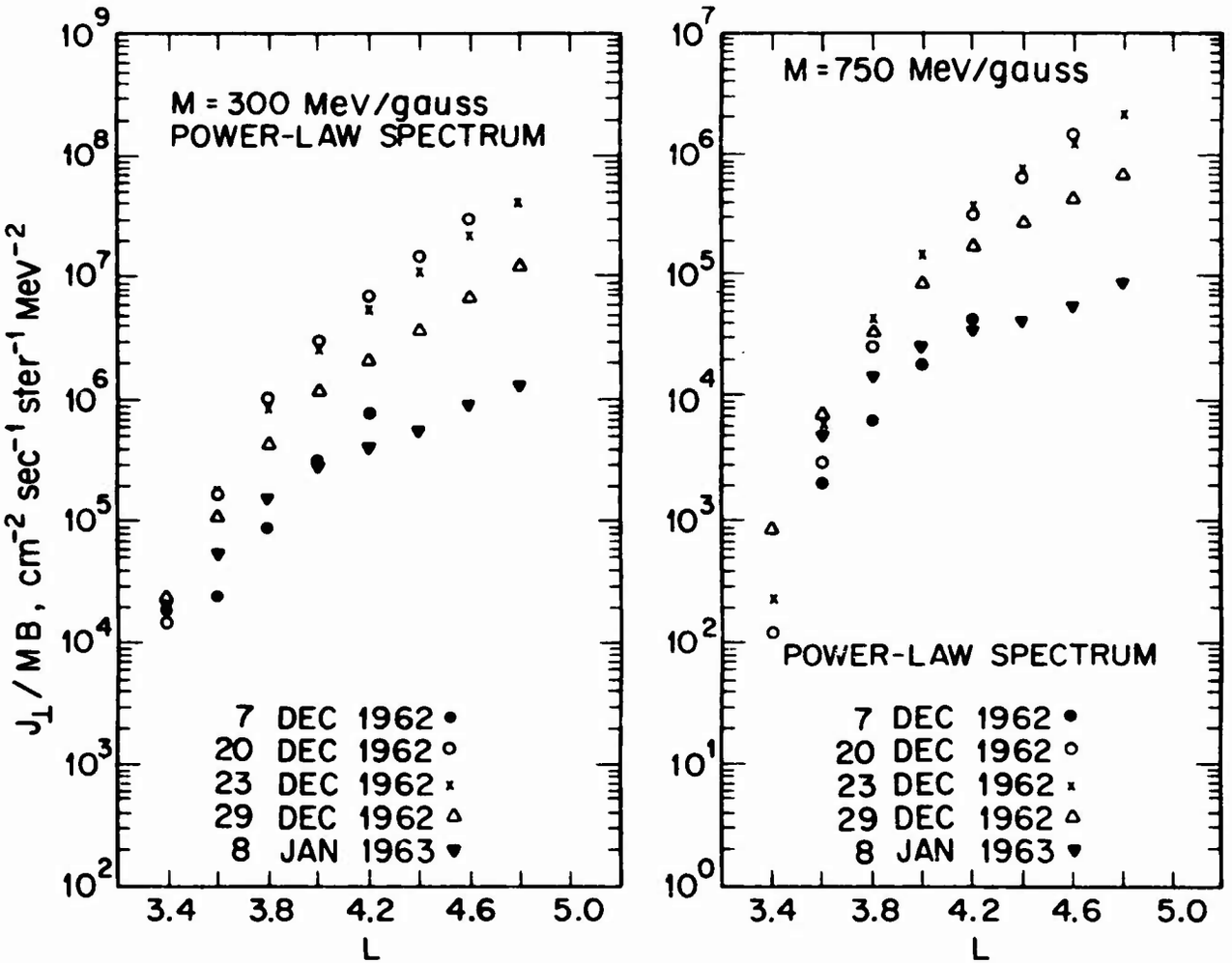

Fig. 18. Electron distribution functions ($\times 2m_0$) at J = 0, as deduced by Lanzerotti et al. (1970) from daily-median intensities of equatorially mirroring electrons observed in two energy channels (E > 0.5 MeV and E > 1.9 MeV) on Explorer 15 before and after the magnetic storm of 17 December 1962.

$D_{LL} = D_n L^n$ for each value of M, with D_n independent of L and time. Defining $F \equiv \ln f$ and

$$\lambda_n(L,t) \equiv D_n L^n \left[\left(\frac{n-2}{L}\right) \frac{\partial F}{\partial L} + \frac{\partial^2 F}{\partial L^2} + \left(\frac{\partial F}{\partial L}\right)^2 \right] - \frac{\partial F}{\partial t}, \quad (15)$$

they proceeded (by a straightforward algebraic operation) to minimize the function

$$G_n(D_n) \equiv \int_{L_1}^{L_2} g(L) \int_{t_1}^{t_2} [\lambda_n^2 - \langle \lambda_n \rangle^2] \, dt \, dL, \quad (16)$$

where g(L) denotes an assigned weighting function and $\langle \lambda_n \rangle$ denotes the temporal mean value of $\lambda_n(L,t)$ at fixed L. The limits of integration were chosen as follows: $L_1 = 3.4$, $L_2 = 4.8$, t_1 = 22 December 1962 and t_2 = 10 January 1963. The derivatives appearing in (15) were evaluated numerically (using symmetric first differences) from the daily-median particle data.

By requiring $dG_n/dD_n = 0$, Lanzerotti et al. (1970) obtained $D_n \approx 6 \times 10^{-10} \times 4^{10-n}$ day^{-1} for each value of M considered. The corresponding lifetimes $\tau \equiv \langle \lambda_n \rangle^{-1}$ are shown in Figure 19. The most reasonable (theoretical) choice for n is n = 10, which would imply $D_{LL} \approx 6 \times 10^{-10} L^{10}$ day^{-1}. The decay rates $1/\tau$ correspond to pitch-angle diffusion. The variation of τ with L at fixed M corresponds in part to the variation of energy with L at fixed M (cf. Figure 10, in

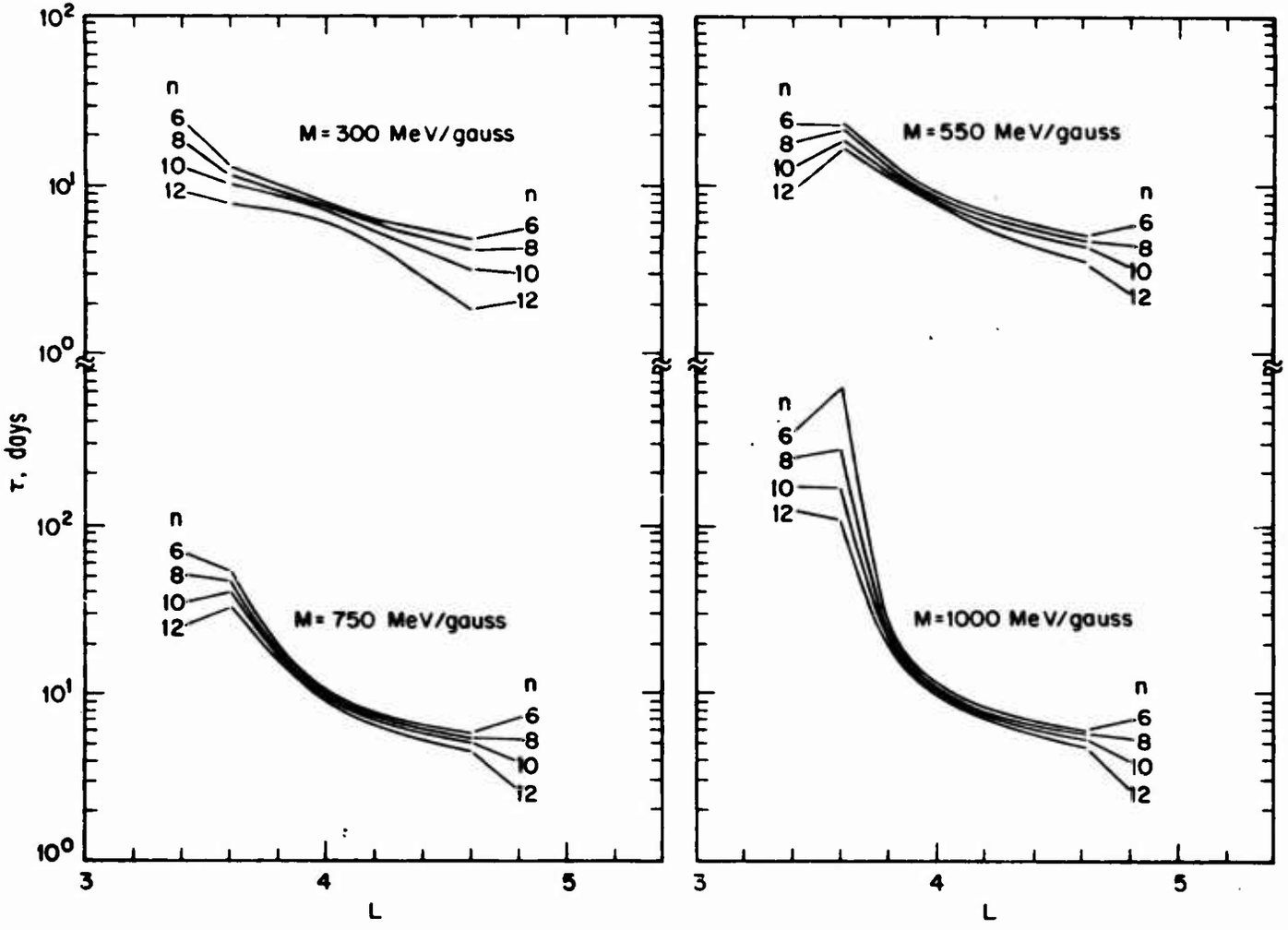

Fig. 19. Optimal electron lifetimes obtained by Lanzerotti et al. (1970) from variational analysis of post-storm data (22 December 1962 to 10 January 1963) on outer-zone electron fluxes.

which τ is an increasing function of E, as well as a decreasing function of L).

The functions D_{LL} and $\tau(L)$ thus obtained were tested by Lanzerotti et al. (1971), who integrated (13) to obtain f as a function of time at each of six L values. The initial configuration was established by the particle data at $t = t_1$ (22 December 1962), and the time-dependent boundary conditions (at $L = 3.4$ and $L = 4.8$) were similarly determined from the observational data at those L values. The predicted evolution of $f(L,t)$ between $L = 3.4$ and $L = 4.8$ was given by a numerical integration of (13). The results, shown in Figure 20 (left panel), serve to vindicate the values of D_{LL} and $\tau(L)$ obtained for this time interval by means of the variational method. The dashed curves represent the prediction; the data points (connected by solid line segments) represent the observation. A different set of transport coefficients, as proposed by Newkirk and Walt (1968b), is similarly tested in the right panel of Figure 20. The larger value of D_{LL} ($= 5 \times 10^{-9} L^{10}$ day^{-1}) is plainly excessive for this time interval, viewed as a whole.

If, however, one considers the time interval 20-31 December 1962, the larger value of D_{LL} (i.e., $5 \times 10^{-9} L^{10}$ day^{-1}) turns out to be preferable. This was the interval originally selected for analysis by Newkirk and Walt (1968b). The comparisons between prediction and observation are shown in Figure 21, in which 20 December is used as the starting point (vs. 22 December in Figure 20) for numerical integration.

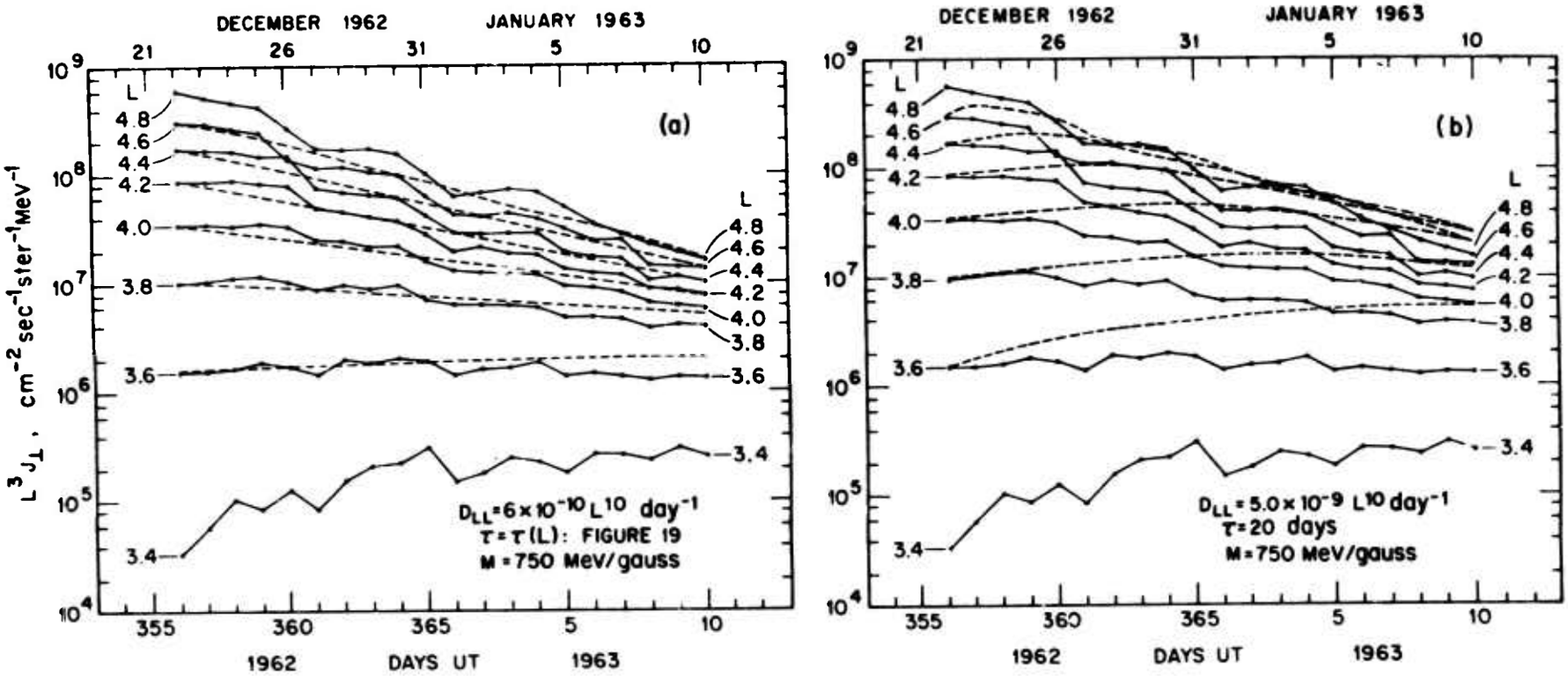

Fig. 20. Evolution of $L^3J_\perp$ for outer-zone electrons, beginning with 22 December 1962. Observational data points (joined by solid line segments) are as given by Lanzerotti et al. (1970). Dashed curves are predictions generated by numerical integration with time-dependent boundary conditions imposed by the data at L = 3.4 and L = 4.8 (Lanzerotti et al., 1971).

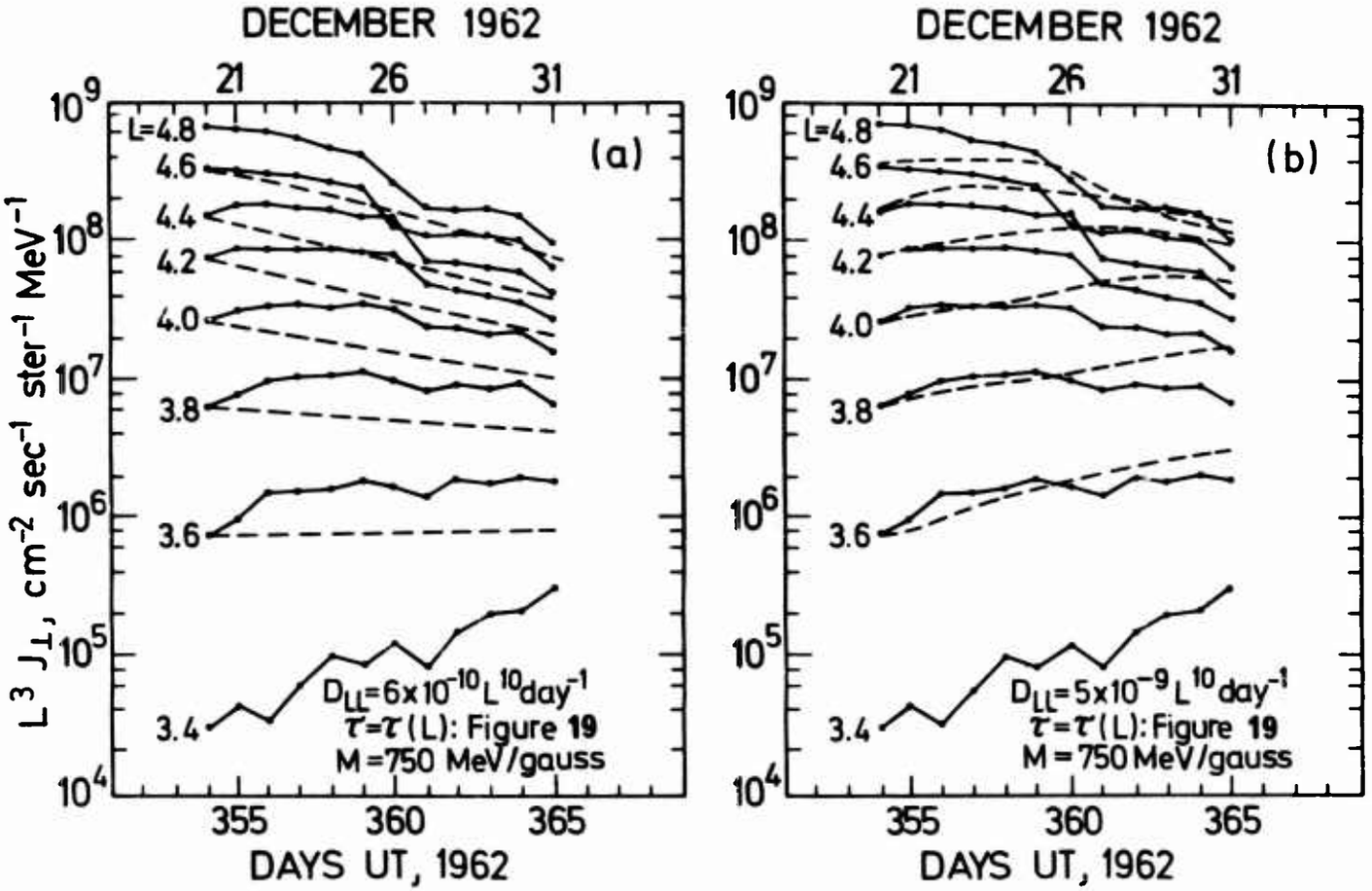

Fig. 21. Evolution of $L^3 J_\perp$ for outer-zone electrons, beginning with 20 December 1962. Observational data points (joined by solid line segments) are as given by Lanzerotti et al. (1970). Dashed curves are predictions generated by numerical integration with time-dependent boundary conditions imposed by the data at L = 3.4 and L = 4.8 (Schulz and Lanzerotti, 1974; based on personal communication from C. G. Maclennan, 1972).

Figures 20 and 21 thus suggest a temporally decreasing magnitude for D_{LL} (perhaps $5 \times 10^{-9} L^{10}$ day^{-1} through 25 December 1962, and $6 \times 10^{-10} L^{10}$ day^{-1} thereafter). This should not be surprising, since geomagnetic conditions (e.g., as measured by the index K_p) were undoubtedly more disturbed during the period 17-25 December 1962 than during the subsequent period between storms. It is noteworthy in this context that, according to Mozer (1971), the spectrum of electrostatic impulses at balloon altitudes is proportional to exp (0.4 K_p). If electrostatic impulses detected at balloon altitudes are indeed of magnetospheric origin, they would thus lead to a radial-diffusion coefficient $D_{LL}^{(e)}$ that is also proportional to exp (0.4 K_p). Lanzerotti and Morgan (1974) have made a similar analysis of magnetic-disturbance spectra observed on the ground, and have concluded (within the framework of the three-term Mead field model) that magnetic impulses produce a radial-diffusion coefficient $D_{LL}^{(m)} \sim 10^{-11}$ exp (2.3 K_p) L^{10} day^{-1} for particles mirroring at the equator. Results compiled by Williams et al. (1968) suggest that D_{xx} varies much more weakly than D_{LL} with K_p, and that any such variation of D_{xx} is confined to the "slot" region ($2.5 \leq L \leq 3.5$).

In a totally separate empirical analysis, based on the method of spatial quadrature, Farley (1969) extracted a radial-diffusion coefficient $D_{LL} \sim 6 \times 10^{-7} (1.2/L)^{85 \pm 15}$ day^{-1} from compilations of data (Paulikas et al., 1967; Imhof et al., 1967) on inner-zone electrons. The apparent decay rate ($-\partial F/\partial t$) during the three years following Starfish (see Table 1,

above) was considerably smaller at $L \leq 1.2$ than one would have predicted from the known effects of Coulomb collisions. The discrepancy is illustrated in Figure 22 (right panel). Some process must have partially counteracted the effects of Coulomb collisions. Using the intensity profile shown in Figure 22 (left panel), Farley (1969) properly neglected wave-particle interactions (i.e., set $\tau_w = \infty$) and integrated (13) for D_{LL}. Since (13) is a first-order differential equation for D_{LL}, there is one arbitrary constant (taken by Farley to be the value of D_{LL} at $L = 1.15$). The results, for various choices of the arbitrary constant, are shown in Figure 23 (smooth curves).

The most acceptable curve in Figure 23 is the one that corresponds to $D_{LL} = 3 \times 10^{-5}$ day^{-1} at $L = 1.15$; this curve is roughly approximated by the formula $D_{LL} \approx 6 \times 10^{-7} (1.2/L)^{92}$ day^{-1}. The strongly inverse variation of D_{LL} with L had been anticipated by Newkirk and Walt (1968a), whose earlier analysis of the same data (by a less reliable method) had yielded the "staircase" function shown in Figure 23. It is difficult to imagine any physical process except atmospheric scattering that would vary so strongly with L. This consideration led Roederer et al. (1973) to propose shell splitting by internal geomagnetic multipoles (cf. Figure 8) as the agent responsible for translating atmospheric pitch-angle diffusion into radial diffusion at very low L values. The implications of this suggestion remain to be worked out in quantitative detail. Moreover, the testing of this hypothesis will require the curves in

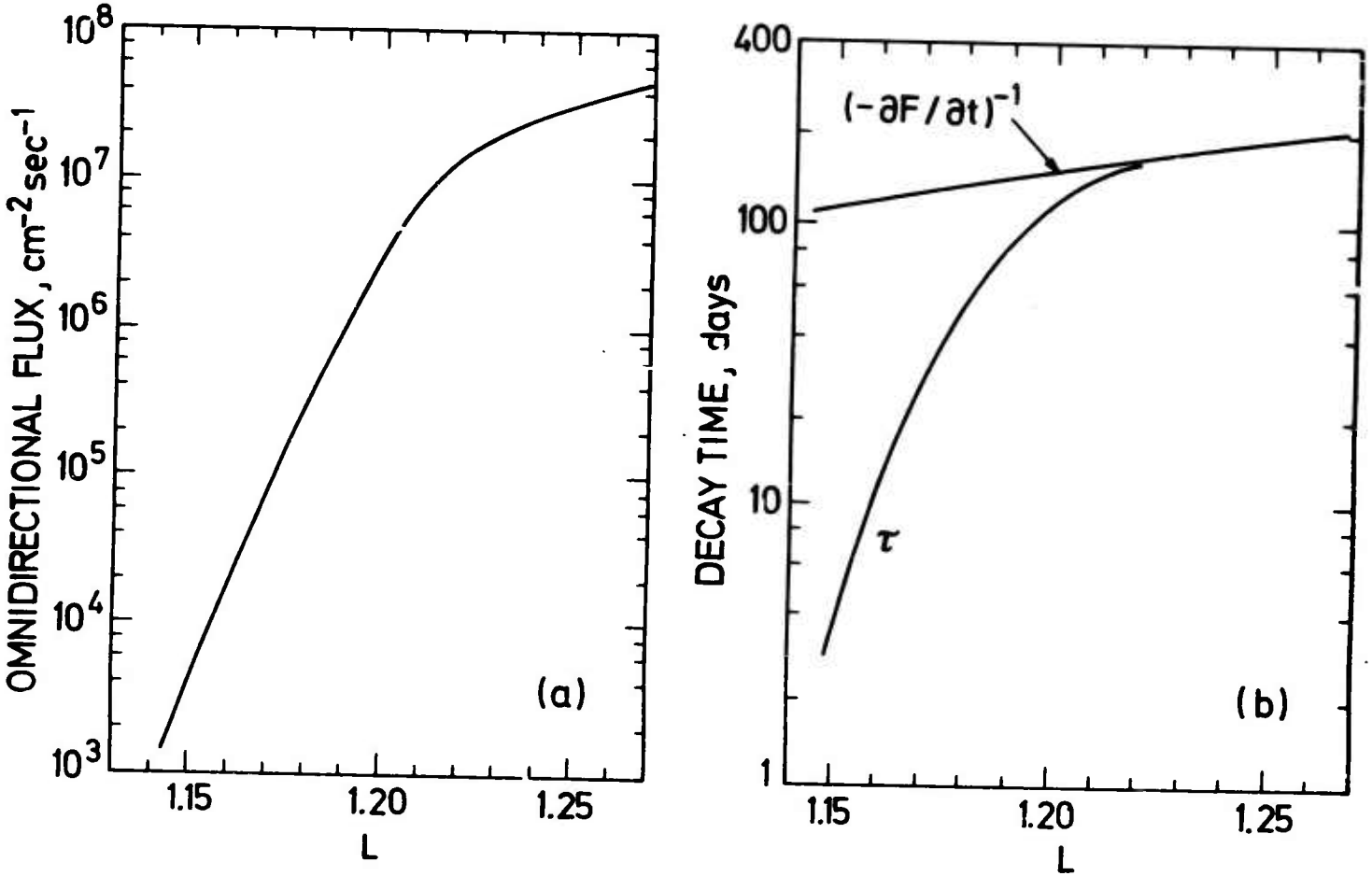

Fig. 22. (a) Inner-zone equatorial electron-flux profile for E > 1.6 MeV observed (Paulikas et al., 1967) on spacecraft 1964-45A during December 1964; (b) decay times τ and $(-\partial F/\partial t)^{-1}$ derived from atmospheric-scattering theory (Walt, 1966) and from a three year compilation (Imhof et al., 1967) of inner-zone electron data (1962-65; E > 0.5 MeV), respectively (Newkirk and Walt, 1968a).

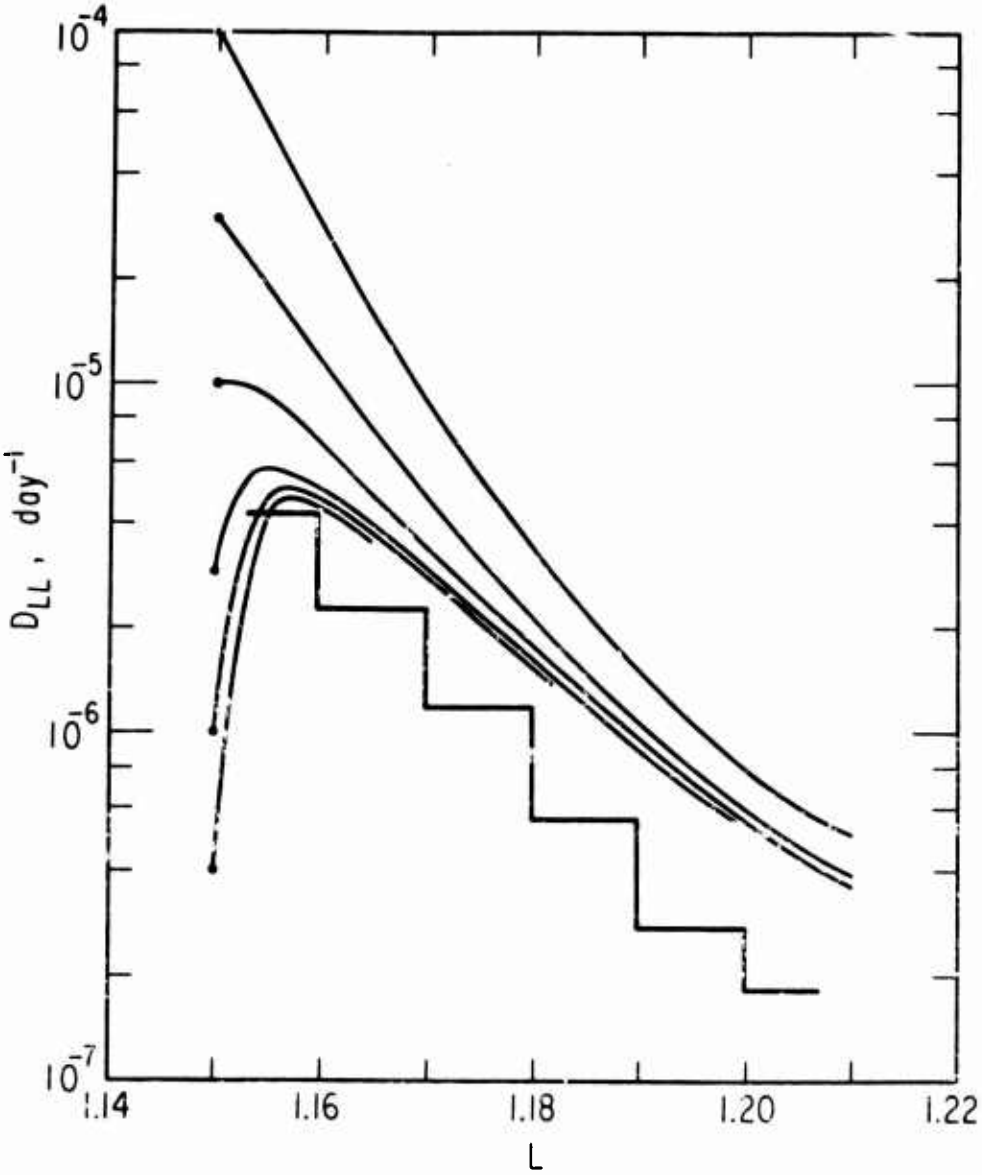

Fig. 23. Radial diffusion coefficients obtained from data in Figure 22, assuming fission spectrum to obtain $\bar{f}(M, J, \Phi)$ at constant M and J. Staircase function (Newkirk and Walt, 1968a) follows from self-inconsistent quadrature. Smooth curves are self-consistent, but require assignment of arbitrary values (filled circles) to D_{LL} at L = 1.15 (Farley, 1969).

Figure 23 to be replaced by solutions of the alternative equation

$$\frac{1}{L^2 f}\ \frac{\partial}{\partial L}\left[L^2 D_{LL}\ \frac{\partial f}{\partial L}\right] = \frac{\partial F}{\partial t} + \frac{1}{\tau_c}\ , \qquad (17)$$

with the flux profile evaluated at fixed energy, as in Figure 22a. Newkirk and Walt (1968a) had postulated a radial-diffusion process conserving M and J, and so had used (14) to transform the flux profile in Figure 22a to a distribution function at constant M and J prior to numerical differentiation. One does not, however, expect to find serious discrepancies (either in magnitude or in functional form) between the solutions of (17) and those of (13) for D_{LL}.

7. INNER-ZONE PROTONS

A major development in radiation-belt theory (Farley et al., 1970) was the inclusion of radial-diffusion effects in the analysis of high-energy inner-zone protons. It seems surprising in retrospect that previous authors (including Dragt, 1971) had chosen to neglect so pervasive a process as radial diffusion in attempting to predict the spatial and spectral structure of the inner proton belt. Before 1970, one had vainly hoped to understand this structure as a dynamical balance between Coulomb drag (ionization loss) and a source known as CRAND (the beta decay of albedo neutrons ejected from the atmosphere by incident cosmic rays).

Farley et al. (1970) showed that the major deficiencies of such a treatment are corrected by the inclusion of radial diffusion and the appropriate boundary conditions. The improvement is illustrated dramatically in Figure 24, from a slightly more refined calculation by Farley and Walt (1971). The basic form of the Fokker-Planck equation for protons, neglecting pitch-angle diffusion, is

$$\frac{\partial f}{\partial t} + \sum_i \frac{\partial}{\partial J_i}\left[\left(\frac{dJ_i}{dt}\right)_\nu f\right] = \frac{\partial}{\partial \Phi}\left[D_{\Phi\Phi}\frac{\partial f}{\partial \Phi}\right] + S - \frac{f}{\tau_q}, \qquad (18)$$

where the subscript ν designates a nonstochastic (frictional) change in the invariant action integral J_i, the symbol S denotes the source term derived from CRAND, and the symbol τ_q denotes the particle lifetime against charge exchange and nuclear collisions in the atmosphere. Charge exchange is completely negligible at the high energies of interest here, but can be very important at ring-current energies (see Section 8).

It is convenient to transform (18) from the "old" variables (M, J, Φ) to the "new" variables (M, K, L), where $K^2 \equiv J^2/8m_0M$ and $L \equiv 2\pi a^2 \left|g_1^0/\Phi\right|$. The Jacobian of this transformation has the absolute value

$$\left|\partial(M, J, \Phi)/\partial(M, K, L)\right| = (8m_0M)^{1/2}\,(2\pi a^2/L^2)\left|g_1^0\right|, \qquad (19)$$

and the quantity K is conserved by the operative dynamical processes.

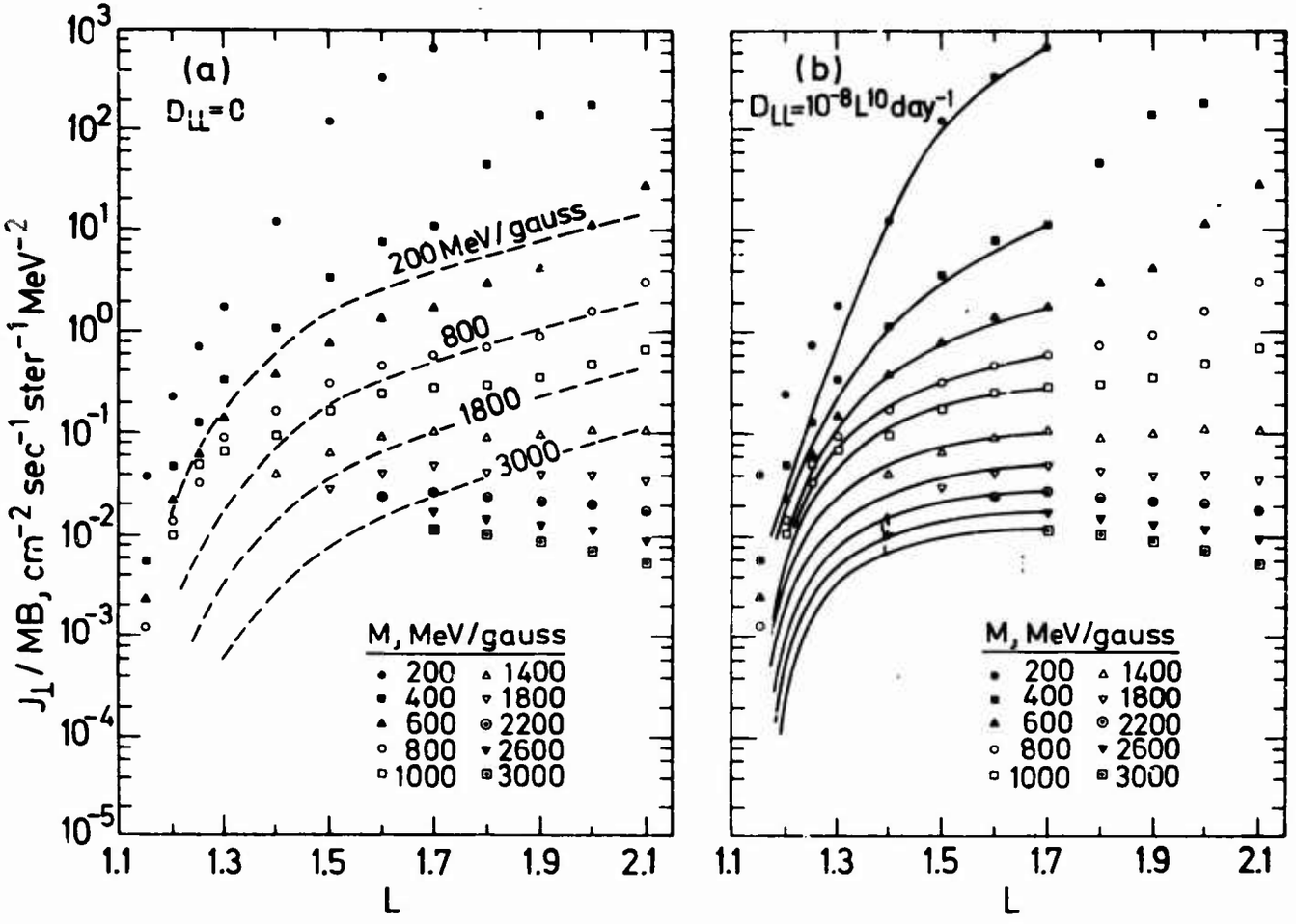

Fig. 24. Inner-zone proton distribution function ($\times 2m_0$) for J = 0 and selected values M, based on OV3-4 data (Thede, 1969) and numerical integration (Farley ar Walt, 1971). Dashed curves (a) are steady-state solutions of the Fokker-Planck equation with $D_{LL} = 0$ and S defined by the Lingenfelter (1963) spectr Solid curves (b) are steady-state solutions of the same Fokker-Planck equation, with the same source term S, but with $D_{LL} = 10^{-8}L^{10}day^{-1}$ and boundary conditions imposed by the data at L = 1.1 (where f = 0) and L = 1.7 (Farley and Walt, 1971).

It follows that

$$\frac{\partial f}{\partial t} + M^{-1/2} \frac{\partial}{\partial M}\left[M^{1/2}\left(\frac{dM}{dt}\right)_\nu f\right] = L^2 \frac{\partial}{\partial L}\left[\frac{1}{L^2} D_{LL} \frac{\partial f}{\partial L}\right] + S - \frac{f}{\tau_q}, \tag{20}$$

where (cf. Farley and Walt, 1971; White, 1973)

$$M^{1/2}(dM/dt)_\nu = M^{1/2}(\gamma/B_m)(dE/dt)_\nu$$

$$= (4\pi q_p^2 q_e^2/m_e)(m_0/2B_m^3)^{1/2}\sigma \tag{21a}$$

and

$$\sigma = \langle N_e[\gamma^2 - 1 - \gamma^2 \ln(\lambda_D m_e v/\hbar)]\rangle$$

$$+ \sum_i \langle N_i\rangle Z_i\{\gamma^2 - 1 - \gamma^2 \ln[2m_e c^2(\gamma^2 - 1)/I_i]\}. \tag{21b}$$

Here the angle brackets denote an average over the particle drift period; the subscript i denotes the atmospheric constituent having density N_i (particles per unit volume), nuclear charge number Z_i, and mean excitation energy I_i per atomic electron; and the symbol m_e denotes the rest mass of an electron. The plasmaspheric Debye length λ_D is equal to $(\kappa T_e/4\pi N_e q_e^2)^{1/2}$, where κ is Boltzmann's constant. The charge of a proton is denoted q_p.

Since $f = J_\perp/2m_0MB$, the source term S must be given (Dragt et al., 1966) by

$$S = (1/p^2\gamma\tau_n)(\Omega_2/2\pi v) \oint \underset{\sim}{J}^n \cdot d\underset{\sim}{\ell} \qquad (22)$$

where τ_n ($\approx$1013 sec) is the mean life of a neutron at rest, $\underset{\sim}{J}^n$ is the differential neutron flux per unit solid angle in velocity space, and $d\underset{\sim}{\ell}$ is the element of length along a proton's spiral path between mirror points. Since inner-zone drift shells are offset from the geocenter, the quantity S given by (22) can vary with azimuth. The source term in (18) and (20) should ideally be written $\langle S \rangle$, so as to indicate the drift average.

In obtaining Figure 24, Farley and Walt (1971) set $\tau_q = \infty$ and solved for the steady state ($\partial f/\partial t = 0$). With $D_{LL} = 0$, equation (20) reduces to a first-order differential equation in M, having the boundary condition that $f = 0$ at $M = \infty$ (actually imposed at $M = 4$ GeV/gauss for numerical convenience). The predicted distribution function (dashed curves) is thus deficient at low M (e.g., $M = 200$ MeV/gauss), excessive at high M (e.g., $M = 3$ GeV/gauss), and generally in poor agreement with the data. With $D_{LL} = 10^{-8} L^{10}$ day^{-1}, one is free to impose suitable boundary conditions in L, and the resulting predictions (solid curves) for $J_\perp/MB$ at $L < 1.7$ agree remarkably well with the observational data.

Farley et al. (1972) added the refinement of including the geomagnetic secular variation ad hoc in the basic equations. Since the secular variation

in fact conserves the adiabatic invariants of charged-particle motion, its inclusion as a term in (20) can only simulate the phenomenon approximately. However, if one views the field configuration as fixed (frozen in time), then the secular contraction of dipolar drift shells can be simulated by a radial convection of particles, an increase in K (to preserve the equatorial pitch angle), and a decrease in M (to characterize the net energy gain correctly). One must specify

$$(\dot{M}/M)_{sec} = (\dot{L}/L)_{sec} = -2\,(\dot{K}/K)_{sec} = \dot{g}_1^0/g_1^0 \qquad (23)$$

for the purpose of this simulation. An equation of the form

$$\frac{\partial f}{\partial t} + M^{-1/2}\frac{\partial}{\partial M}\left[M^{1/2}\left(\frac{dM}{dt}\right)_\nu f\right] + (\dot{g}_1^0/g_1^0)\,L^2\frac{\partial}{\partial L}\left[\frac{f}{L}\right]$$
$$- (\dot{g}_1^0/2g_1^0)\frac{\partial}{\partial K}\left[Kf\right] + (\dot{g}_1^0/g_1^0)\,M^{-1/2}\frac{\partial}{\partial M}\left[M^{3/2} f\right]$$
$$= L^2\frac{\partial}{\partial L}\left[\frac{1}{L^2} D_{LL}\frac{\partial f}{\partial L}\right] + S - \frac{f}{\tau_q} \qquad . \qquad (24)$$

thus emerges. Farley et al. (1972) obtained quasi-static solutions of (24) in the limit K = 0, taking the realistic case $g_1^0/\dot{g}_1^0 = -1933$ yr and (for comparison) the unrealistic case $\dot{g}_1^0/g_1^0 = 0$. The outcome is shown in Figure 25. The effect of the geomagnetic secular variation is to enhance the predicted proton flux at each M, thus improving the agreement with observation (notably at M = 0.8 GeV/gauss).

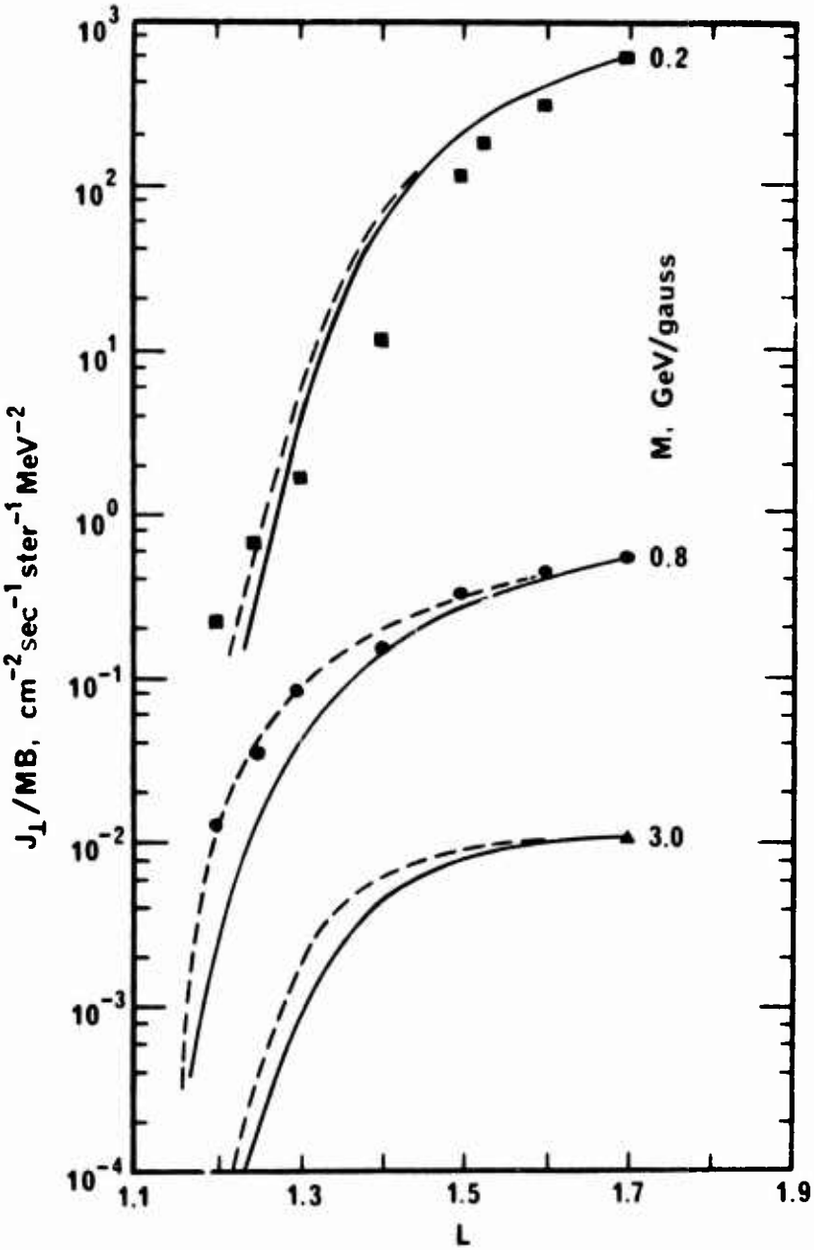

Fig. 25. Inner-zone proton distribution function ($\times 2m_0$) for J = 0 and selected values of M, based on data points from Figure 24 and numerical integration (Farley et al., 1972). Solid curves are steady-state solutions of the Fokker-Planck equation (neglecting the geomagnetic secular variation) with $D_{LL} = 2.1 \times 10^{-9} L^{10} \times |m_0c^2/g_1^0 M|$ and S defined by the Lingenfelter (1963) spectrum. Dashed curves are quasi-static solutions of the Fokker-Planck equation augmented to simulate secular contraction of the geomagnetic dipole moment (Farley et al., 1972).

The foregoing results were obtained by using an albedo-neutron spectrum predicted by Lingenfelter (1963) from a theoretical extrapolation of observations made at energies $E < 10$ MeV. This extrapolation follows the dashed line in Figure 26. The subscript 2π denotes angular integration over the upward hemisphere in velocity space. For this presentation the extrapolated spectrum of Lingenfelter (1963) has been evaluated at a magnetic colatitude $\theta = 50^{\circ}$. Until September 1971, there had been no direct measurement of the albedo-neutron flux in the energy range $E =$ 10-100 MeV, i.e., in the range of relevance to the majority of inner-zone proton observations. This deficiency was rectified by Preszler et al. (1972), whose balloon-borne neutron detectors yielded the data points shown in Figure 26. It is noteworthy that the neutron fluxes observed by Preszler et al. (1972) far exceeded the extrapolation of Lingenfelter's prediction. However, more recent theoretical (Monte Carlo) calculations by Merker (1972) and Armstrong et al. (1973) have yielded results that agree with the measurements reported by Preszler et al. (1972, 1974).

Fortified by these new theoretical and observational data, Claflin and White (1974) used the CRAND-proton source derived therefrom in the radial-diffusion code that had been developed by Farley et al. (1972). Claflin and White (1974) included nuclear collisions (the term f/τ_q) in their analysis and expressed the radial-diffusion coefficient as the sum of two terms: $D_{LL} = D_{LL}^{(e)} + D_{LL}^{(m)}$, arising from electrostatic impulses and magnetic impulses, respectively. Taking $D_{LL}^{(e)} = 5 \times 10^{-11} L^{10} \times$

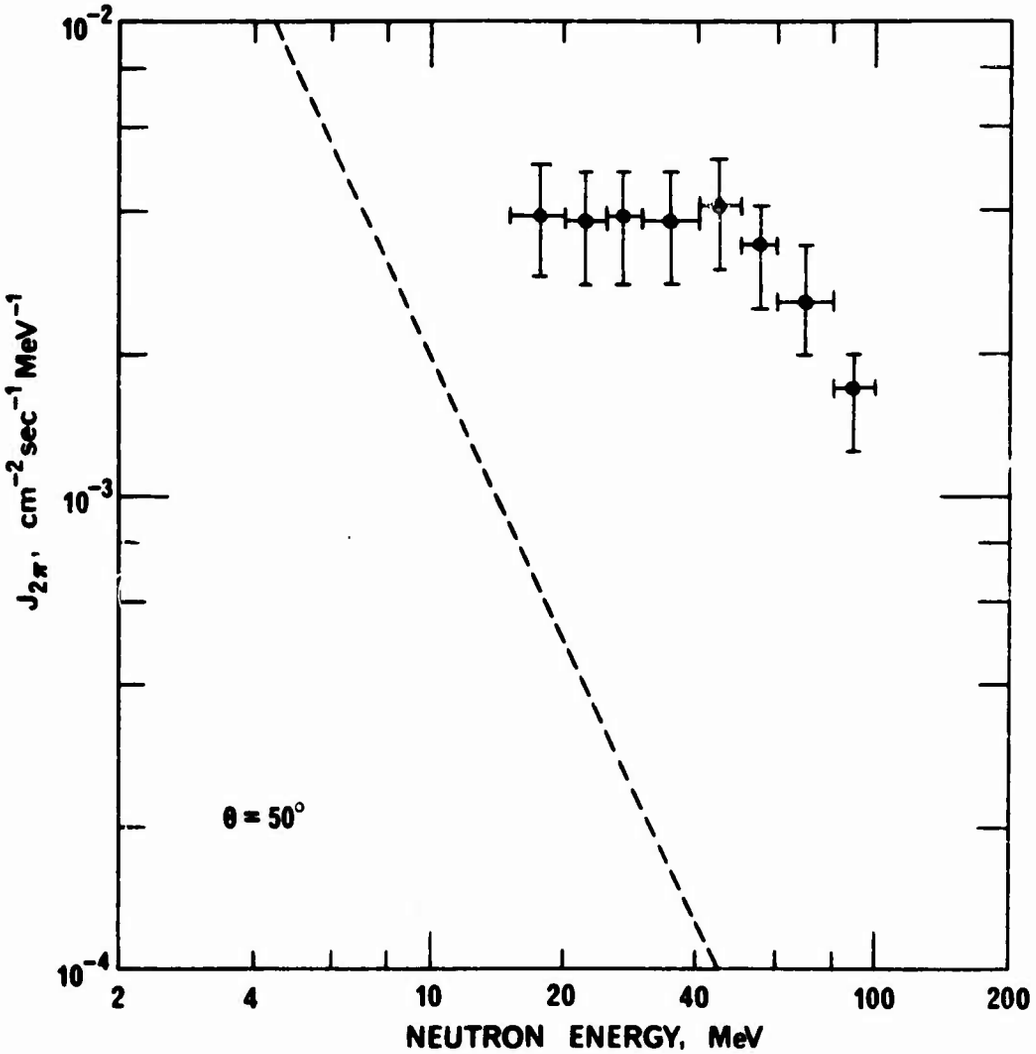

Fig. 26. Data points specify the omnidirectional flux of albedo neutrons at magnetic latitude 40°N, altitude 36 km, as measured by Preszler et al. (1972). The dashed line is an extrapolation of the spectrum obtained by Lingenfelter (1963) at energies E < 10 MeV.

$(M_0/M)^2$ day^{-1} and $D_{LL}^{(m)} = 8 \times 10^{-9} L^{10}$ day^{-1}, where $M_0 \equiv 1$ GeV/gauss, they obtained the theoretical (dashed and solid) curves shown in Figure 27. The solid curves correspond to the atmospheric model used earlier by Farley and Walt (1971). The dashed curves correspond to the same neutral-atmospheric model, but require a plasmaspheric electron density five times that used by Farley and Walt (1971). Agreement with observation is thereby improved, but observational confirmation of the required plasmaspheric electron density is lacking. One must therefore regard the corresponding determination of $D_{LL}^{(e)}$ and $D_{LL}^{(m)}$ as tentative, although the two-term representation of D_{LL} in such an analysis is definitely a step forward. A more detailed review of progress on the problem of inner-zone protons is given by White (1973).

A word of caution seems appropriate at this point. The use of (24) to simulate the behavior of inner-zone protons is an expedient that remains to be justified in fundamental terms. It is true that one can obtain quasi-static solutions of (24) by inserting transport coefficients and sources that have been averaged over the solar cycle. One can further obtain quasi-periodic solutions of (24) by allowing the transport coefficients and sources to vary over the solar cycle (cf. Dragt, 1971). However, there is no assurance that such mathematical solutions correspond to geophysical reality, even in principle, because there is no assurance that the geomagnetic secular variation can be treated properly in the quasi-static approximation.

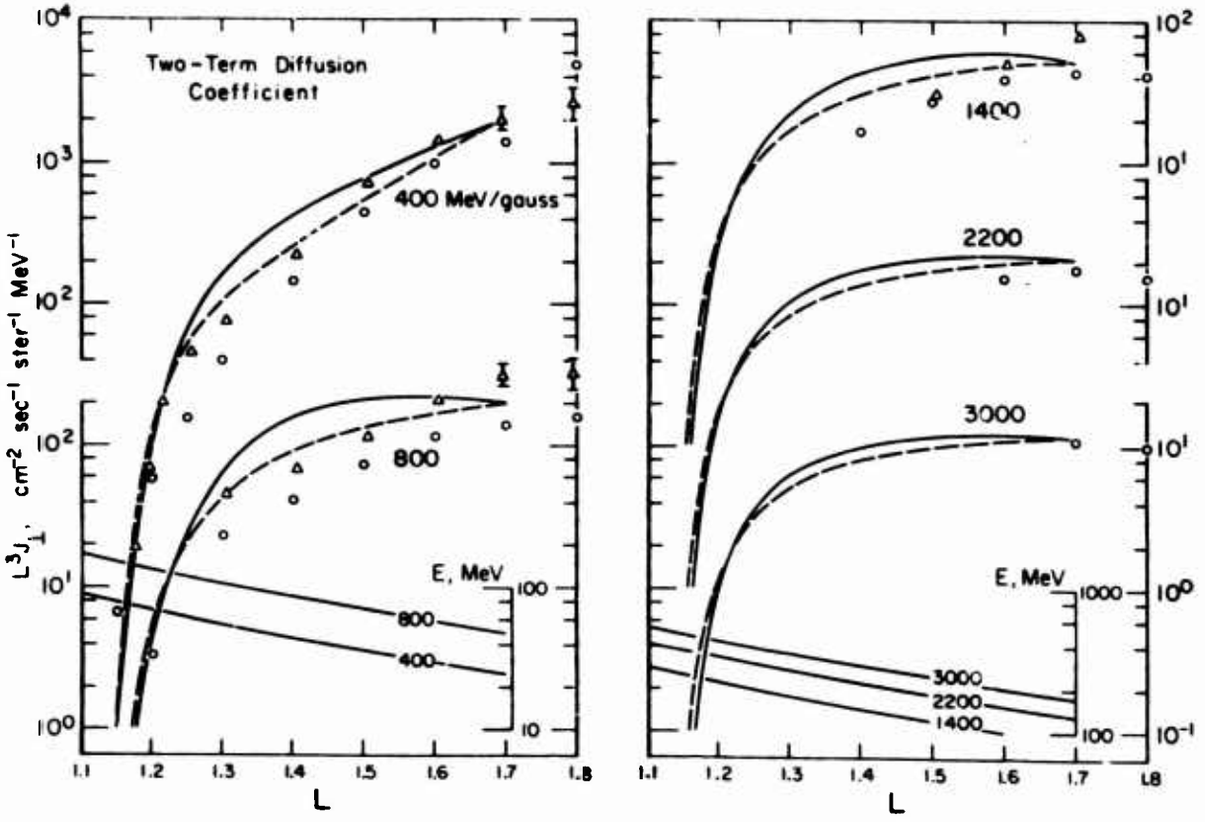

Fig. 27. Profiles of proton $L^3J_\perp$ for J = 0 and selected values of M, MeV/gauss. Triangles denote data points derived from Hovestadt et al. (1972a). Circles denote data points derived from Thede (1969), as in Figure 24. Solid curves represent quasi-static solution of augmented Fokker-Planck equation used previously by Farley et al. (1972) to simulate secular contraction of geomagnetic dipole moment (Claflin and White, 1974). Dashed curves represent quasi-static solutions of the same Fokker-Planck equation, but with plasmaspheric electron density quintupled. Subsidiary scale indicates variation of kinetic energy E with L at fixed M.

It seems probable, at least for M >1 GeV/gauss, that some proton residence times in the inner zone are comparable to the 8000-year period of the geomagnetic cycle. If so, the present configuration of the inner proton belt would be the product of its past evolution, an evolution dependent upon the whole history of the earth's field. (Most serious investigators reject the contrary hypothesis, that the inner proton belt has remained immutable since its sudden creation in the distant past.)

The proper evolutionary treatment of inner-zone protons follows naturally from (18). One must attempt to model the transport coefficients, source term, and boundary conditions (in Φ) as functions of time. All consequences of the secular variation must enter at this level, and not as distinct terms in the Fokker-Planck equation. The distribution function $f(M, J, \Phi; t)$ must be stored as a function of the adiabatic invariants (M, J, Φ) and the time (t). One may presume that $f(M, J, \Phi; t)$ is quasi-periodic on the time scale of 8000 years. Thus, if $t = 0$ deontes the present, one may set $f(M, J, \Phi; -8000\ \text{yr}) = f(M, J, \Phi; 0)$ as an initial condition based on the observational data. One next integrates forward in time (from $t = -8000$ yr to $t = 0$). The chosen normalization of $D_{\Phi\Phi}$ is thereby vindicated if the solution for $f(M, J, \Phi; 0)$ matches the observational data at the present epoch, and the historical description of the inner proton belt is thus completed. (One may instead integrate from the initial condition that $f = 0$ at the time of the last geomagnetic field reversal; see Cox, 1969.)

8. ALPHA-PROTON RATIO

Minor ionic constituents of the geomagnetically trapped radiation are becoming recognized as a valuable probe for the dynamics of radiation belts in general. To the extent that such minor ions (e.g., He^{+}, He^{++}, C^{+m}, N^{+n}, O^{+p}) respond differently from protons (or from each other) to the fluctuating fields responsible for various transport processes, the relative abundances of such ions can serve to indicate the relative importance of the various transport mechanisms. To the extent that their relative abundances differ from the abundances inherent in various plausible radiation sources, these relative abundances can help one to assess the relative importance of the various sources.

It has become conventional, for valid theoretical reasons, to compare the intensities (fluxes) of various radiation-belt ions having the same velocity, i.e., the same amount of energy per nucleon and (preferably) the same pitch angle, at a given location in space. Moreover, since helium is the most prevalent minor ion in the radiation belts, the alpha/proton (α/p) intensity ratio is the ratio that has been studied most thoroughly. (Since it would be very difficult to distinguish between He^{+} and He^{++} with instruments presently available on spacecraft, the observed "alpha-particle" intensity is understood to include the contributions from both charge states.) Typical values of the α/p ratio observed off-equator at $L \sim 3$ have been compiled by Krimigis (1970) and are shown in Figure 28. The ratio is somewhat enhanced (as shown)

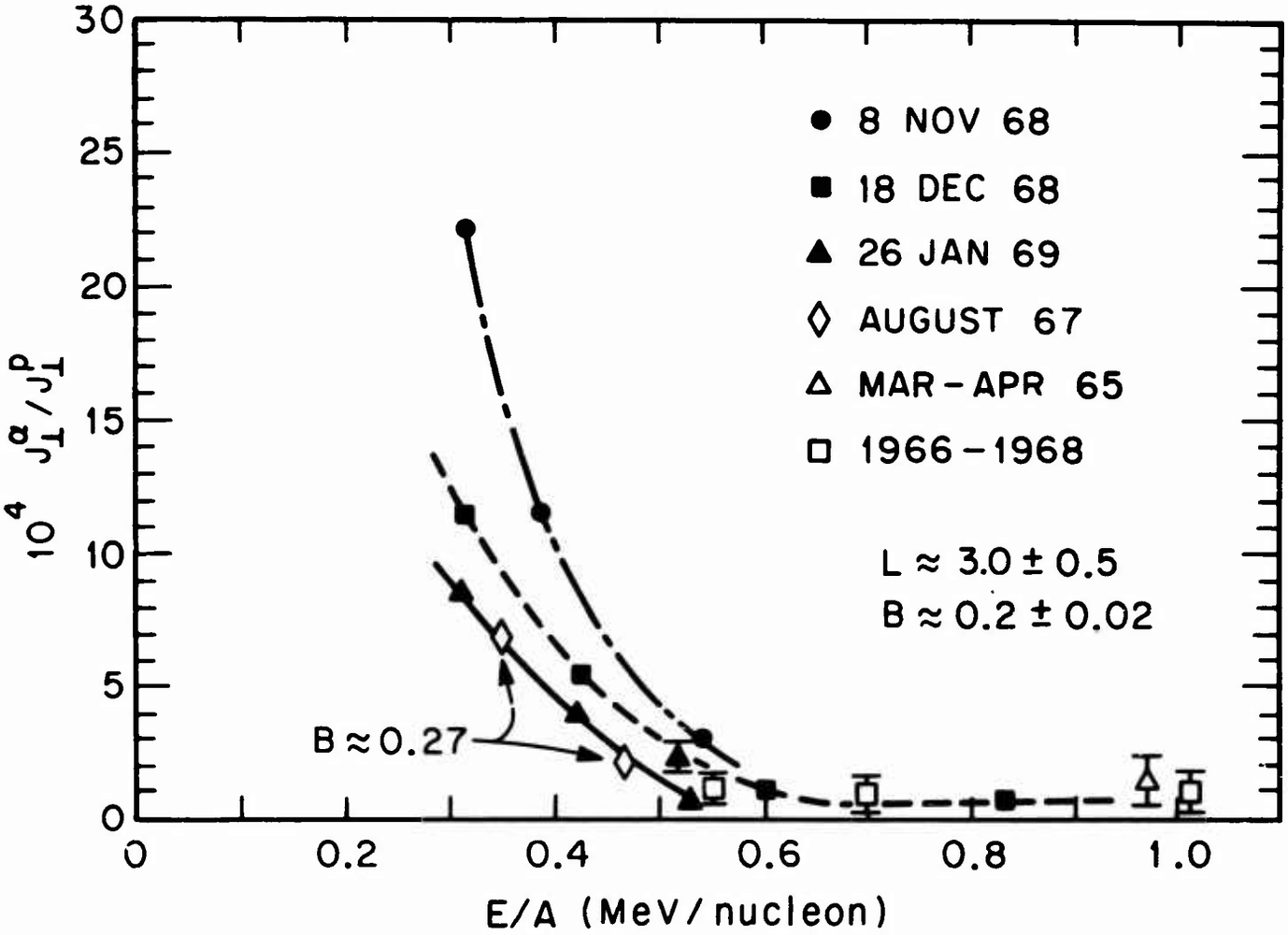

Fig. 28. Low-Altitude observations of α/p ratio at several different epochs (Krimigis, 1970).

during periods of geomagnetic disturbance (e.g., November 1968), but is limited even under these conditions to values $\sim 1\text{-}30 \times 10^{-4}$ for $E/A \geq 0.3$ MeV/nucleon.

The magnetospheric α/p ratio (as observed off-equator at $L \sim 3$) is thus appreciably smaller than the α/p ratio in the solar wind ($\sim 4 \times 10^{-2}$), which is the most plausible source for magnetospheric hydrogen and helium ions. Cornwall (1972a) has successfully accounted for this superficial discrepancy by attributing magnetospheric radial diffusion (off-equator) to electrostatic impulses. The resulting diffusion coefficient $D_{LL}^{(e)}$ is proportional to $(Z/A)^2$ at fixed energy/nucleon, among particles having drift periods ≤ 20 min (the postulated decay time of an electrostatic impulse). The magnitude of $D_{LL}^{(e)}$ for energetic H^+ ($Z = 1$, $A = 1$) thus exceeds the magnitude of $D_{LL}^{(e)}$ for He^{++} ($Z = 2$, $A = 4$) and He^+ ($Z = 1$, $A = 4$) by factors of four and sixteen, respectively. Consequently, protons have more efficient access than helium ions to the inner magnetosphere ($L \leq 4$) from an external source.

In reproducing the trend of quiet-time data shown in Figure 28, Cornwall (1972a) neglected pitch-angle diffusion, since the observational evidence does not yet require the inclusion of this process for the particle population under study. He did, however, include both ionization loss (Coulomb drag) and charge exchange, both of which are included in (20) as far as protons are concerned. Ionization loss for helium ions is described by (21) if the correct ionic charge (q_p for He^+, $2q_p$ for He^{++})

is inserted in place of the proton charge q_p. Charge exchange (τ_q) is an especially important process here. It leads not only to the neutralization of H^+, as in (20), but also to the alternation of helium ions between the singly charged state and the doubly charged state. To describe this alternation, one requires a pair of coupled transport equations having the form

$$\frac{df_1}{dt} = L^2 \frac{\partial}{\partial L}\left[\frac{1}{L^2} D_{LL}^{(1)} \frac{\partial f_1}{\partial L}\right] + \frac{f_2}{\tau_{21}} - \frac{f_1}{\tau_{10}} - \frac{f_1}{\tau_{12}} \qquad (25a)$$

$$\frac{df_2}{dt} = L^2 \frac{\partial}{\partial L}\left[\frac{1}{L^2} D_{LL}^{(2)} \frac{\partial f_2}{\partial L}\right] + \frac{f_1}{\tau_{12}} - \frac{f_2}{\tau_{21}} , \qquad (25b)$$

where the total derivative (df/dt) includes the Coulomb-drag term, as on the left-hand side of (20). Distributed sources (S) are unimportant here. The charge-exchange lifetime τ_{ij} in (25) refers to the conversion of He^{+i} (distribution function f_i) into He^{+j} (distribution function f_j). The observable α/p ratio $J_\perp^\alpha/J_\perp^p$ is equal to $(16/f_p)(f_1 + f_2)$ at fixed E/A, where $f \equiv J_\perp/2m_0MB$ for each species.

The foregoing discussion refers to particles mirroring far off the geomagnetic equator. The situation is much different for particles that mirror near the equator, where $J_\perp^\alpha/J_\perp^p \sim 10^{-2}$ according to the initial observations by Fritz and Williams (1973). Full equatorial pitch-

angle distributions of inner-zone alpha particles and protons, as obtained by Blake et al. (1973), are shown in Figure 29. The alpha-particle distribution is considerably narrower in pitch angle (α) than the proton distribution. This finding is compatible with the previous observational results, namely that $J_\perp^\alpha/J_\perp^p$ on the equator greatly exceeds $J_\perp^\alpha/J_\perp^p$ far off the equator along the same field line.

Both pitch-angle distributions in Figure 29 are sharply peaked at $\alpha = 90^\circ$. For the lowest eigenmode of pitch-angle diffusion, one might have expected a distribution like $\sin\alpha$ or $\sin^2\alpha$. It is natural, therefore, to neglect pitch-angle diffusion in seeking to explain the observed distributions. Nakada et al. (1965) confronted the same problem years ago, and concluded that radial diffusion from an external source is sufficient to produce a sharply peaked pitch-angle distribution at $L \lesssim 3$. The point is that particles from a common source gain relatively more energy per unit change in L at small values of K than at large values of K. The dashed curves in Figure 30 (which converge to a common value of $E \approx 9$ keV at $L \approx 12$) illustrate this effect for nonrelativistic particles. The specified angles (90°, 30°, 20°, 10°) represent the equatorial values of α at L = 7. Thus, particles contributing to a given energy channel at $L \sim 2$ (Figure 29) at small α (large K) must have arisen from a higher energy on the source spectrum than particles contributing to the same channel at $\alpha = 90^\circ$ (K = 0).

Since the source (plasma-sheet) spectrum has an e-folding energy of only $\lesssim 6$ keV for protons, it is a steeply falling function of energy for

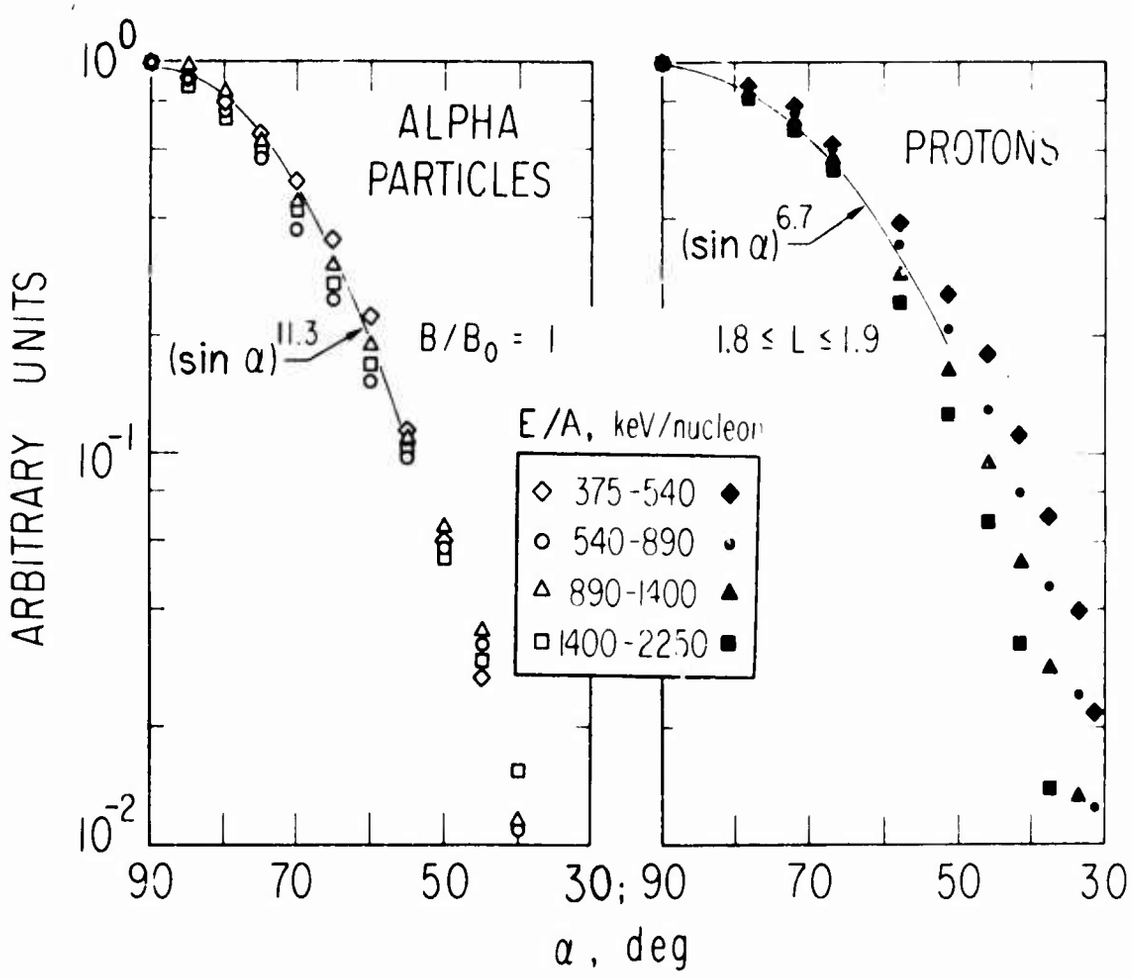

Fig. 29. Equatorial pitch-angle distributions of alpha particles (left panel) and protons (right panel) in the same four energy/nucleon passbands, as observed on spacecraft OV1-19 (Blake et al., 1973). Statistical error bars would be about as large as the data-point symbols themselves.

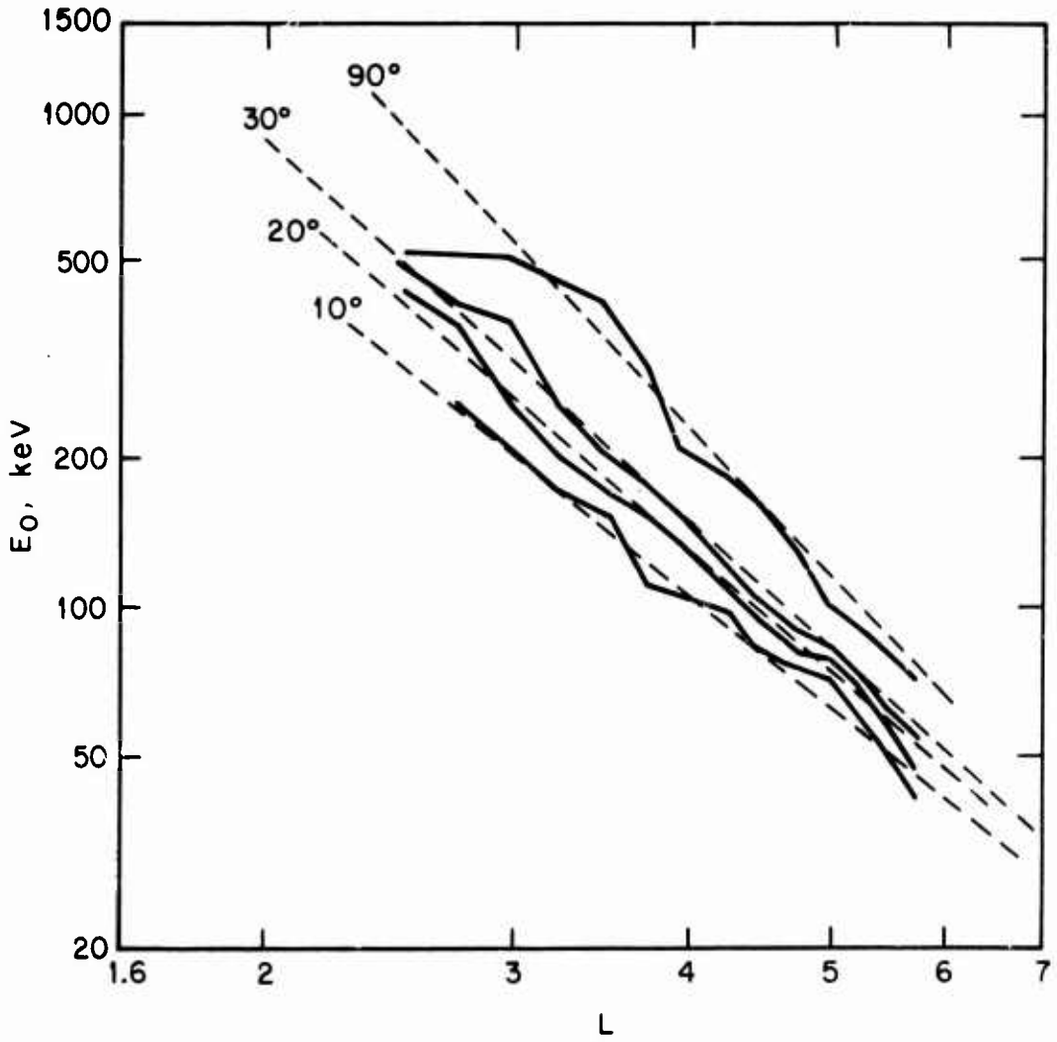

Fig. 30. Empirical e-folding energies (solid curves) of observed proton spectra (Davis and Williamson, 1963) at equatorial pitch angles consistent with conservation of M and J; expected variation (dashed curves) of energy with L for individual protons having constant M and J, for selected values of energy and equatorial pitch angle at L = 7 (Nakada et al., 1965).

$E \gtrsim 20$ keV. This feature is translated by radial diffusion into a sharply peaked pitch-angle distribution at sufficiently high energies and low L values. Nakada et al. (1965) expressed the same result somewhat differently, in terms of the e-folding energies E_0 of the exponential spectra observed at various values of K and L. Using the proton data of Davis and Williamson (1963), they made the empirical observation that the spectral index E_0 varies with L in roughly the same manner as the kinetic energy of an individual particle would vary. This property is illustrated by the solid "curves" in Figure 30, where the value of K is uniquely determined by specifying the equatorial value of α (90°, 30°, 20°, 10°) at $L = 7$.

Under very restrictive conditions, one can prove a theorem which holds that the e-folding energy of an exponential spectrum of nonrelativistic particles should indeed behave as the energy of an individual particle. The proof requires neglect of Coulomb loss $(dM/dt)_\nu$ and distributed sources (S), the assumption of a steady state ($\partial f/\partial t = 0$), and the existence of an M-independent inner boundary (L_1) at which f vanishes. Then, if $\tau_q D_{LL}$ is independent of M, the solution of (20) for f at fixed K factors such that $f(L, M) = g(L)\, h(M)$. Should h(M) be of the form

$$h(M) = M^{-\ell} \exp(-M/M_0), \tag{26a}$$

the spectrum of nonrelativistic energies will vary with L as

$$h(M) = (B_m/E)^{l} \exp(-E/E_0), \qquad (26b)$$

where $E_0 = M_0 B_m$. Thus, the e-folding energy E_0 varies with L as would the energy of an individual particle conserving M ($=M_0$) and K, thereby tracing an L-dependent mirror-point field B_m. This proof includes the limiting cases $\tau_q = \infty$ (negligible charge exchange), $M_0 = \infty$ (power-law energy spectrum for $J_\perp$), and $l = 1$ (exponential energy spectrum for $J_\perp$). The most doubtful asumption (if $\tau_q < \infty$) is the M-independence of $\tau_q D_{LL}$.

It remains to understand why the alpha-particle distribution is even narrower in pitch angle than the proton distribution (Figure 29). One possibility, suggested by Cornwall (1972a) in a different context, is that the "temperature" of the alpha-particle source is less than four times the "temperature" of the proton source. Although E/A is the same for alpha particles and protons in the solar wind up to the bow shock, it is at least conceivable that the two species would exchange energy (partially thermalize) in the turbulent magnetosheath. Further thermalization in the plasma sheet hardly seems avoidable, in view of the turbulence required there to dissipate the neutral-sheet current and thereby maintain the dawn-dusk magnetospheric electric field.

Another possibility is that radial diffusion by magnetic impulses can affect the pitch-angle distribution of alpha particles (more so than for protons). The rationale for this thought is illustrated schematically in Figure 31. The known functional form of $D_{LL}^{(m)}$, as given by Fälthammar

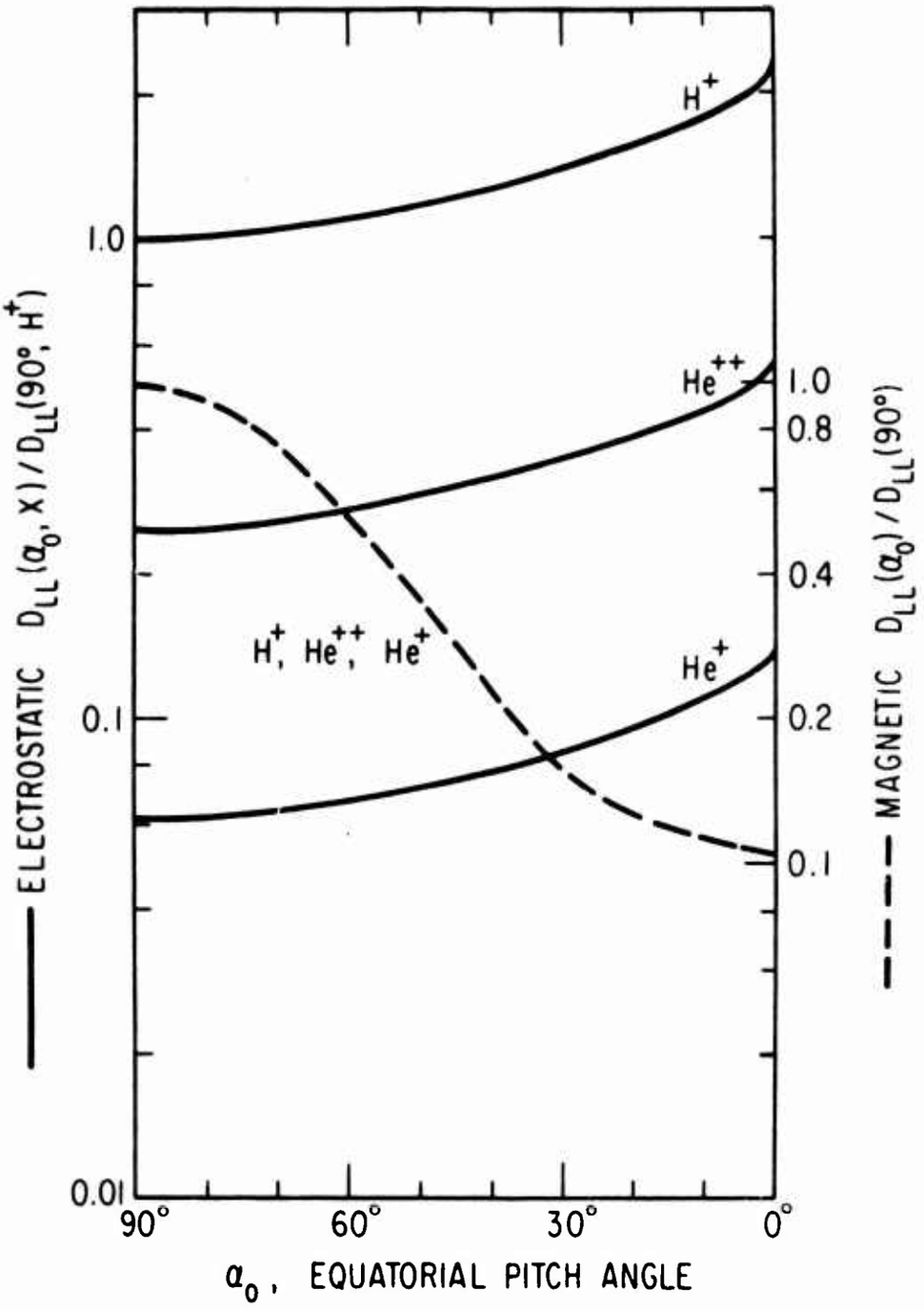

Fig. 31. Schematic representation of pitch-angle and charge-state dependence of radial-diffusion coefficient resulting from step-like electrostatic impulses (solid curves) or magnetic impulses (dashed curve). The relative displacement of right and left ordinates remains to be determined empirically (Fennell et al., 1974) for given E/A and L.

(1968), strongly favors the access of particles having equatorial pitch angles α_0 near 90°. The magnitude of $D_{LL}^{(m)}$ is independent of particle species, charge state, and energy. Conversely, the known functional form of $D_{LL}^{(e)}$ slightly favors the access of particles having small values of sin α_0. At fixed energy/nucleon, the magnitude of $D_{LL}^{(e)}$ varies as $(Z/A)^2$ for drift periods $2\pi/\Omega_3 \leq 20$ min. Since $D_{LL}^{(e)}$ also varies as $(\gamma/p^2)^2$ for fixed Z and A, there should be a range of E/A values for which the functions $D_{LL}^{(e)}$ and $D_{LL}^{(m)}$ overlap as illustrated (Figure 31). This condition would tend to make the alpha-particle distribution narrower in pitch angle than the proton distribution.

Lest there be any doubt that inner-zone alpha particles in fact have an external source, a near-equatorial profile of $2m_0 f$ at fixed K and M is shown in Figure 32. (A convenient unit for measuring K^2 and Φ is the giga-weber, GWb. For example, a particle having $B_m/B_0 \sim 5$ at $L \sim 2$ yields $K^2 \sim 3$ GWb and $\Phi \sim 4$ GWb.) The diffusion "current", whose "divergence" appears in (20), is equal to $-D_{LL}(\partial f/\partial L)_{M,K}$. It is directed inward. It is found (Blake et al., 1973) that a diffusion coefficient $D_{LL} \approx 1.2 \times 10^{-8} L^{10}$ day^{-1} would be required to maintain the profile shown in Figure 32 against Coulomb loss, so as to make $\partial f/\partial t$ vanish.

Although it is tacitly assumed in several of the paragraphs above that radiation-belt particles are ultimately derived from the solar wind, this assumption has not yet been verified conclusively. Thus, Axford (1970) has suggested that perhaps the earth's plasma sheet is populated also by ionospheric plasma, which is believed to escape along open field

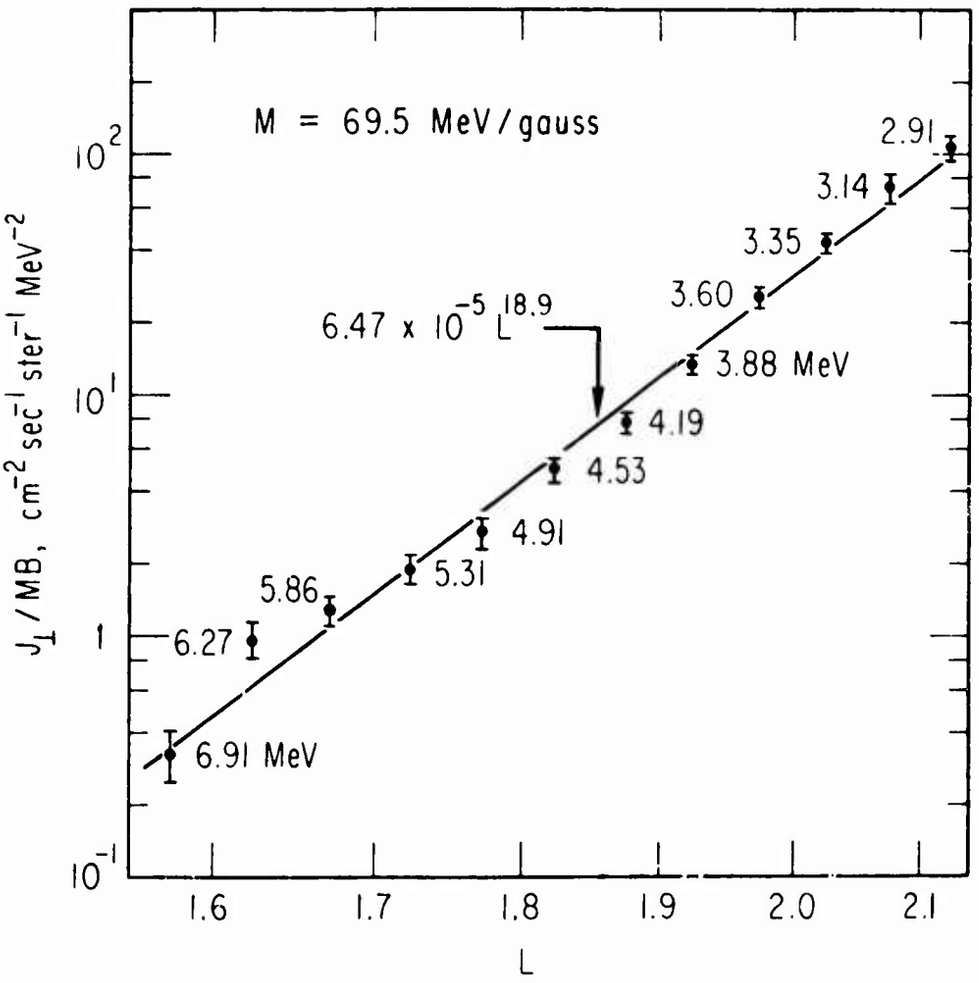

Fig. 32. Distribution function ($\times 2m_0$) of inner-zone alpha particles having M = 69.5 MeV/gauss and $K^2 = 27.6$ MWb, based on OV1-19 data (Blake et al., 1973). This value of K^2 corresponds to a mirror-point field $B = 1.3\ B_0$ at L = 2.125, and to $B < 1.3\ B_0$ at lower L values.

lines in the form of a "polar wind" (e.g., Banks and Holzer, 1968). Various tests have been proposed to distinguish between the solar-wind and polar-wind source hypotheses. Axford (1969, 1970) has noted that the two sources differ significantly with respect to isotopic and charge-state abundances of ionic helium. Mogro-Campero and Simpson (1970) have noted that they differ with respect to the ionic abundances of carbon, nitrogen, and oxygen (CNO). Blake (1973) has determined that a measurement of the C/O intensity ratio in the radiation belts would provide the most decisive test, since the two proposed sources differ by at least five orders of magnitude in their C/O abundance ratios. Observations reported by Mogro-Campero (1972) indicate that $C/O \sim 1\text{-}10$ at $L = 4$, for $E/A \sim 15\text{-}30$ MeV/nucleon. This result would exclude the polar wind (in which $C/O < 10^{-5}$) as a source of such radiation-belt ions, and favor the solar wind, in which $C/O \sim 1$ (Blake, 1973). However, the C/O intensity ratio remains to be measured at the lower values of E/A that would be compatible with Figure 28, i.e., at energies which trace back (at constant M and K) to the nearly thermal component of the plasma sheet.

Finally it is of interest to comment on the radiation-belt ions that are suddenly lost through charge exchange at $L \gtrsim 3$, in particular on their reappearance as a partial radiation belt at L values between 1.00 and 1.15. Hovestadt et al. (1972b) have observed such a partial belt of protons at $E \gtrsim 500$ keV, while Mizera and Blake (1973) have extended the observations down to 12.4 keV (i.e., through energies typical of the ring current). The formation of such partial radiation belts has been explained

by Moritz (1972). Charge exchange converts an energetic ion (H^+, for example) into a fast-moving neutral atom, whose trajectory is tangential to the adiabatic spiral path of the ion at the instant of neutralization. Most such rectilinear trajectories allow the fast neutral atom to escape from the magnetosphere, but a certain fraction are directed toward the dense atmosphere. In this latter case, there arises a significant probability for the dense atmosphere (e.g., at altitudes $\lesssim 120$ km) to strip away the fast atom's electron, thus recreating an energetic ion. Ions thus formed at low altitudes drift westward to form a partial radiation belt, but are ultimately degraded by Coulomb loss. Successive charge-exchange and stripping reactions within the dense atmosphere can lead to a novel form of radial diffusion. However, ions trapped at very low L values ($L \lesssim 1.1$) cannot complete a drift period around the earth. They are doomed to lose their energy at the longitude of the South Atlantic "anomaly", if not before. The equatorial pitch-angle distributions of such recreated ions are sharply peaked about 90°, because the source protons at $L \gtrsim 3$ are similarly anisotropic (Moritz, 1972; Mizera and Blake, 1973).

9. COLD-PLASMA INJECTION

Recent theoretical and observational studies suggest rather strongly that the plasmapause (see Figure 2) is a boundary of great importance in the context of magnetospheric wave-particle interactions. This importance

arises mainly from the fact that momentum-space instabilities of radiation-belt particles typically have growth rates that are very sensitive to the local density of cold plasma. Thus, the electromagnetic ion-cyclotron waves responsible for precipitation of ring-current protons (Cocke and Cornwall, 1967; Cornwall et al., 1970) and for the electron heating prerequisite to the formation of stable auroral red (SAR) arcs (Cole, 1965; Cornwall et al., 1971) in the atmosphere should be unstable (spontaneously generated) only within the plasmasphere. Ring-current observations analyzed by Russell and Thorne (1970) and SAR-arc observations analyzed by Chappell et al. (1971) seem to confirm this prediction.

The knowledge that cold-plasma density should similarly affect electron-cyclotron instabilities (e.g., Kennel and Petschek, 1966) led Brice (1970, 1971) to propose the experimental injection of artificial plasma clouds into the magnetosphere as a means of simulating such wave-amplifying properties of the plasmasphere. The effect of increasing the cold-plasma density (N_c) is to decrease the phase velocity ($\omega/k_\parallel$) of an electromagnetic cyclotron wave propagating in the whistler mode. This decreases the electron energy required for resonance, in the sense of (8), with a wave of frequency $\omega/2\pi$. Since the lower-energy electrons are typically the more numerous, the magnitude of the growth rate is thereby enhanced. Cuperman and Landau (1974) have investigated this effect quite thoroughly for a bi-Maxwellian plasma (of density N_h) in which $T_\perp^e = (A+1)\, T_\parallel^e$. The parameter A (> 0) is known as the anisotropy.

If $N_h \ll N_c$ and $\beta_\perp^e$ ($\equiv 8\pi N_h \kappa T_\perp^e / B^2$) is much less than unity, the growth rate Im ω is well approximated by the formula

$$\text{Im } \omega = -v_g N_h (q/n\omega)^2 [\Omega + (\omega - \Omega)(A+1)] (2\pi^3 / m_e \kappa T_\parallel^e)^{1/2} \times \exp [-(n_e c^2 / 2n^2 \omega^2 \kappa T_\parallel^e)(\Omega - \omega)^2], \quad (27)$$

where n is the refractive index and v_g is the group velocity. The former is given by

$$n^2 = 1 + (4\pi N_c c^2 / m_e \omega)(\Omega - \omega)^{-1} \gg 1, \quad (28)$$

where $\Omega/2\pi$ is the electron gyrofrequency and $\omega \gtrsim 10^{-3}\Omega$. For a given wave frequency $\omega/2\pi$, the temporal growth rate Im ω is maximized in absolute value (Cuperman and Landau, 1974) by setting the argument of the exponential equal to 1/2. The more relevant spatial growth rate (Im ω/v_g) is maximized in absolute value by setting the argument of the exponential equal to unity. This requires the condition

$$N_h / N_c = \omega \Omega^2 \beta_\parallel^e (\Omega - \omega)^{-3}. \quad (29)$$

Since Im $\omega > 0$ requires $\omega/\Omega < A/(A+1)$, the optimum cold-plasma density for wave <u>growth</u> has the property that $N_h/N_c < A\beta_\parallel^e (A+1)^2$. For $\beta_\parallel^e \ll 1$, the frequency corresponding to the maximum value of Im ω/v_g lies just

slightly below $\omega/2\pi = [A/(A+1)](\Omega/2\pi)$, and so the optimum ratio N_h/N_c is in fact a number of order $A\beta_{\parallel}^{e}(A+1)^2$.

Since realistic conditions often invalidate the foregoing assumptions (e.g., that $\beta_{\perp}^{e} \ll 1$ and that $N_h \ll N_c$), Cuperman and Landau (1974) have extended their calculation analytically to conditions far more general than those admitted by (27)-(29). They find, for example, that the value of Im ω (not Im ω/v_g) is maximized (with respect to both N_c and ω) by setting $[1 + (N_c/N_h)]\beta_{\parallel}^{e}A(A+1)^2 = 2$. Thus, the presence of a cold plasma (N_c) enhances the maximum temporal growth rate (Im ω) if $\beta_{\parallel}^{e}A(A+1)^2 < 2$. Cuperman and Salu (1974) have checked this and other analytical results numerically.

The calculations described above invoke an energy-independent anisotropy A. Lucas and Brice (1973) have called attention to the effects of an energy-dependent anisotropy. They have pointed out that on the distant night side of the magnetosphere (Figure 7, left panel), the pitch-angle anisotropy at high particle energies is strongly unfavorable for wave growth. By reducing the particle energy required for cyclotron resonance at a given frequency $\omega/2\pi$, the addition of cold plasma in this region of space would enable the wave to interact with electrons having a more favorable anisotropy ($A > 0$) for inducing wave growth. Detailed calculations (Lucas and Brice, 1973) have supported this heuristic argument. Moreover, the natural plasma in this region of space is so tenuous ($N_c \ll N_h \sim 1$ cm^{-3}) that even a modest experimental injection of cold plasma ($\Delta N_c \sim 3$ cm^{-3}, for example) would constitute a large relative perturbation of the medium.

The growth-rate enhancement of an electron-cyclotron wave does not depend on the ionic species of the injected plasma. Thus, barium and cesium plasmas are just as effective (per unit density N_c) as lithium and hydrogen plasmas in promoting electron-cyclotron instabilities. However, the electron population contains only a minor fraction of the total magnetospheric particle energy. The great majority of magnetospheric particle energy is concentrated in the population of ring-current protons ($E \sim 10$-100 keV). Phase velocities of electromagnetic ion-cyclotron waves are reduced (and growth rates thereby enhanced) by cold-plasma injection only at frequencies below the gyrofrequency of the injected ion. Since the natural value of Im ω/v_g attains its maximum at an appreciable fraction of the critical frequency $\omega^*/2\pi = A\Omega_p/2\pi(A+1)$, efficient enhancement of Max Im ω/v_g by cold-plasma injection requires the use of a fairly light ion (Märk, 1974). Moreover, the dimensions of the plasma cloud must exceed the wavelength of the alleged instability. Technological considerations related to this last point led Cornwall (1972b) to dismiss barium- and cesium-plasma injections in favor of lithium-plasma injection as a means of tapping the free energy inherent in the proton ring current. (Still lighter ions such as helium and hydrogen cannot be produced in sufficient numbers with conventional energy sources on spacecraft. Substances that are easily photo-ionized by the sun, e.g., alkali metals, circumvent this technological difficulty.)

The calculation of growth rates γ ($\equiv$ Im ω) in the earth's natural ring current (located beyond the plasmasphere) is complicated

by the virtual absence of cold plasma and by the fact that $\beta_{\parallel}^{p} \sim 1$ there. Thus, a treatment modeled after (27)-(29) is inappropriate, and a treatment based on the full plasma dispersion equation is ultimately required. Indeed, if the cold-plasma dispersion relation

$$n^2 = 1 + (c/v_A)^2 \left[1 - (\omega/\Omega_p)\right]^{-1} \gg 1 \tag{30}$$

is used in order to compute the phase velocity ω/k for $\underset{\sim}{k}$ parallel to $\underset{\sim}{B}$, the result is that shown by the dashed curve in Figure 33, where v_A is the Alfvén speed. The temporal growth rate that would follow, assuming a sharp resonance at the value of $v_{\parallel}$ given by (8), is

$$\gamma = 2N_p v_g (\pi q/nc\omega)^2 (2\pi m_p \kappa T_{\parallel}^{p})^{-1/2} \left[A\Omega - (A+1)\omega\right] \times \exp\left[-(\Omega_p - \omega)^3/\beta_{\parallel}\omega^2\Omega_p\right] \tag{31}$$

if the plasma electrons are cold. This result is shown as the dashed curve in Figure 34. However, the correct phase velocity Re $\omega/k_{\parallel}$ and growth rate Im ω for a bi-Maxwellian plasma are given by solutions of the dispersion equation

$$c^2 k_{\parallel}^2 = \omega^2 + (4\pi N_e q^2 \omega/\Omega_p m_p) + (4\pi N_p q^2/m_p)\left\{A - \left[A\Omega_p - (A+1)\omega\right] \times (m_p/2\kappa T_{\parallel}^{p} k_{\parallel}^2)^{1/2} Z(\zeta)\right\}, \tag{32}$$

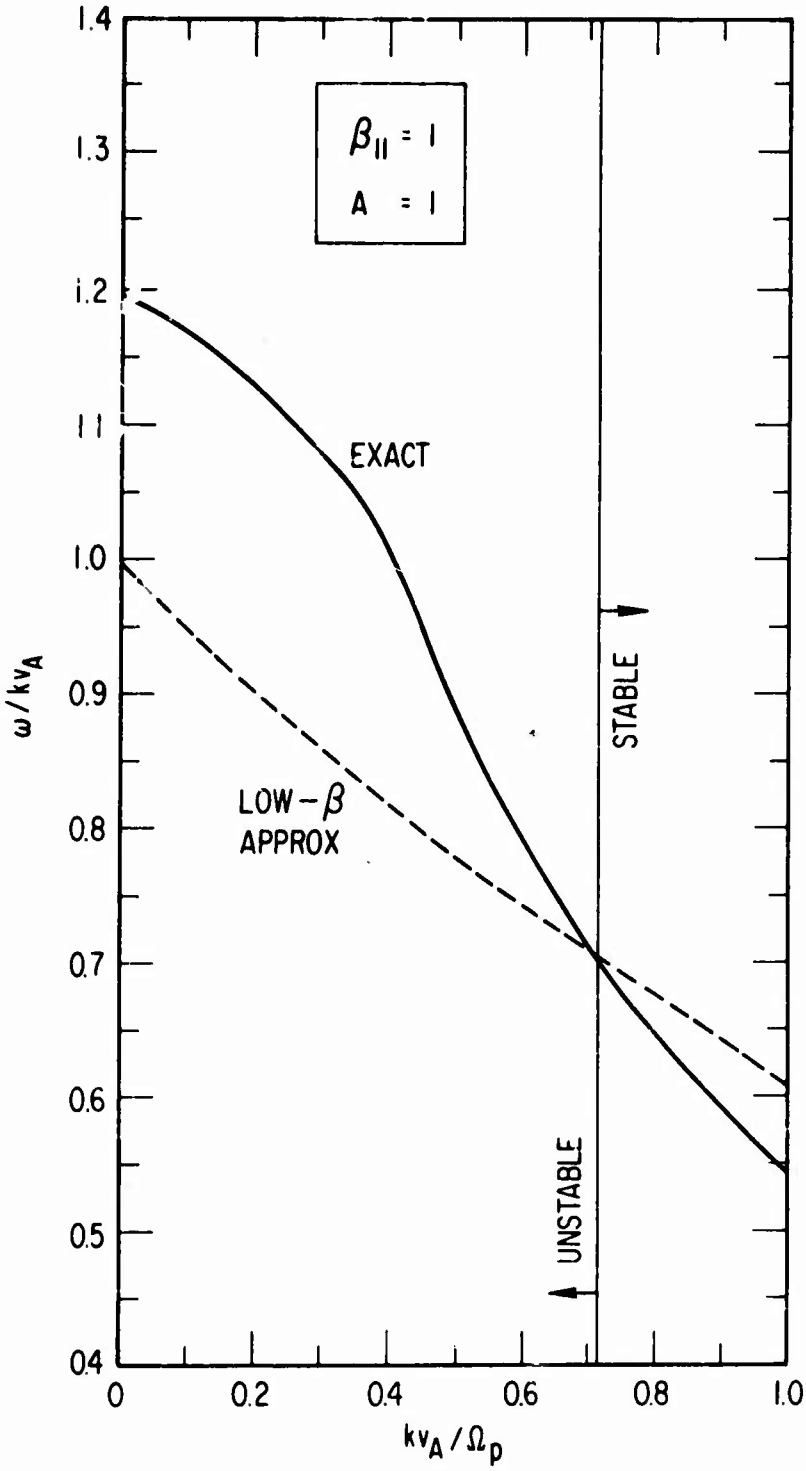

Fig. 33. Normalized phase velocities of electromagnetic ion-cyclotron waves from exact numerical calculation (solid curve) and from lowest-order (low-beta) approximation (dashed curve) in a plasma whose electrons are cold (Cornwall and Schulz, 1971).

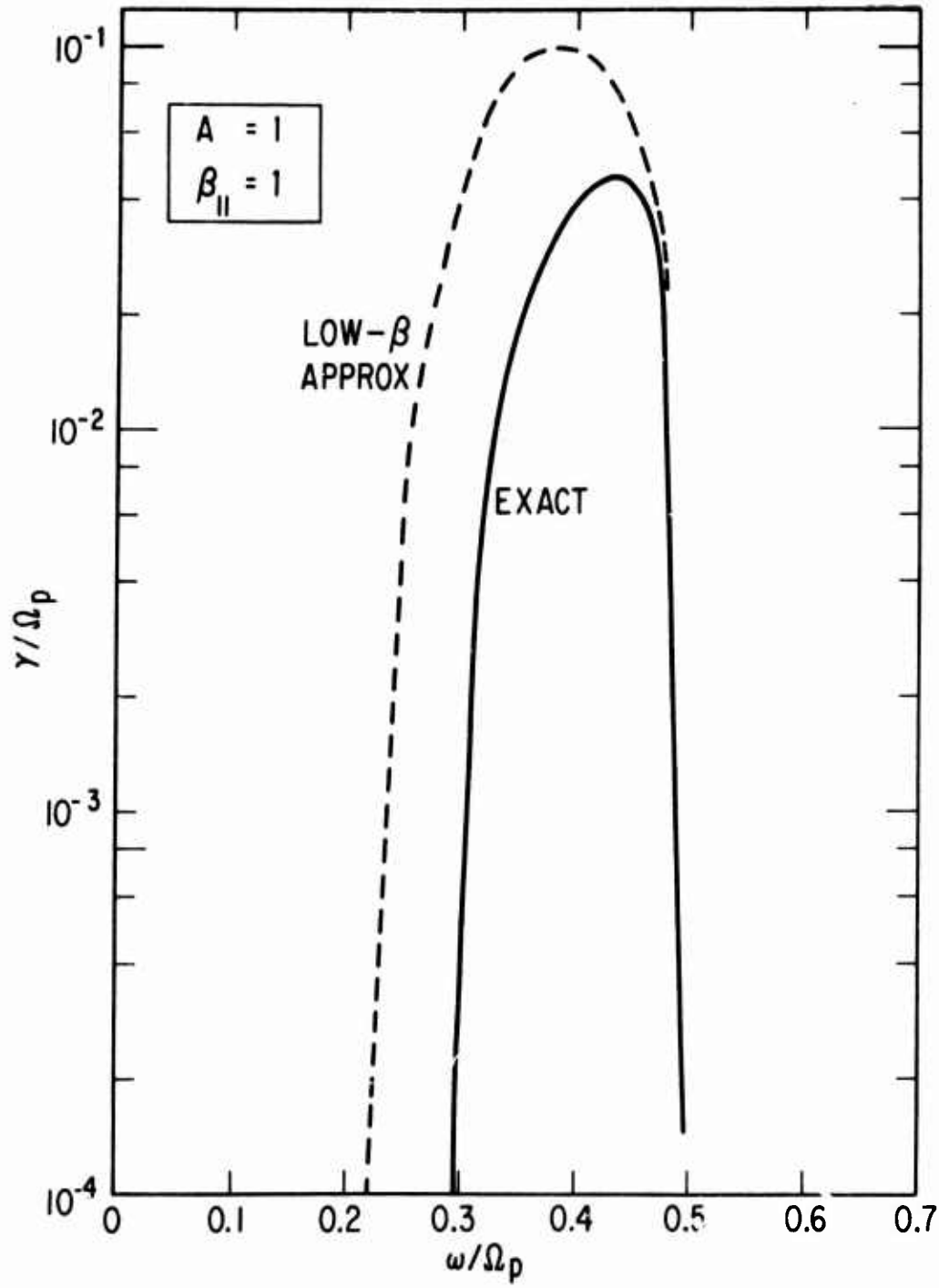

Fig. 34. Normalized growth rates of electromagnetic ion-cyclotron waves from exact numerical calculation (solid curve) and from lowest-order (low-beta) determination of phase velocity (dashed curve). The exact treatment increases the phase velocity (cf. Figure 33), and thereby reduces the growth rate, at frequencies $\omega/2\pi < A\Omega_p/2\pi(A+1)$. This figure originally appeared with incorrect normalization in Cornwall and Schulz (1971). Normalization was corrected by Cornwall and Schulz (1973).

where $\mathrm{Re}\,\omega < \Omega_p$ and where $Z(\zeta)$ is the plasma dispersion function of Fried and Conte (1961). The (complex) argument ζ is equal to $(m_p/2\kappa T_\parallel^p k_\parallel^2)^{1/2}(\omega - \Omega_p)$. The resulting values of $\mathrm{Re}\,\omega/k_\parallel v_A$ and $\mathrm{Im}\,\omega/\Omega_p$ (where positive) are plotted as solid curves in Figures 33 and 34 (Cornwall and Schulz, 1971; 1973; based on personal communication from T. Samec, 1971). The exact and (lowest-order) approximate phase velocities (Figure 33) agree at marginal stability, i.e., at $\omega = A\Omega_p/(A+1)$, because the square-bracketed coefficient of $Z(\zeta)$ in (32) vanishes there.

The quantitative consequences of injecting various species of cold plasma into such a proton ring current have been investigated by Märk (1974). His results are shown in Figure 35. The phase velocities in this case were calculated by retaining the first three terms ($n = 0, 1, 2$) of the asymptotic expansion

$$\zeta Z(\zeta) \sim -\pi^{-1/2} \sum_{n=0}^{\infty} \zeta^{-2n}\, \Gamma(n + \tfrac{1}{2}), \qquad (33)$$

which holds for $\mathrm{Im}\,\zeta > 0$ (Fried and Conte, 1961). Retention of only the first term ($n = 0$) leads to the "low-beta" approximation shown in Figures 33 and 34. The validity of Märk's "second-order" approximation (expansion of ζZ through $n = 2$ rather than $n = \infty$) can be checked by comparing the peak values of γ/Ω_p in Figures 34 and 35 for the case of absent cold plasma. One thus obtains $\mathrm{Max}\ \gamma/\Omega_p = 0.100$ by retaining only one term in (33), $\mathrm{Max}\ \gamma/\Omega_p = 0.035$ by retaining three terms (Figure 35), and $\mathrm{Max}\ \gamma/\Omega_p = 0.044$ by retaining all terms (Figure 34).

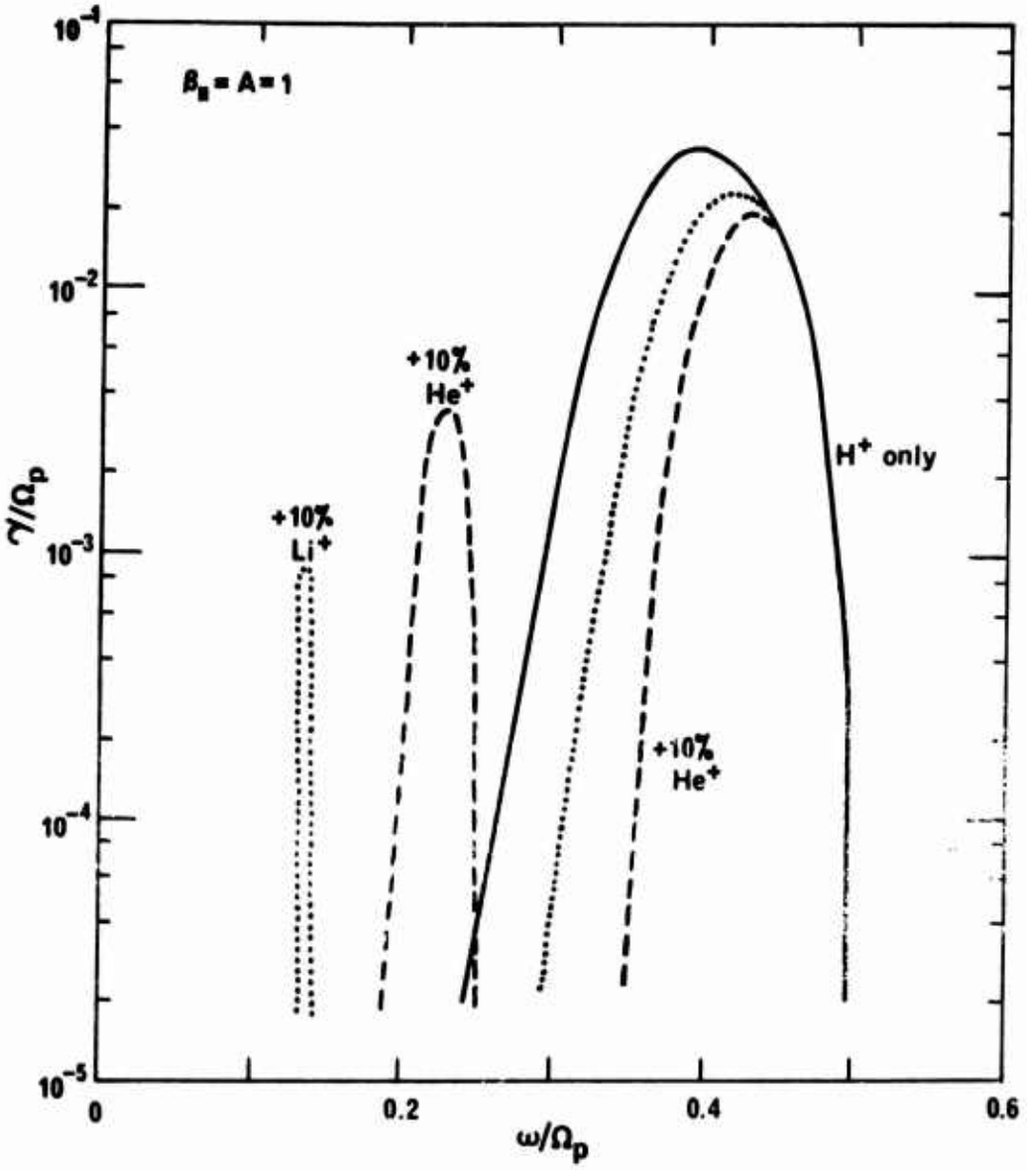

Fig. 35. Normalized growth rates of electromagnetic ion-cyclotron waves in plasmas consisting of hot protons, cold electrons, and (in two cases) additional cold plasma at 10% of the proton number density (personal communication based on Märk, 1974). Asymptotic expansion of the plasma dispersion function (Fried and Conte, 1961) was truncated after three terms in this calculation (cf. Figure 34 for H^+ only).

The addition of cold plasma (in Figure 35, a 10% increase in N_e) enhances the growth rate at $\omega < \Omega_c$ as expected, and reduces the growth rate at $\omega > \Omega_c$, where $\Omega_c/2\pi$ is the gyrofrequency of the ionic additive. However, since Max γ/Ω_p occurs at $\omega \sim 0.4\,\Omega_p$ in the absence of cold plasma for this situation ($\beta_\parallel = A = 1$), there is no technologically feasible ionic additive that can act to enhance the existing peak in γ/Ω_p. One must hope instead to create a new maximum in γ/Ω_p at $\omega \lesssim \Omega_c$ (by means of a cold-plasma admixture $\gg 10\%$). The natural maximum in γ/Ω_p would occur in the vicinity of $\omega \sim \Omega_p/7$ ($\sim \Omega_c$ for Li^+) only for rather small values of A and/or rather large values of $\beta_\parallel$, i.e., under conditions that are already rather disturbed even in the absence of cold-plasma additives. Thus, the conditions most favorable to efficient experimental enhancement of γ/Ω_p are the conditions most likely to preclude unequivocal detection of such enhancement.

For this reason and others, the idea of injecting cold plasma to stimulate electromagnetic ion-cyclotron instabilities has (in recent years) fallen into some disfavor as an experimental project. Besides implying the above objection, Märk (1974) has argued that the natural value of Max γ/v_g typically exceeds the reciprocal plasma dimension ($\sim 1/La$) even beyond the plasmasphere. Thus, local wave growth would exceed convective wave loss, and there would be instability even in the absence of a cold-plasma additive (a point conceded by Cornwall and Schulz, 1973). Moreover, Coroniti et al. (1972) have shown that ring-current protons having $\beta_\parallel \sim 1$ and $A \geq 1$ beyond the plasmapause should destabilize a

quasi-electrostatic wave mode (e.g., Post and Rosenbluth, 1966). Indeed, Burch (1973) and Mizera (1974) have observed precipitating ring-current protons in strong pitch-angle diffusion beyond the plasmasphere. Such protons are probably responsible for hydrogen arcs. The electrostatic loss-cone mode is stabilized by an increase in the cold-plasma density (Coroniti et al., 1972). Thus, the plasmapause should serve as a boundary between regions in which electromagnetic and electrostatic ion-cyclotron instabilities are respectively predominant. However, the experimental consequences of cold-plasma injection are much more subtle for ring-current protons than one had originally expected (e.g., Cornwall, 1972b). A concise review of present uncertainties in this area of investigation, as applied to the natural environment, is given by Coroniti (1973).

Theoretical problems posed by the idea of cold-plasma injection include the identification of a limit on stably trapped particle flux, the concept described by Kennel and Petschek (1966). This limit is the supposed maximum particle intensity that can remain trapped in the geomagnetic field without provoking the spontaneous excitation of large-amplitude electromagnetic cyclotron waves. Its evaluation is based on the requirement that

$$R \exp(2\gamma La/v_g) \leq 1, \tag{34}$$

where La is the effective path length over which wave amplification occurs, and R is the effective reflection coefficient to which the wave

energy is subjected at the "end" of the amplification path. Stability requires that the upper bound on γ/v_g, namely $(1/2\,La)\left|\ln R\right|$, be imposed at all relevant wave frequencies $\omega/2\pi$.

If, following Kennel and Petschek (1966), one imposes a pitch-angle distribution ($\sin^{2A}\alpha$, with $A \sim 1$ and energy spectrum (E^{-n}, with $n \sim 4$) at the outset, then one derives a limiting magnitude

$$I_{4\pi}^{*}(E^{*}) \sim 7 \times 10^{10}\, L^{-4}\, (B_0/B)^{A}\ \mathrm{cm}^{-2}\ \mathrm{sec}^{-1} \tag{35}$$

for the integral omnidirectional flux above the critical energy E^{*}. The critical energy for evaluating $I_{4\pi}^{*}$ is given by

$$E^{*} = B_0^2/8\pi N_e (A+1)^2 A \tag{36a}$$

for electrons and

$$E^{*} = B_0^2/8\pi N_p (A+1) A^2 \tag{36b}$$

for protons (e.g., Cornwall, 1972). Thus, the addition of cold plasma reduces E^{*}. The value of B/B_0 in (35) determines the location along a field line (L), with $B/B_0 = 1$ on the equator and $B/B_0 > 1$ off equator.

If, following Brice and Lucas (1971), one imposes only the pitch-angle distribution as above, then a limiting (nonrelativistic) spectrum of the form

$$E\, J_{4\pi}^{*}(E) \sim 10^{10}\, L^{-4}\, (E_0/B)^{A}\ \mathrm{cm}^{-2}\ \mathrm{sec}^{-1} \tag{37}$$

emerges for $E \gg E^*$. Here the symbol $J_{4\pi}(E)$ denotes the differential omnidirectional particle flux. The integral flux $I_{4\pi}^*(E^*)$ derived from (37) would diverge logarithmically. There is no possibility of reconciling (37) with (35), since different assumptions about the particle spectrum have been invoked in deriving the respective equations.

Both of the foregoing procedures have been criticized by Etcheto et al. (1973), who argue that neither the energy spectrum nor the pitch-angle distribution should be specified a priori in a theoretical calculation of the other. Instead, they advocate the steady-state solution of coupled equations for the wave spectrum $\mathcal{B}_\perp(\omega/2\pi)$ and particle distribution function $f(v_\parallel, v_\perp)$ in the presence of a particle source S. Similarly, Haerendel (1970) views the observable pitch-angle distribution and energy spectrum as a consequence of the balance between radial diffusion and pitch-angle diffusion. The main difficulty in implementing these approaches has been that the waves were assumed to propagate only parallel to $\underset{\sim}{B}$. Thus, for reasons outlined in Section 3, the resulting pitch-angle distributions have tended to form a cusp ($A = +\infty$?) at $\alpha_0 = 90^\circ$. This feature makes it impossible to define E^*, and (of course) disagrees with the observational data.

It is evident, however, that the advocates of self-consistently determining $f(v_\parallel, v_\perp)$ and $\mathcal{B}_\perp(\omega/2\pi)$ are on the right track. A similar procedure had been proposed by Cornwall (1966). What remains is to model the multitude of interactions more realistically, as Lyons et al. (1972) have done for the case of parasitic pitch-angle diffusion. Thus,

one must include off-equatorial resonances and oblique wave propagation (as well as radial diffusion of particles) in order to obtain a realistic distribution function. It will be inevitable in a realistic treatment, therefore, that waves generated on a given L shell will interact later with particles on another. The various drift shells are not dynamically isolated, even with respect to pitch-angle diffusion. Rather, the entire magnetosphere (including the ionosphere, according to the most thoughtful investigators) constitutes a single dynamical entity.

Pending a theoretical solution of the whole problem, however, there can be no serious objection to the use of observed pitch-angle distributions and particle-energy spectra in estimating the consequences of cold-plasma injection. This was the procedure adopted by Lucas and Brice (1973), for example. It is always hazardous, of course, to predict the consequences of a major environmental perturbation before a full understanding of the natural equilibrium has evolved. It is therefore to be hoped that future efforts in space will be directed as much toward an understanding of the natural magnetosphere as toward methods of its optimal contamination.

10. SUMMARY

The foregoing review of recent developments in radiation-belt physics is intended as a general overview of the topics selected. The

literature contains many papers not mentioned here, and the selection of citations has admittedly been somewhat parochial. The reader is asked to be tolerant of these shortcomings, as the subject of geomagnetically trapped radiation is too large in scope to be covered thoroughly in the space available here. However, it seems appropriate in closing to mention once again the outstanding questions that remain open in the general areas of investigation reviewed above.

On the subject of adiabatic drift shells, there is still the question of whether quasi-trapping affects any particles having $K = 0$ (neglecting electrostatic-field effects) in a realistic model of the outer magnetosphere, i.e., in a model whose surrounding electrical currents close in a reasonable way. On the topic of pitch-angle diffusion, one can hope to include self-consistently the exchange of energy between waves and particles, so as to identify the source(s) of waves responsible for parasitic diffusion. This procedure, and the inclusion of propagation effects, would enable one to obtain the spectrum, angular distribution, and spatial distribution of wave energy self-consistently, without recourse to the fiat of a given wave distribution. Moreover, the inclusion of radial diffusion and pitch-angle diffusion on an equal footing would make it possible to calculate both the radial distribution and the pitch-angle distribution of inner-zone and outer-zone electrons.

Temporal variations of the transport coefficients represent the major uncertainty in empirical and theoretical studies involving radial diffusion. In the case of outer-zone protons and electrons, the problem

is to account for temporal variations of the particle intensities in terms of temporal variations of D_{LL} with K_p. In the case of inner-zone protons, the problem is to model the variation of transport coefficients and boundary conditions (a) over the solar cycle, and (b) over the quasi-periodic (~ 8000-yr) variation of the earth's magnetic-dipole moment. Temporal variations also play a complicating role in the interpretation of data on the alpha/proton intensity ratio. In this problem it is certainly best to view the alpha-particle and proton distributions as two separate dynamical entities occupying the same environment. Temporal variations of their intensity ratio thus emerge as incidental consequences of the more interesting temporal variations that affect each particle species separately. Finally, to predict the consequences of cold-plasma injection into the magnetosphere (an experimental project), one requires a deeper understanding of the various processes that control the natural magnetospheric environment and its particle populations.

These comments conclude the present review of recent progress in the field of radiation-belt phenomenology, with emphasis on the past four years of research. Significant steps have been taken to consolidate and refine a variety of ideas that had previously occupied the realm of qualitative speculation. Despite this progress, many of the quantitative questions remain open. Thus, in view of the work that must yet be done, one can only hope that radiation-belt physics will survive as an active discipline for at least "four more years".

REFERENCES

Armstrong, T. W., Chandler, K. C., and Barish, J.: 1973, J. Geophys. Res. 78, 2715.

Axford, W. I.: 1969, in B. M. McCormac and A. Omholt (eds.), Atmospheric Emissions, Van Nostrand Reinhold, New York, p. 317.

Axford, W. I.: 1970, in B. M. McCormac (ed.), Particles and Fields in the Magnetosphere, Reidel, Dordrecht, p. 46.

Banks, P. M., and Holzer, T. E.: 1968, J. Geophys. Res. 73, 6846.

Bird, M. K., and Beard, D. B.: 1972, Planetary Space Sci. 20, 2057.

Blake, J. B.: 1973, J. Geophys. Res. 78, 5822.

Blake, J. B., Fennell, J. F., Schulz, M., and Paulikas, G. A.: 1973, J. Geophys. Res. 78, 5498.

Brice, N.: 1970, J. Geophys. Res. 75, 4890.

Brice, N.: 1971, J. Geophys. Res. 76, 4698.

Brice, N., and Lucas, C.: 1971, J. Geophys. Res. 76, 900.

Brown, W. L.: 1966, in B. M. McCormac (ed.), Radiation Trapped in the Earth's Magnetic Field, Reidel, Dordrecht, p. 612.

Burch, J. L.: 1973, J. Geophys. Res. 78, 6569.

Carter, R. E., Reines, F., Wagner, J. J., and Wyman, M. E.: 1959, Phys. Rev. 113, 280.

Chapman, S., and Bartels, J.: 1940, Geomagnetism, Clarendon, Oxford, pp. 611 and 651.

Chappell, C. R., Harris, K. K., and Sharp, G. W.: 1970, in B. M. McCormac (ed.), Particles and Fields in the Magnetosphere, Reidel, Dordrecht, p. 148.

Chappell, C. R., Harris, K. K., and Sharp, G. W.: 1971, J. Geophys. Res. 76, 2357.

Claflin, E. S., and White, R. S.: 1974, J. Geophys. Res. 79, 959.

Cocke, W. J., and Cornwall, J. M.: 1967, J. Geophys. Res. 72, 2843.

Cole, K. D.: 1965, J. Geophys. Res. 70, 1689.

Cornwall, J. M.: 1966, J. Geophys. Res. 71, 2185.

Cornwall, J. M.: 1972a, J. Geophys. Res. 77, 1756.

Cornwall, J. M.: 1972b, Rev. Geophys. Space Phys. 10, 993.

Cornwall, J. M., and Schulz, M.: 1971, J. Geophys. Res. 76, 7791.

Cornwall, J. M., and Schulz, M.: 1973, J. Geophys. Res. 78, 6830.

Cornwall, J. M., Coroniti, F. V., and Thorne, R. M.: 1970, J. Geophys. Res. 75, 4699.

Cornwall, J. M., Coroniti, F. V., and Thorne, R. M.: 1971, J. Geophys. Res. 76, 4428.

Coroniti, F. V.: 1973, in W. Campbell, S. Matsushita, and T. Speiser (eds.), Proceedings of the Chapman Memorial Symposium on Magnetospheric Motions, NOAA (ERL) and NCAR (HAO), Boulder, p. 118.

Coroniti, F. V., Fredricks, R. W., and White, R.: 1972, J. Geophys. Res. 77, 6243.

Cox, A.: 1969, Science 163, 237.

Crowther, D. L., and Harless, W. H.: 1971, in J. B. Cladis, G. T. Davidson, and L. L. Newkirk (eds.), The Trapped Radiation Handbook, ch. 8, DNA 2524H, DASA Info. Analysis Ctr., Santa Barbara.

Cuperman, S., and Landau, R. W.: 1974, J. Geophys. Res. 79, 128.

Cuperman, S., and Salu, Y.: 1974, J. Geophys. Res. 79, 135.

Davidson, G. T.: 1973, J. Geophys. Res. 78, 7569.

Davidson, G. T., and Hendrick, R. W.: 1971, in J. B. Cladis, G. T. Davidson, and L. L. Newkirk (eds.), The Trapped Radiation Handbook, ch. 7, DNA 2524H, DASA Info. Analysis Ctr., Santa Barbara.

Davis, L. R., and Williamson, J. M.: 1963, Space Res. 3, 365.

Dragt, A. J.: 1971, J. Geophys. Res. 76, 2313.

Dragt, A. J., Austin, M. M., and White, R. S.: 1966, J. Geophys. Res. 71, 1293.

Etcheto, J., Gendrin, R., Solomon, J., and Roux, A.: 1973, J. Geophys. Res. 78, 8150.

Fälthammar, C.-G.: 1968, in B. M. McCormac (ed.), Earth's Particles and Fields, Reinhold, New York, p. 157.

Farley, T. A.: 1969, J. Geophys. Res. 74, 377.

Farley, T. A., and Walt, M.: 1971, J. Geophys. Res. 76, 8223.

Farley, T. A., Tomassian, A. D., and Walt, M.: 1970, Phys. Rev. Letters 25, 47.

Farley, T. A., Kivelson, M. G., and Walt, M.: 1972, J. Geophys. Res. 77, 6087.

Fennell, J. F., Blake, J. B., and Paulikas, G. A.: 1974, J. Geophys. Res. 79, 521.

Frank, L. A.: 1971, J. Geophys. Res. 76, 2512.

Fried, B. D., and Conte, S. D.: 1961, The Plasma Dispersion Function, Academic Press, New York.

Fritz, T. A., and Williams, D. J.: 1973, J. Geophys. Res. 78, 4719.

Haerendel, G.: 1970, in E. M. McCormac (ed.), Particles and Fields in the Magnetosphere, Reidel, Dordrecht, p. 416.

Hess, W. N.: 1968, The Radiation Belt and Magnetosphere, Blaisdell, Waltham, p. 155.

Hovestadt, D., Achtermann, E., Ebel, B., Häusler, B., and Paschmann, G.: 1972a, in B. M. McCormac (ed.), Earth's Magnetospheric Processes, Reidel, Dordrecht, p. 115.

Hovestadt, D., Häusler, B., and Scholer, M.: 1972b, Phys. Rev. Letters 28, 1340.

Imhof, W. L., Reagan, J. B., and Smith, R. V.: 1967, J. Geophys. Res. 72, 2371.

Kennel, C. F., and Petschek, H. E.: 1966, J. Geophys. Res. 71, 1.

Krimigis, S. M.: 1970, in B. M. McCormac (ed.), Particles and Fields in the Magnetosphere, Reidel, Dordrecht, p. 364.

Lanzerotti, L. J., and Morgan, C. G.: 1973, J. Geophys. Res. 78, 4600.

Lanzerotti, L. J., Maclennan, C. G., and Schulz, M.: 1970, J. Geophys. Res. 75, 5351.

Lanzerotti, L. J., Maclennan, C. G., and Schulz, M.: 1971, J. Geophys. Res. 76, 5371.

Lenchek, A. M., Singer, S. F., and Wentworth, R. C.: 1961, J. Geophys. Res. 66, 4027.

Lingenfelter, R. E.: 1963, J. Geophys. Res. 68, 5633.

Lucas, C., and Brice, N.: 1973, J. Geophys. Res. 78, 8338.

Lyons, L. R.: 1974, J. Plasma Phys. 9, 0000.

Lyons, L. R., and Thorne, R. M.: 1972, J. Geophys. Res. 77, 5608.

Lyons, L. R., and Thorne, R. M.: 1973, J. Geophys. Res. 78, 2142.

Lyons, L. R., Thorne, R. M., and Kennel, C. F.: 1971, J. Plasma Phys. 6, 589.

Lyons, L. R., Thorne, R. M., and Kennel, C. F.: 1972, J. Geophys. Res. 77, 3455.

Märk, E.: 1974, J. Geophys. Res. 79, 3218.

Mead, G. D.: 1964, J. Geophys. Res. 69, 1181.

Mead, G. D., and Beard, D. B.: 1964, J. Geophys. Res. 69, 1169.

Merker, M.: 1972, Phys. Rev. Letters 29, 1531.

Mizera, P. F.: 1974, J. Geophys. Res. 79, 581.

Mizera, P. F., and Blake, J. B.: 1973, J. Geophys. Res. 78, 1058.

Mogro-Campero, A.: 1972, J. Geophys. Res. 77, 2799.

Mogro-Campero, A., and Simpson, J. A.: 1970, Phys. Rev. Letters 25, 1631.

Morfill, G.: 1975, Space Sci. Rev. 17, this issue.

Moritz, J.: 1972, Z. Geophys. 38, 701.

Mozer, F. S.: 1971, J. Geophys. Res. 76, 3651.

Nakada, M. P., Dungey, J. W., and Hess, W. N.: 1965, J. Geophys. Res. 70, 3529.

Newkirk, L. L., and Walt, M.: 1968a, J. Geophys. Res. 73, 1013.

Newkirk, L. L., and Walt, M.: 1968b, J. Geophys. Res. 73, 7231.

Northrop, T. G., and Teller, E.: 1960, Phys. Rev. 117, 215.

Paulikas, G. A., Blake, J. B., and Freden, S. C.: 1967, J. Geophys. Res. 72, 2011.

Pfitzer, K. A., Lezniak, T. W., and Winckler, J. R.: 1969, J. Geophys. Res. 74, 4687.

Post, R. F., and Rosenbluth, M. N.: 1966, Phys. Fluids 9, 730.

Preszler, A. M., Simnett, G. M., and White, R. S.: 1972, Phys. Rev. Letters 28, 982.

Preszler, A. M., Simnett, G. M., and White, R. S.: 1974, J. Geophys. Res. 79, 17.

Roberts, C. S.: 1969, Rev. Geophys. 7, 305.

Roederer, J. G.: 1967, J. Geophys. Res. 72, 981.

Roederer, J. G., and Schulz, M.: 1969, J. Geophys. Res. 74, 4117.

Roederer, J. G., and Schulz, M.: 1971, J. Geophys. Res. 76, 1055.

Roederer, J. G., Hilton, H. H., and Schulz, M.: 1973, J. Geophys. Res. 78, 133.

Russell, C. T., and Thorne, R. M.: 1970, Cosmic Electrodynamics 1, 67.

Schulz, M., and Lanzerotti, L. J.: 1974, Particle Diffusion in the Radiation Belts, Springer, Heidelberg.

Shabansky, V. P., and Antonova, A. E.: 1968, Geomagn. i Aeronomiya 8, 844.

Smart, D. F., Shea, M. A., and Gall, R.: 1969, J. Geophys. Res. 74, 4731.

Stern, D. P.: 1971, J. Geophys. Res. 76, 7787.

Stone, E. C.: 1963, J. Geophys. Res. 68, 4157.

Taylor, H. E., and Hastie, R. J.: 1971, Cosmic Electrodynamics 2, 211.

Thede, A. L.: 1969, Report AFWL-TR-68-128, Air Force Weapons Lab., Albuquerque.

Vampola, A. L.: 1972, in E. A. Warman (ed.), Proceedings of the National Symposium on Natural and Manmade Radiation in Space, p. 539, NASA TM X-2440, Washington.

Van Allen, J. A.: 1966, in B. M. McCormac (ed.), Radiation Trapped in the Earth's Magnetic Field, Reidel, Dordrecht, p. 575.

Walt, M.: 1966, in B. M. McCormac (ed.), Radiation Trapped in the Earth's Magnetic Field, Reidel, Dordrecht, p. 337.

Walt, M.: 1970, in B. M. McCormac (ed.), Particles and Fields in the Magnetosphere, Reidel, Dordrecht, p. 410.

Walt, M.: 1971, in J. B. Cladis, G. T. Davidson, and L. L. Newkirk (eds.), The Trapped Radiation Handbook, ch. 6, DNA 2524H, DASA Info. Analysis Ctr., Santa Barbara.

West, H. I., Buck, R. M., and Walton, J. R.: 1973, J. Geophys. Res. 78, 1064.

White, R. S.: 1973, Rev. Geophys. Space Phys. 11, 595.

Williams, D. J., and Mead, G. D.: 1965, J. Geophys. Res. 70, 3017.

Williams, D. J., Arens, J. F., and Lanzerotti, L. J.: 1968, J. Geophys. Res. 73, 5673.

LABORATORY OPERATIONS

The Laboratory Operations of The Aerospace Corporation is conducting experimental and theoretical investigations necessary for the evaluation and application of scientific advances to new military concepts and systems. Versatility and flexibility have been developed to a high degree by the laboratory personnel in dealing with the many problems encountered in the nation's rapidly developing space and missile systems. Expertise in the latest scientific developments is vital to the accomplishment of tasks related to these problems. The laboratories that contribute to this research are:

Aerophysics Laboratory: Launch and reentry aerodynamics, heat transfer, reentry physics, chemical kinetics, structural mechanics, flight dynamics, atmospheric pollution, and high-power gas lasers.

Chemistry and Physics Laboratory: Atmospheric reactions and atmospheric optics, chemical reactions in polluted atmospheres, chemical reactions of excited species in rocket plumes, chemical thermodynamics, plasma and laser-induced reactions, laser chemistry, propulsion chemistry, space vacuum and radiation effects on materials, lubrication and surface phenomena, photosensitive materials and sensors, high precision laser ranging, and the application of physics and chemistry to problems of law enforcement and biomedicine.

Electronics Research Laboratory: Electromagnetic theory, devices, and propagation phenomena, including plasma electromagnetics; quantum electronics, lasers, and electro-optics; communication sciences, applied electronics, semiconducting, superconducting, and crystal device physics, optical and acoustical imaging; atmospheric pollution; millimeter wave and far-infrared technology.

Materials Sciences Laboratory: Development of new materials; metal matrix composites and new forms of carbon; test and evaluation of graphite and ceramics in reentry; spacecraft materials and electronic components in nuclear weapons environment; application of fracture mechanics to stress corrosion and fatigue-induced fractures in structural metals.

Space Physics Laboratory: Atmospheric and ionospheric physics, radiation from the atmosphere, density and composition of the atmosphere, aurorae and airglow; magnetospheric physics, cosmic rays, generation and propagation of plasma waves in the magnetosphere; solar physics, studies of solar magnetic fields; space astronomy, x-ray astronomy; the effects of nuclear explosions, magnetic storms, and solar activity on the earth's atmosphere, ionosphere, and magnetosphere; the effects of optical, electromagnetic, and particulate radiations in space on space systems.

THE AEROSPACE CORPORATION
El Segundo, California

. . .